Synthetic Expression Systems for Controlled Perturbation of Mammalian Cellular Regulatory Networks

Von der Fakultät für Lebenswissenschaften

der Technischen Universität Carolo-Wilhelmina

zu Braunschweig

zur Erlangung des Grades einer

Doktorin der Naturwissenschaften

(Dr. rer. nat.)

genehmigte

D i s s e r t a t i o n

von Stephanie Sievers
aus Goslar

1. Referentin: Professor Dr. Petra Dersch
2. Referent: apl. Professor Dr. Peter Paul Müller
eingereicht am: 27.04.2011
mündliche Prüfung (Disputation) am: 04.07.2011

Druckjahr 2011

Vorveröffentlichungen der Dissertation

Teilergebnisse aus dieser Arbeit wurden mit Genehmigung der Fakultät für Lebenswissenschaften, vertreten durch die Mentorin der Arbeit, in folgenden Beiträgen vorab veröffentlicht:

Tagungsbeiträge

Sievers S, Hauser H, Wirth D (2008) Synthetic regulatory modules for controlled perturbation of the interferon network (poster P3). 2nd International PhD Symposium of the Helmholtz International Research School for Infection Biology, Braunschweig

Sievers S, May T, Hauser H, Wirth, D (2009) Synthetic expression systems for the modulation of endogenous cellular networks (talk and poster). Clinigene 2nd Training Course, Barcelona

Sievers S, May T, Goncalves J, Eccleston L, Hauser H, Wirth, D (2009) Towards genetic perturbation of cellular networks in mammals (poster). German Symposium on Systems Biology, Heidelberg

Sievers S, Rand U, Köster M, Teixeira A, Hauser H, Wirth, D (2009) Towards genetic perturbation of cellular networks in mammals (poster P47). 3rd International PhD Symposium of the Helmholtz International Research School for Infection Biology, Braunschweig

Sievers S (2010) Synthetic Expression Systems for Controlled Perturbation of Cellular Regulatory Networks (talk). Progress Seminar of the Helmholtz Centre for Infection Research, Braunschweig

Sievers S (2010) Synthetic Expression Systems for Controlled Perturbation of Cellular Regulatory Networks (talk T11). 4th International PhD Symposium of the Helmholtz International Research School for Infection Biology, Braunschweig

Table of contents

Summary

Synthetic biology is a young research field which aims at the design of artificial networks as well as the redesign of existing networks to obtain insight into complex biological relations. Since lately, synthetic approaches are used to interfere with mammalian networks.

In this work, perturbation of the virus-induced IFN-β induction pathway was forced. For this purpose, synthetic cassettes were used. The interference was realized by exploiting natural, viral counteracting proteins. The viral proteins that were used in this work are the influenza A virus NS1 protein and the hepatitis C virus NS3/4A protein complex. The viral genes were fused to a tag to allow fluorescent ligand labeling of the proteins and besides, visualization on the single cell level. The respective fusion was expressed from a tetracycline-dependent promoter within IFN-β reporter cells. These cells showed controlled regulation in response to the tetracycline derivative doxycycline and displayed graded induction on the single cell level. Both proteins were able to strongly interfere with IFN-β induction, whereas NS3/4A showed more pronounced effects already at low amounts of the protein. On the single cell level, this system allowed to correlate the virus-induced IFN-β expression course with the ectopically induced expression of the viral perturbators. The latter was clearly associated with an arrest of IFN-β signal increase. The results suggest that even an ongoing IFN-β induction can be interrupted by expression of NS1 and NS3/4A. This was confirmed by monitoring intracellular localization of tagged IRF-7 which translocates to the nucleus upon activation of the IFN-β induction pathway. Indeed, perturbation experiments showed that the relocation of activated IRF-7 into the cytosol occurred in direct temporal correlation to NS1 induction. Importantly, the herein chosen viral proteins were highly specific in their action and were proven to have no impact on IFN-induced JAK/STAT signaling. In addition, any effect on the type I IFN post-transcriptional level could be excluded. Together, the results underline the benefit of synthetic expression modules/circuits to specifically perturb individual steps within complex regulatory cascades in a highly controlled way – a prerequisite to establish mathematical models towards systems biology based understanding.

This work further provides first results on the realization of a complex, synthetic network. Cassettes for the establishment of a synthetic oscillatory expression circuit were stably integrated into mammalian cells. While final proof remains to be shown, the results highlight the requirements and challenges to realize such complex circuits in mammalian cells.

1 Introduction

1.1 Synthetic biology approaches in mammalian cells

Synthetic biology is a young research field addressing scientific problems by engineering systems. The main topics are the design of synthetic components or networks that do not exist in nature on the one hand and the rebuilding of existing systems on the other hand. Certainly, these methods contribute to solving complex problems in biological systems that are not understood, yet.
Initial work in this field was performed in prokaryotes or *Saccharomyces cerevisiae* due to their accessible genome and easier handling in the case of genetic manipulation and cultivation. However, the recent progress in mammalian genetics and manipulation strategies as well as the development of a great number of mammalian transgene control networks within the past years enabled the use of mammalian models (reviewed in Tigges & Fussenegger, 2009). Also, synthetic biology approaches can probably be used for drug discovery and pharmaceutical applications (reviewed in Neumann & Neumann-Staubitz, 2010). Especially in the last two years, impressive approaches for complex synthetic networks could be demonstrated, even though they still lack stable integration into mammalian cells (Tigges et al, 2010; Tigges et al, 2009).
A main goal addressed by synthetic biology is to gain information about the dynamics and mechanisms of biological systems ranging throughout the cellular hierarchy. Up to now, much is known about specific individual components and mechanisms within cellular networks, but it lacks knowledge on spatiotemporal dynamics and the interplay of these networks.
Systems biology, on the other hand, contributes to the understanding of complex biological systems by converting biological facts (e.g. experimental data) into mathematical models. With such models, the simulation and prediction of the behavior of a distinct factor or system is possible as very recently demonstrated (Maiwald et al, 2010). Also, the behavior of synthetic circuits can be predicted, facilitating the work in the field of synthetic biology. *Vice versa*, quantitative and qualitative data for the construction of mathematical models can be provided by synthetic biology approaches. However, the modeling results still have to be verified by experimental procedures. Approaches like this are time-consuming and demand strong collaborations between the respective scientists.

1.2 Cellular networks

Within biological signaling networks, information processing is performed at intra- and extracellular stages. They are composed of many components like (co-) activators, enzymes or substrates which have specific functions and are organized in certain levels (reviewed by Scott & Pawson, 2009). The response of the cell to a certain signal can be multifaceted. Often, secondary cascades are induced, but anyway, at the end of the cascade(s), activation of gene expression, modification in the cellular metabolism, cell death or other alterations within the cell occur.
Formerly, signal transduction was regarded as separate transmission of linear information, but this view has changed drastically. There is a tremendous variety of examples for crosstalk between signaling pathways that often have huge impact on cellular fate. For example, different receptors are able to induce the same signal transduction pathway and also the components are shared by multiple networks. This creates the possibility of a limited number of components to induce a variety of biological processes. The spatiotemporal organization of signaling networks certainly is of central importance for its outcome.

1.3 Interfering with cellular networks for determining protein functions and dynamics

Today, there is deep knowledge about the single components of many networks, but their spatiotemporal and dynamical interplay is hardly understood. For obtaining information about the "where-and-when" of signal transduction as well as connections between the networks and the discovery of key functions, perturbation of cellular pathways can be a good tool. Targeted interference with a cellular network allows the examination of an altered cellular phenotype. Up to date, there exist several methods to perturb cellular functions which all have assets and drawbacks.

- Irreversible perturbation: Genetic knock-out
- Reversible perturbation: RNA interference (RNAi)
  Chemical perturbation
  Perturbation via synthetic constructs

The use of chemical agents can be efficient but is frequently unspecific due to possible down-regulation of related proteins. Furthermore, cell permeability and low toxicity is required which strongly reduces the choice of small compounds. Another technique is the creation of a genetic knock-out, which is time-consuming and irreversible. Furthermore, the permanent deletion of a gene can have detrimental or even lethal effects on the cell or organism. Conditional knock-out strategies can overcome some of these problems. RNA interference allows targeted transcript deletion while a complete block usually cannot be achieved. All of these techniques lack true reversibility and the possibility of temporal regulation.

Since recent studies in synthetic biology demonstrated successful results in mammalian cells, an interesting and demanding approach would be the usage of these tools to establish modules specifically perturbing signaling networks with biological molecules in a regulable and reversible manner. However, only minor data of related approaches are published. Few attempts for synthetic perturbation were demonstrated as it is the conditional immortalization (May et al, 2004).

For synthetic perturbation, mammalian cells have to be repeatedly modified. Constructs need to be stably introduced into the cells to verify robustness, reliability and reproducibility of the system. Such constructs would harbor a factor that specifically interferes with the desired signaling process. Unspecific effects should be excluded.

A further advantage is the usage of an inducible expression system in order to externally control the perturbation in a time- and dose-dependent manner. With such cells, temporal dynamics of a system could be determined in more detail in a predictable, reproducible and reversible manner.

1.4 The tetracycline (Tet) responsive system

Inducible expression systems are useful tools to control the level of a gene product of interest (GOI) within a mammalian cell. The most prominent among them is the Tet system (Gossen & Bujard, 1992). This system was developed from the Tn*10*-specific tetracycline-resistance operon of *Escherichia Coli* (*E. Coli*). It relies on the homodimerization of the Tet repressor (TetR; Postle et al, 1984) and the binding to cognate tetracycline operator sequences (*tet*Os). Gossen and Bujard fused the *tetR* binding domain to the transactivating domain of Herpes Simplex Virus VP16 (Triezenberg et al, 1988). This fusion, namely tetracycline transactivator (tTA), can transactivate the synthetic promoter consisting of *tet*O repeats and a downstream minimal eukaryotic promoter. The first synthetic tetracycline-responsive promoter (Gossen & Bujard, 1992)

consisted of seven *tet*O repeats and a minimal Cytomegalovirus (CMV) promoter (P_{hCMV}) (Boshart et al, 1985) devoid of its enhancer which is further on designated as P_{Tet}. Upon administration of the inducer tetracycline, the tTA undergoes a conformational change and dissociates from the promoter, leading to the arrest of gene expression (Tet-Off system).
The originally described Tet system worked reliable and gave predictable expression for bulk assays. However, some drawbacks concerning regulation and leakiness of the promoter were connected with its use.

The reverse tetracycline transactivator (rtTA)

In the Tet-Off system, the constant presence of tetracycline is needed to keep synthetic gene expression silent. This is disadvantageous in long-term experiments, transgenic animals and for gene therapeutic approaches. Consequently, Gossen et al. (1995) designed a *tetR* domain with four amino acid exchanges, which exhibited reversed tetracycline dependence. The mutagenized *tetR* was fused to the HSV VP16 transactivating domain creating the so-called reverse tetracycline transactivator (rtTA). The rtTA exhibited binding to the *tet*O sequences only in the presence of tetracycline (Tet-On system, see fig. 1). This reverse transactivator led to strongest activation of gene induction upon administration of the tetracycline derivative doxycycline (Dox), which is nowadays commonly used. However, inducibility of this initial rtTA was inefficient, which led to the construction of improved versions like rtTA2(S)-M2 (consecutively called rtTA2). This transactivator is more stable in eukaryotic cells, works at 10-fold lower doxycycline concentrations and shows a significant reduction in background activation of the respective promoter in the absence of doxycycline (Urlinger et al, 2000). Further improvements are reviewed by Berens and Hillen (2003).

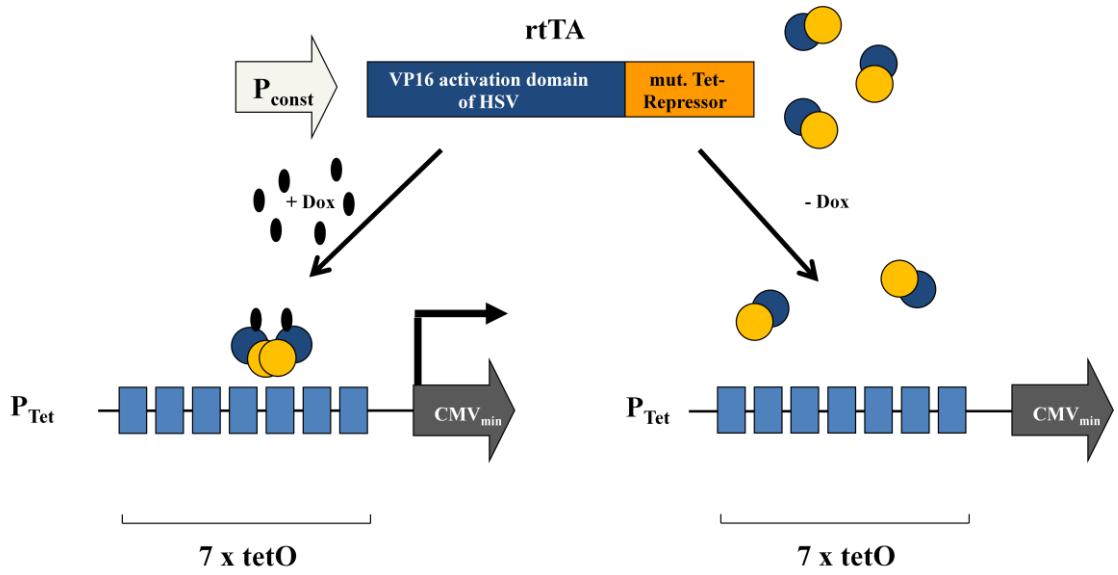

Figure 1: Functionality of the Tet-On system.

In the presence of doxycycline (Dox), rtTA dimerizes and associates with *tet*O sequences leading to the onset of downstream gene expression. In the absence of Dox, rtTA cannot dimerize or bind to the *tet*O repeats.

Tetracycline-induced repression: the KRAB repressor

Margolin et al. (1994) described that Krüppel-associated boxes (KRAB) can act as transcriptional repressors when fused to the DNA-binding domain of yeast Gal4 promoter. Fusion of *tetR* to the KRAB domain of the human Kox1 zinc finger motif led to the design of a tetracycline-dependent transcriptional suppressor, the KRAB repressor, (consecutively for simplicity called KRAB) for the use in eukaryotes (Deuschle et al, 1995). KRAB recognizes the operator sequences within the P_{Tet} and induces transcriptional repression of RNA polymerases I-III within the range of a few kilobases in the absence of doxycycline by an epigenetic silencing mechanism causing the induction of heterochromatin. Administration of doxycycline, in turn, enables the dissociation of the repressor from the *tet*O sites. Consequently, the TetR-KRAB fusion could be exploited for the repression of basal leakiness of the P_{Tet}.
Since KRAB exhibits opposite binding capacities as the rtTA, it could be combined with the activation via the rtTA in one system. KRAB and rtTA could be provided with different DNA recognition and/or protein dimerization capabilities to overcome heterodimerization of the two compounds or competition for the same DNA binding sites (Forster et al, 1999). The KRAB repressor was improved for further silencing basal expression and for different ways to avoid heterodimerization of KRAB and the transactivator (Freundlieb et al, 1999; Hayakawa et al, 2006).

The Tet-dependent promoter

In the initial Tet system, Gossen and Bujard designed a tetracycline-responsive promoter consisting of seven *tet*Os that were placed upstream of a minimal promoter (fig. 1). The arrangement of the promoter arised the idea to construct a bidirectional, tetracycline-dependent promoter ($P_{bidiTet}$) which allows simultaneous expression of two GOIs (Baron et al, 1995). In this construct, heptamerized *tet*O sequences are flanked by two minimal promoters.
An IFN-α stimulated response element (ISRE)-like element was discovered between the *tet*O repeats of P_{Tet} (Rang & Will, 2000). Consequently, improved variants of P_{Tet} were developed. One of these promoters, P_{Tight} from Clontech (2003), is purchasable and already commonly used. Other improvements to reduce leakiness of the promoter were e.g. performed by (Agha-Mohammadi et al, 2004; Loew et al, 2010; Pluta et al, 2005).

1.5 The coumermycin (Cou) responsive system

The mammalian expression Tet system is a well characterized and improved tool. However, in order to express two genes in one organism independent from each other, different systems are necessary. Up to date, there exist many of these systems exploiting e.g. light, temperature or steroid hormones. Those and further genetic switches have been reviewed by several groups (Aubel & Fussenegger, 2010; Botezatu et al, submitted; Weber & Fussenegger, 2010). Indeed, the controlled expression by a second inducer would be easy to manage and therefore favored. Besides the Tet system there exist several other systems responding to antibiotic as a transcription inducer as e.g. macrolide- or streptogramin-responsive systems (Fussenegger et al, 2000; Weber et al, 2002).
Another antibiotic-responsive system, the coumermycin (Cou) system was developed (Zhao et al, 2003). This system was already shown not to interfere with the Tet system (Kästner, 2007). In principal, this system works similar to the Tet system being composed of a transactivator and a corresponding promoter. The coumermycin transactivator (CouTA) is a chimeric protein built of the bacterial phage λ repressor-binding domain fused to the bacterial gyrase B subunit (GyrB) and the p65 activation domain of nuclear factor (NF)-κB. The coumermycin-responsive promoter (P_{Cou}) consists of 12 λ operator sequences located upstream of the P_{hCMV*} minimal promoter. The addition of coumermycin induces dimerization of the transactivator which causes the binding of the phage λ repressor to the cognate λ operator sequences, thereby transactivating expression of the downstream gene. Administration of the coumermycin

antagonist novobiocin abolishes dimerization of the transactivator what leads to its dissociation from P_{Cou}, thereby interrupting gene expression. Basal expression levels by this system were already reduced by site-directed mutagenesis of the λ repressor-binding domain. Inductions of four orders of magnitude can be reached by this system (Zhao et al, 2003).

1.6 Synthetic modules for the use in eukaryotic cells

Synthetic biology aims at designing modules with the goal to resemble natural expression patterns. Even though pioneering work was performed in prokaryotes and lower eukaryotes, many approaches could be successfully transferred for the use in mammalian cells. Genetic switches serve as a platform for these approaches in eukaryotic cells (compare with chapter 1.5).
It was shown that two different antibiotic-responsive switches, Pip-On and E-On (Fussenegger et al, 2000; Weber et al, 2002), can be combined to design an epigenetically controlled circuit (Kramer et al, 2004). The KRAB transrepressor is fused to the erythromycin or pristinamycin response regulators in this circuit. Thereby, it is directed to the respective responsive promoter and the two systems are able to repress each other's expression. Upon a transient dosage of the respective antibiotic, the binding of one of the fusions to the respective promoter is impaired and sustained expression of the second module can occur even in the presence of the transrepressor. A toggle-switch like phenotype can be obtained by this circuit. With this tool, long-term antibiotic administration to obtain desired expression levels can be circumvented. Also, a bimodal expression pattern could be realized by this constellation.
Bimodal expression is a natural pattern occurring e.g. in the response of mouse embryonic stem cells to leukemia inhibitory factor (LIF) (Davey et al, 2007). By the usage of a positive feedback system, this pattern can be artificially induced. In the case of the Tet system, a construct harboring the rtTA and a reporter gene under control of P_{Tet} are induced via a feedback mechanism after administration of doxycycline (Kramer & Fussenegger, 2005; May et al, 2008). For this purpose, a bidirectional tetracycline-dependent promoter controlling the expression of rtTA and the gene of interest can also be exploited. Increasing concentrations of doxycycline rather affect the probability that a gene will be expressed than its expression strength. If expression is turned on, it shows reduced variability.
The Tet system can also be used to generate graded gene expression by constitutive expression of rtTA while the GOI is expressed from P_{Tet}. Increasing

concentrations in this case lead to a continuous increase in the expression intensity of the GOI.
Another naturally appearing expression pattern is the oscillation. This pattern appears e.g. for circadian clock genes (reviewed by Jolma et al, 2010). The work mechanism for this pattern is similar for these genes: it is based on a negative feedback loop after a time delay caused by the self-inhibition of the own gene product (reviewed by Van Gelder et al, 2003). Indeed, the design of an adequate system to mimic this expression pattern underlies a more complex composition than for graded or bimodal expression.
The basic knowledge of oscillatory behavior was exploited to design diverse oscillating constructs. First works on complex multiple gene oscillators were also performed in bacteria or lower eukaryotes (Elowitz & Leibler, 2000).
However, for mammalian cells, no stable oscillator could be introduced up to now. Indeed, a transient approach succeeded to obtain oscillations in single cells (Tigges et al, 2009). A synthetic low-frequency oscillator, which shows oscillation with a period of 26 h, was also introduced by Tigges et al. (2010). The current state of synthetic oscillator performance was reviewed (Purcell et al, 2010).

1.7 Viruses and type I IFNs

As part of the innate immunity, the IFN system is one of the first host cell responses to intruding pathogens like viruses and is able to quickly induce a multitude of antiviral genes. Type I IFNs are directly induced in response to virus infection (early type I IFN genes) and in a response to early type I IFNs (late type I IFNs). 14 α genes as well as each one β, δ, ε, κ and ω gene belongs to the type I IFNs in mice (reviewed by Seo & Hahm, 2010). They can be produced from all nucleated cells, whereas plasmacytoid dendritic cells are often the major producers (reviewed by Barchet et al, 2005a; Barchet et al, 2005b).
Today, recombinant interferon is used as a therapeutic for diverse diseases like multiple sclerosis, hepatitis C and some kinds of cancer. On the other hand, altered IFN induction can cause systemic autoimmune disorders like lupus erythematosus, rheumatoid arthritis or Sjögren's syndrome. Consequently, IFNs are of major interest for several clinical purposes.
Type I IFNs are produced in response to pathogens like viruses and their products which are described as pathogen-associated molecular patterns (PAMPs). These PAMPs, e.g. viral nucleic acids, bind to specialized pattern recognition receptors (PRRs) which reside within the cell membrane or in the cytoplasm. PRRs can be divided in two groups: the transmembrane sensors

namely Toll-like receptors (TLRs) and the cytosolic sensors. The latter group is divided in two further groups: The RIG-I-like receptors (RLR) retinoic acid-inducible gene I (RIG-I), melanoma differentiation-associated gene 5 (MDA-5) and laboratory of genetics and physiology (LGP-2) as well as the NOD-like receptors (NLR) (reviewed by Thompson & Locarnini, 2007).
Recently, further intracellular DNA sensors DAI, IFI16 and Ku70 were discovered (Takaoka et al, 2007; Unterholzner et al, 2010; Zhang & Brann TW, 2011).

1.7.1 Virus-induced signaling via RLRs

Specific PAMPs can be recognized by the host cell using currently discovered cytoplasmic sensor proteins of the RLR family. These ubiquitously expressed proteins have a helicase domain in common, but differ in their N- and C-termini. The prototypical member of the RLR family is the RIG-I protein which was originally identified as a gene induced in retinoic acid-treated cells (Sun, 1997). At the N-terminus, RIG-I contains two caspase recruitment domains (CARD), whereas the C-terminus exhibits repressor functions to keep RIG-I inactivated in the absence of the ligand inducer (Saito et al, 2007). The use of knock-out mouse models revealed that RIG-I is the major recognition receptor for RNA virus infection. It is specifically activated by 5’ triphosphated ssRNA which contains partial dsRNA motifs. Such a structure occurs e.g. during influenza A virus (IAV) infection, also exposing a genomic panhandle RNA. Also, it responds to short fragments (~300 bp) of the dsRNA analogon poly I:C Furthermore, T7 in vitro transcripts and poly (rU) tract of HCV RNA are responsible for activating RIG-I (reviewed by Onoguchi et al, 2011).
After recognition of an adequate substrate, RIG-I undergoes a conformational change leading to its activation and the exposure of CARD to interact with the mitochondrially anchored adaptor protein IFN-β promoter stimulator (IPS-1). This protein also contains a CARD domain leading to CARD-CARD association with RIG-I. The tripartite motif 25 (Trim25) E3 ubiquitin ligase was demonstrated to be essential for the ubiquitination of the RIG-CARDs (Gack et al, 2007). The translocase of outer membrane 70 (Tom70) interacts with IPS-1 and causes the recruitment of downstream effectors of IFN-β induction, TBK1 and the IFN regulatory factor (IRF) 3, to the mitochondria (Liu et al, 2010). At the surface of the mitochondria, around IPS-1, a number of further effectors accumulate like the ubiquitin ligase tumor necrosis factor (TNF)-receptor associated factor 3 (TRAF3) which activates Tank-binding kinase 1 (TBK1) and IκB kinase (IKK)-related kinase IKKε. These two kinases phosphorylate the

transcription factors IRF-3 and IRF-7 at distinct serine residues causing their homo- or heterodimerization. Subsequently, IRF-3/7 translocate to the nucleus (reviewed by Kumar et al, 2011; Onoguchi et al, 2011; Takeuchi & Akira, 2009; compare with fig. 2).
Furthermore, IPS-1 initiates a second signaling targeting in NF-κB activation via the IKK complex (consisting of the kinases IKKα and IKKβ; compare with fig. 2).
Newcastle Disease Virus (NDV) is a potent inducer of type I IFN expression. As other viruses, it also exerts an IFN antagonistic effect by its V protein. However, MDA-5, but not RIG-I-mediated signaling is affected by this mechanism (Childs et al, 2007). For this reason, NDV is used as a model virus in this work.

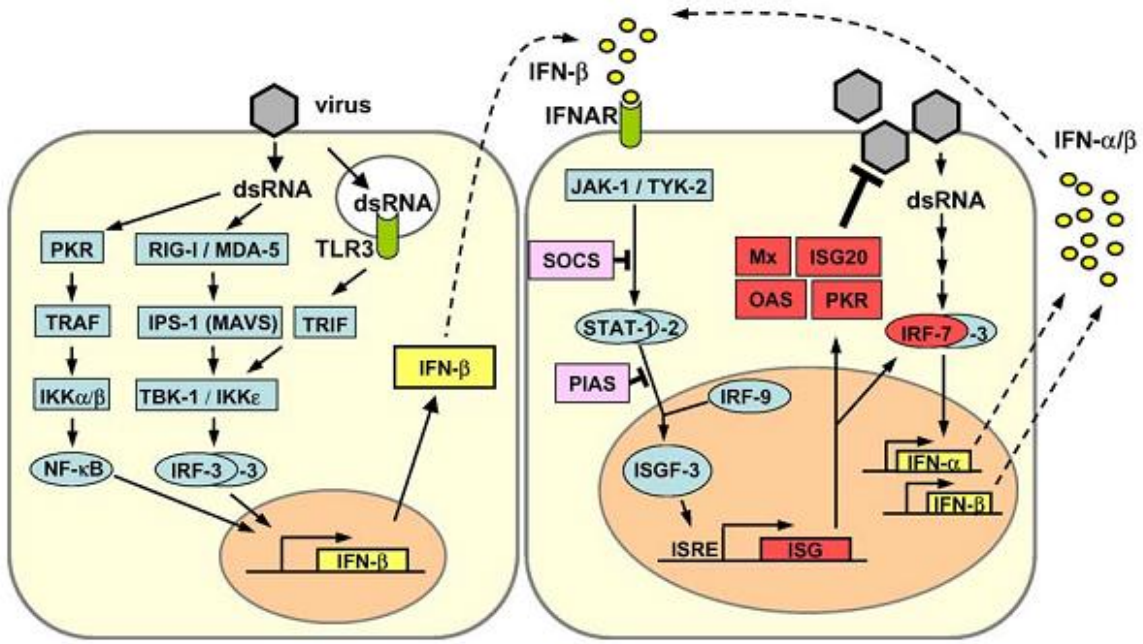

Figure 2: Early IFN induction and IFN-mediated signaling.

Cytoplasmic viral dsRNA causes the activation of NF-κB and IRF-3. These proteins, together with other transcription factors, bind to the promoter region of early type I IFNs (see here IFN-β) and initiate their expression. The resulting IFN proteins are secreted from the cell and bind to their cognate receptor IFNAR in an auto- or paracrine manner. IFN stimulated genes (ISGs) are expressed as a result of JAK/STAT signaling. One of these ISGs, IRF-7, amplifies the IFN response by inducing several type I IFNs. SOCS and PIAS negatively regulate JAK/STAT signaling. Mx, ISG20, OAS and PKR are ISGs having antiviral activity (figure according to Haller et al, 2006).

1.7.2. Virus-induced signaling via TLRs

Another family of PRRs is the transmembrane sensors (TLRs). Those glycoproteins are encoded by 10 genes in humans and 12 genes in mice. They consist of extracellular leucin rich repeats which are necessary for ligand

binding and a cytoplasmic Toll/interleukin-1 receptor (TIR) which is indispensable for downstream signaling.
From the family of TLRs, the receptors 3, 7/8 and 9 are located in intracellular, endosomal compartments and capable to induce type I IFNs (reviewed by Chaturvedi & Pierce, 2009). TLR3 is specialized for sensing dsRNA (Alexopoulou et al, 2001). Signaling occurs through the adaptor protein TRIF which activates the noncanonical IKK kinases TBK-1 and IKK-ε. Those cause the phosphorylation of IRF-3 and thereby its translocation to the nucleus. The IKK-α, β and γ kinases are also stimulated by TRIF leading to the phosphorylation of NF-κB and its translocation to the nucleus. TLR-7 and 8 recognize ssRNA (Heil et al, 2004), whereas TLR-9 senses unmethylated cytosine phosphatidyl guanine (CpG) motifs (Hemmi et al, 2000).
TLRs use the myeloid differentiation primary-response gene 88 (MyD88) as a signaling adaptor causing the activation of IRF-7 (reviewed by Honda & Taniguchi, 2006; Takeuchi & Akira, 2009; Thompson & Locarnini, 2007).

1.7.3 The interferon regulatory factors 3 and 7

The family of interferon regulatory factors consists of nine members contributing to immune response, cytokine signaling, cell cycle and growth as well as apoptosis, tumor suppression and hematopoietic development. They share high homology especially in the N-terminal DNA binding domain. This domain mediates binding to the interferon-stimulated response element (ISRE) within the promoter region of IFN-stimulated genes (ISGs).
Of all the IRFs, IRF-3 and IRF-7 share the greatest homology and are directly associated with RIG-I-mediated signaling. Both factors are activated through phosphorylation of their C-terminal serine/threonine residues by TBK-1 or/and IKK-ε (Fitzgerald et al, 2003; Sharma et al, 2003). Also, they share similarities concerning dimerization and translocation (Hiscott, 2007; Lin et al, 1999; Marié et al, 2000). Indeed, they also exhibit distinct behavior caused by the C-terminus which is less conserved transmitting uniqueness to every IRF (reviewed by Servant et al, 2002).
Since IRF-3 is constitutively expressed in all cell types, it is able to directly respond to virus infection and leads to the induction of early type I IFN genes (IFN-α4 and IFN-β). Meanwhile, IRF-7 is mainly induced by these secreted type I IFNs in most cell types (Sato et al, 1998). In lymphoid cells and some DC subsets, IRF-7 is constitutively expressed which causes high antiviral potential of these cell types.

Indeed, cytoplasmic IRF-7 molecules can also be activated by IKK-ε and TBK1 kinases and induce the expression of type I IFNs differentially (Marié et al, 1998). Despite the time delay in IRF-3 and IRF-7 presence, they also show specificities concerning type I IFN activation (Yeow et al, 2000).
The existence of three promoter proximal IRF elements (B, C and D) within respective promoter regions of IFN-α genes was displayed (Civas et al, 2006). They show distinct preferences for IRF-3 and IRF-7 binding which leads to the differential activation of IFN-α genes by the two IRFs (reviewed by Hiscott, 2007).

1.7.4 The induction of early type I interferons

Signaling of the RLR pathway ends up in the induction of early type I IFNs mediated by the specific binding of transcription factors to IFN-α4 and IFN-β promoter regions. Individual activity of these factors is not sufficient to induce efficient expression from these promoters. In order to verify proper expression of the desired gene, all factors that are necessary for efficient initiation, reinitiation and pursuing of expression are assembled in one enhanceosome. Engaged into this stable protein complex are ATF-2/c-Jun and the high mobility group protein (HMGI(Y)), NF-κB, IRF-3 and, if present, IRF-7. The enhanceosome promotes the recruitment of these activators and further co-activators (CREB-binding proteins (CBP/p300)) as well as the RNAPII complex to the active site of transcription (Kim et al, 1998; Wathelet et al, 1998). Efficient (re-) initiation of transcription is promoted by these co-activators (Yie et al, 1999). Acetylation of HMG I(Y) by the co-activators leads to the termination of transcription (reviewed by Ford & Thanos, 2010; Vo & Goodman, 2001).

1.7.5 The induction of interferon stimulated genes

After efficient transcription and translation of the early IFNs α4 and β, the proteins are secreted from the cell. In an auto- or paracrine manner, they bind to their cognate receptor IFN-α receptor (IFNAR) which consists of the subunits IFNAR1 and 2 (Cutrone & Langer, 2001). IFNAR associated Janus kinases (JAK) JAK1 and TYK2 activate the signal transducer and activator of transcription (STAT) 1 and 2 by phosphorylation. Their activated forms build heterodimers which associate with IRF-9 building the IFN-stimulated gene factor 3 (ISGF-3) complex (Horvath et al, 1996; Levy et al, 1989; Martinez-Moczygemba et al, 1997). In the nucleus, ISGF-3 recognizes the interferon stimulated response element (ISRE) within the promoter regions of ISGs by the

DNA-binding domain of IRF-9. STAT2 leads to the activation of gene transcription via its C-terminal transcriptional activation domain. ISGs comprise a group of more than 300 antiviral effectors such as the myxovirus-resistance protein (Mx) GTPase, RNA-dependent protein kinase (PKR), ribonuclease L (RNase L), oligo-adenylate synthetase (OAS) and IRF-7.
Rapid onset and termination of JAK/STAT signaling is considered to be characteristic for JAK/STAT signaling (Schindler & Plumlee, 2008). In agreement with this, STATs are known to interact with several regulators. In the last years, the suppressors of cytokine signaling (SOCS) have been discovered and well characterized. Inhibition of IFN signaling was assigned to SOCS1 and SOCS3, both of them containing a kinase inhibitory region (KIR) which interacts with Janus kinase (Sasaki et al, 1999). SOCS-1 was also shown to directly interact with the IFNAR1 subunit (Fenner et al, 2006).
Expression of the ISG IRF-7 is strongly induced upon JAK/STAT signaling. Synthesized IRF-7 proteins can be activated upon stimulation via virus-activated IKK kinases. After homo- or hetero-dimerization with IRF-3, they translocate to the nucleus and contribute to the induction of the second wave of IFNs, the late type I IFNs.
Another important ISG is the Mx guanosine 5´triphosphatase (GTPase) which exerts essential influences in host immune response against various viruses, especially influenza A virus (Koerner et al, 2007). *Mx* genes (two in mice and humans) are present in most vertebrates and share high molecular weight. The importance of these genes became obvious when mice harboring a mutated *Mx1* gene were more susceptible to orthomyxovirus infection than those with the native *Mx1* gene. Mx consists of three domains that are highly conserved in all species; an N-terminal GTPase domain, a linker domain and a GTPase effector domain at the C-terminus. Viral ligands are recognized by a central interacting domain and a C-terminal leucine zipper. By recognizing and detracting viral nucleocapsid proteins, Mx interferes with virus entry into the nucleus and the assembly of virus particles after replication (reviewed in Boo & Yang, 2010; Sadler & Williams, 2008).

1.7.6 Dynamics of interferon induction

Early and fast induction of type I IFNs after viral infection is essential for the clearance of a pathogen. As one of the first antiviral mechanisms, it needs to be tightly regulated at various levels. Indeed, many components are found to contribute to IFN induction and new factors are regularly identified. However, the discrete time points of the respective steps within the cascade as well as their

relation to each other are not well understood. Also, key functions and intracellular localization at various time points post infection are not fully discovered, yet. Consequently, only marginal information exists about the spatiotemporal dynamics of IFN induction.
Despite the general lack of data, few publications could give at least indications suiting to this topic. Zawatzky et al (1985) postulated that only a couple of infected cells transcribe IFN-β mRNA. The topic recently gained interest due to modern experimental procedures and mathematical modeling. The alleles of the gene are unequally transcribed, what is proposed to occur from the complexity of the IFN-β enhanceosome (Hu et al, 2007). Indeed, the stochasticity of monoallelic expression was demonstrated to occur from interchromosomal association. Using a YFP knock-in mouse, Scheu et al. (2008) also demonstrated that only a fraction of cells responds to stimulation independent of the origin. They further displayed differential onset of IFN-β in varying cell types. In A549 cells harboring a lentiviral construct on which eGFP is driven by the IFN-β promoter, the induction of a fraction of cells post infection with a variety of negative sense RNA viruses at a high multiplicity of infection (MOI) was demonstrated (Chen et al, 2010). However, MuV infection turned out to give high rates of IFN-β positive cells upon infection which increase overtime. IFN-β positive cells were displayed by a distinct population indicating an on- or off-mechanism of IFN-β induction.
Contradictory results concerning this point were obtained from U. Rand (2010), who demonstrated a great variety in IFN-β intensity following NDV infection or poly I:C transfection. He also demonstrated that successfully infected cells do not necessarily induce IFN-β production.

1.8 Perturbation of the interferon system by pathogens

The IFN system plays a major role in early recognition and counteraction of virus infection (McInerney & Karlsson Hedestam, 2009; Randall & Goodbourn, 2008). It is an unspecific mechanism to quickly induce an antiviral state of the infected cell and neighboring cells. However, viruses co-evolved with the immune system and are able to evade the host immune response by diverse mechanisms encoded by the viral genome. Some of these mechanisms were shown to act on multiple levels and signaling pathways. Up to now, more than 170 viral IFN antagonists were identified from 93 different virus strains. Every virus has evolved distinct strategies to interfere with the host immune response to allow the verification of replication and persistence within host cells, but some overall strategies arise regularly.

- Minimizing PAMP production (e.g. poxviruses, picornaviruses)
- Sequestration/inactivation of host proteins/viral PAMPs (e.g. IAV NS1, Poxvirus E3L)
- Interference with cellular gene expression (e.g. Bunyamwera NSs protein, foot-and-mouth-disease virus L proteinase)
- Direct (proteolytic) cleavage of host proteins (e.g. HCV NS3/4A; Poliovirus 3C protein)
- Recruitment of the host cell ubiquitin proteasome system to induce degradation of host targets (e.g. Rotavirus NS1, N proteases of classical swine fever)

(reviewed by Haller et al, 2006; Haller & Weber, 2009; McInerney & Karlsson Hedestam, 2009; Randall & Goodbourn, 2008; Versteeg & García-Sastre, 2010)

In the following chapters, the main antagonistic functions of two major viruses are described in detail with respect to their main IFN antagonist.

1.9 Influenza A virus and its general perturbation mechanisms against the IFN response

The influenza A virus, a member of the *Orthomyxoviridae*, is responsible for seasonal outbreaks of influenza, a disease which infects epithelial cells of the upper and lower respiratory tract. In the last century, three severe influenza pandemics occurred of which the Spanish flu from 1918 resulted in up to 40 million deaths. Every year, 500 million of infections are estimated to occur, with 250-500 thousand of deaths, mostly caused by seasonal influenza.
The viral genes contain 3’ and 5’ non-translated regions (NTR) that are necessary for replication and the formation of the capsid. Importantly, in contrast to cellular transcripts, 5’ ends of viral RNAs carry uncapped triphosphate groups that are recognized as foreign by the cellular IFN system, namely the RIG-I protein. Nevertheless, IAV is able to successfully infect host cells. This is caused by its IFN antagonistic functions supported by regularly occurring genetic drift. Recently, the protein PB1-F2, derived from an alternative open reading frame of IAV, was demonstrated to cause alteration in the cytokine response, but a concrete link to innate immunity has not yet been demonstrated. Indeed, the non-structural protein 1 (NS1) which was initially described to have regulatory functions on the viral life cycle, was shown to have multiple effects on the immune response caused by IAV infection. In the next chapter, NS1 will be introduced with a focus on its ability to interfere with type I IFN induction (further reviewed by Arias et al, 2009; Ehrhardt et al, 2010).

1.9.1 The influenza A virus non-structural protein 1 – evasion from the host immune system

The non-structural protein 1 (NS1) shows strong IFN antagonistic functions and mutations within NS1 are related to the multifaceted pathogenicity of different IAV subtypes. Within cells, NS1 is highly expressed post infection. The protein comprises a length of 230 to 237 aa with strain-specific C-terminal truncations (Suarez & Perdue, 1998). It is composed of two major domains, the N-terminal RNA binding domain and the variable, C-terminal effector domain (fig. 3). Dimerization of the protein occurs via its RNA-binding domain in the absence and presence of a respective substrate (Nemeroff et al, 1995). Further, NS1 possesses two nuclear localization signals (NLS; Greenspan et al, 1988). These signals mediate the nuclear import of NS1 via importin-α (Melén et al, 2007). The second NLS, which is located at the C-terminus of the protein, also functions as a nucleolar localization signal (NoLS) probably having an influence on pathogenicity of the respective IAV strain.

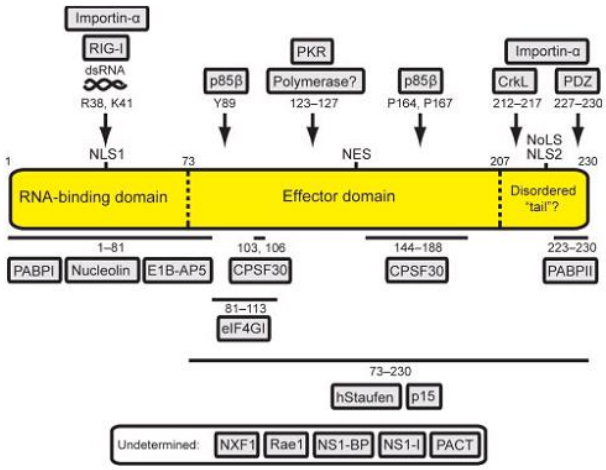

Figure 3: Constitution of the IAV NS1 protein.

The NS1 protein of IAV is composed of an N-terminal RNA-binding domain and an effector domain. The C-terminal tail has varying length between IAV subtypes. Detected nuclear localization signals (NLS), nucleolar localization signals (NoLS) and nuclear export signals (NES) as well as protein binding sites are indicated (figure according to Hale et al, 2008).

Its strong IFN antagonistic effect became obvious when an IAV mutant lacking NS1 was determined for its virulence (García-Sastre et al, 1998). This mutant, designated delNS1, was attenuated in replication within Madin-Darby canine kidney (MDCK) cells. However, in IFN-deficient cells, delNS1 replication could be rescued. While NS1 was firstly proposed to have regulatory functions

in the viral life cycle, it was shown to additionally effectively act as an IFN antagonist on multiple cellular levels.
The first discovered mechanism for evading the innate immune response was the sequestration of dsRNA by NS1. Previous dimerization of NS1 is essential for binding dsRNA (Wang et al, 1999). By this mechanism, dsRNA is withdrawn from recognition by PRRs (Lu et al, 1995). Also, the activation of PKR, which is able to exert antiviral effects, is prevented. The dsRNA-dependent 2'-5' oligo (A) synthetase (OAS) cannot activate RNaseL, which could exert antiviral activity (Min & Krug, 2006). However, the strength of the effect related to this mechanism is controversially discussed, since only minor levels of dsRNA are produced during the replication of negative-strand RNA viruses (Weber et al, 2006). In influenza B virus, mutational deletion of the NS1 dsRNA binding domain revealed that IFN induction is only marginally influenced by this domain (Dauber et al, 2006).
Besides RNA-dependent effects of NS1 on IFN induction, it was shown to interact with cellular proteins depriving them from their further action. NS1 was demonstrated to build a stable complex with RIG-I (Pichlmair et al, 2006). NS1 was further identified to bind TRIM25, thereby inhibiting multimerization of TRIM25 and consequently RIG-I ubiquitination (Gack et al, 2009). In addition, an effect of avian influenza NS1 on JAK/STAT signaling could be demonstrated (Jia et al, 2010). Further, NS1 of some IAV strains exhibits regulatory functions on the posttranscriptional level leading to an alteration of host cell protein production (Chen et al, 1999; Nemeroff et al, 1998; Satterly et al, 2007). Since viral mRNAs are not modified by the 3’ end processing factors, their polyadenylation is not affected. These and other functions of NS1 and other IAV proteins on the host cell metabolism are reviewed in Hale et al (2008).

1.10 The hepatitis C virus

The hepatitis C virus (HCV) is a member of the *Flaviviridae* (genus *Hepaciviridae*) and causes chronic liver disease. HCV has a positive-sense, ssRNA genome with a length of 9.6 kb encoding a single open reading frame (fig. 4). HCV replication, as for all +ssRNA viruses, occurs at intracellular membranes (Ahlquist et al, 2005).
The polyprotein is co- and post-translationally processed by both, cellular and viral proteases. The host cell proteases cleave the polyprotein at the N-terminal region, whereas viral proteases NS2 and NS3 cleave in the middle and C-terminal region (reviewed by Tang & Grisé, 2009).

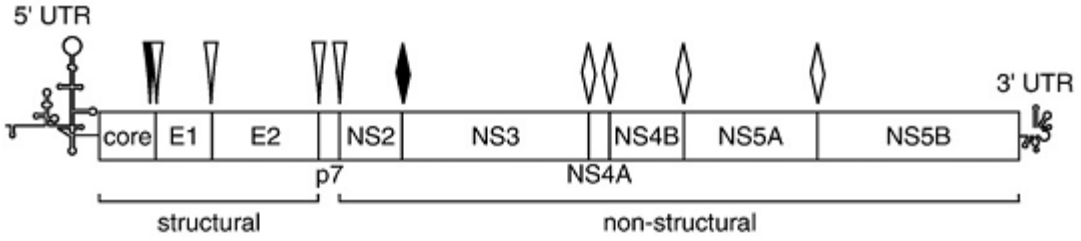

Figure 4: Composition of the HCV genome.

The HCV genome is transcribed as a single polyprotein that is co- and post-translationally processed by viral and cellular proteases. Within the polyprotein reside three structural proteins, one ion channel protein (N-terminus) and six non-structural proteins (C-terminus**).** The cleavage sites are denoted as follows. Filled arrowhead: signal peptide peptidase site; open arrowhead: signal peptidase sites; filled diamond: cleavage site for the NS2/3 protease; open diamond: cleavage sites for the NS3/4A protease (figure according to McLauchlan, 2009).

1.10.1 Counteraction of the host immune response by HCV – the non-structural protein 3/4A complex

The NS3 protein obtains two specific domains. A serine protease at the N-terminus is responsible for cleaving the C-terminal proteins of the polyprotein (Grakoui et al, 1993). The co-factor NS4A is also required for the proteolytic activity of NS3 (Failla et al, 1994). The NS3 C-terminus contains a helicase/NTPase function for unwinding RNA-RNA substrates and was demonstrated to be involved in HCV particle assembly (Ma et al, 2008). The two NS3 domains are connected by a linker peptide. Both functions are necessary for HCV replication (Lam & Frick, 2006; reviewed by Tang & Grisé, 2009).

The protease activity of NS3 and its co-factor NS4A (consecutively named NS3/4A) are also exploited by the virus to interrupt IFN induction. This strong interference causes persistence of the virus within the host. Abrogation of IFN induction occurs via specific cleavage of cellular factors. The RIG-I pathway is disturbed by the cleavage of the mitochondrial adaptor protein IPS-1, thereby disrupting downstream signaling which is targeted in early IFN induction (Foy et al, 2005; Loo et al, 2006). It was further demonstrated that NS3/4A leads to proteolysis of the TLR-3 adaptor protein TIR-domain-containing adapter-inducing IFN-β TRIF in HeLa cells (Li et al, 2005). However, data concerning this item are controversial as it could also be demonstrated that NS3/4A was not able to cleave TRIF in human hepatocytes, regardless of the tested HCV strain (Dansako et al, 2009; Dansako et al, 2007).

Controversial results were shown for the effect of NS3/4A on JAK/STAT signaling. While Cheng and co-workers (2006) could not display any effect of NS3/4A on IFN-induced signaling, Helbig et al. (2008) realized an inhibitory effect on STAT1 phosphorylation.
All these heterogenous effects could be explained by cell type- and species-specificity, since isolate-dependent variations within the NS3/4A sequence exist.

1.11 Reporter genes for the detection of cellular components

The activity of a promoter or the intracellular localization of a certain component can only be detected indirectly. Most accurately, this information is obtained from living cells that can display natural changes and dynamics. This needs non-invasive techniques, e.g. by expressing a reporter gene driven by the promoter of interest or by fusing fluorescent reporters to the GOI. For these purposes, reporters are used that are not naturally present in the cell it is transferred to, meaning that it is "ectopically" expressed. This gene should not interfere with the cellular machinery.
A very common reporter for bulk assays is luciferase being the first non-isotopic reporter assay (De Wet et al, 1987). The *luciferase* gene of *Photinus pyralis* is integrated as a reporter and bioluminescence is measured quickly after administration of the substrate luciferine as well as ATP to the cell lysate. Measurement occurs via a luminometer. With a half-life of approximately 3 h in mammals, this reporter is very suitable for the measurement of protein dynamics (Thompson et al, 1991) in bulk assays. This assay is fast and cheap, but since luminescent reporters need a constant presence of their substrate, the use for microscopic experiments, especially time-lapse experiments, is limited.
Other non-isotopic assays were developed for chloramphenicol acetyltransferase (CAT) or β-galactosidase (β-gal, reviewed by Kain & Ganguly, 2001).
Fluorescent reporter genes are preferred for microscopic analyses, especially of living cells. The first fluorescent gene discovered was the green fluorescent protein (GFP) from *Aquorea victoria* (Shimomura et al, 1962). Further fluorescent proteins were discovered in different organisms and adapted to the respective purpose by modulating e.g. expression intensity, half-life or maturation time (reviewed by Lukyanov et al, 2010).
In addition to the described fluorescence genes, tagging proteins or sequences were developed which can, as the fluorescent reporters, be fused to the GOI. Measurement can be performed after administration of a fluorescence ligand or dye that specifically associates with the tag. A recent, versatile tool is the HaloTag Interchangeable Technology (Promega). The HaloTag V7 (HTV7) can

be used as a reporter or reporter fusion and can sequence-specifically and irreversibly be stained. For this tag, different fluorescent ligands are available (green, blue, and red).
However, a pitfall of all reporter genes in fusion with the GOI is the change in length and secondary structure. Interference with functionality of the protein of interest cannot be excluded and must be checked carefully.
With the tool of a reporter gene, light can be shed on many cellular processes as well as activity and localization of components after integration into a host cell. Indeed, diverse opinions come up concerning the reliability of data in transient or stable expression experiments. By transient expression experiments many data can be gained within a short time period. However, the reliability and reproducibility of these experiments is questionable. For these reasons, stable integration of the GOI into the host cell genome is often preferred. Even though it is more time-consuming to obtain the desired cells, a selected, stable cell clone allows reproducibility and long-term storage.

1.12 Reporter systems for interferon induction and signaling

The integration of a promoter of interest into a new environment can alter certain characteristics like its activity or expression pattern due to the impact of neighboring regulatory elements like enhancers or silencers. Consequently, reporter expression may differ from the native GOI and between single clones harboring the same construct(s). To overcome this so-called “position effect”, bacterial artificial chromosomes (BACs) can be used. These BACs are large DNA constructs based on the F plasmid of *E. coli* and can have a size of 300 kb or more. The sequences can easily be manipulated by homologous recombination. Since genome analysis is nowadays performed in BACs, a large variety of them exists and is commonly used.
Research of promoter activities can be performed precisely by these tools, since the promoter of interest can be provided within its natural surroundings. In the following, murine NIH3T3 fibroblasts were used that stably express the respective BAC. NIH3T3 cells exert beneficial properties as low differentiation rate and the presence of numerous signal transduction pathways which can be investigated. Another important aspect is the ability of stable integration and expression of transgenes within these cells.
For this work, it was necessary to perturb native IFN expression to obtain reliable data on the dynamics of the IFN system and to determine perturbator functions. U. Rand (2010) provided NIH3T3 cells stably harboring a BAC of originally ~ 280 kb of the natural murine locus of IFN-β. The *IFN-β* locus was

replaced by the fast maturing TurboGFP (Evrogen), which is a fluorescent protein based on CopGFP from the copepod *Pontellina plumata*. After induction of the IFN cascade, these cells, consecutively called IFN-β TurboGFP, display asynchronous onset of IFN-β and exert stochastic behavior concerning i) the decision whether IFN-β will be expressed, ii) the starting time of expression and iii) the strength and duration of expression.
Two different kinds of reporter cells were used for the determination of the IFN response. These cells harbor a BAC derived from the murine genome that contains the ISG *Mx2* locus. In this locus, the gene encoding *Mx2* was replaced by either the reporter gene luciferase (Mx2Luc) or by the tandem dimer tomato (tdTomato, Mx2Tom). The cells exhibit high inducibility of the *Mx2* promoter driven reporter upon induction by various stimuli (Pulverer, 2008; Pulverer et al, 2010).

1.13 Single cell analyses of fluorescently labeled cells

For many years, bulk assays were performed to study promoter activities or protein function. However, today many methods for single-cell analyses are established. They give much more insight into the respective function since results are no longer mean values of a population of cells. Some of these analyses are reviewed by Lindström and Andersson-Svahn (2010).
Using fluorescence reporter genes, an effective method to gain data of numerous single microscopic particles like cells is flow cytometry. Here, fluorescence, size and granularity of a high number of individual cells can be analyzed at a certain time point. Indeed, these cells cannot be followed over time. This can be performed using time-lapse microscopy. Here, repeated imaging of a previous selected area of cells can be done for various fluorescence colors. At the end of the measurement, single cells can be analyzed for the function of the fluorescently labeled factor.

2 Aims of this work

So far, synthetic biology approaches have been mainly followed in bacterial systems or lower eukaryotes. While a number of different synthetic modules have been established also for mammalian cells, they were not yet employed to elucidate a cellular network in a time-resolved manner.

The aim of this work was to employ synthetic expression modules for the controlled perturbation of a complex mammalian network. As a model network, the antiviral IFN cascade, i.e. RIG-I-mediated IFN-β induction, should be addressed. For this particular pathway, only marginal data concerning its spatiotemporal dynamics exist. Perturbation of this network should occur via exploitation of antagonistic viral mechanisms to evade this immune pathway. In particular, it was of interest to dissect the dynamics of individual perturbator/host interplay and inhibition kinetics. For monitoring the perturbation, the viral genes should be expressed in reporter cells that allow the visualization of IFN-β, thereby enabling monitoring on the single cell level. Onset and termination of perturbator expression should be mediated by transcriptional regulation which is externally adjustable by the administration or withdrawal of doxycycline (Tet system). Tight regulation of the expression level should be achieved by the dose- or time-dependent administration of the inducer. Furthermore, expression levels, and consequently perturbation levels, should be predictable and reproducible even on the single cell level. The data should further give information about the efficiency and properties of the perturbators.

In addition, the results of this work should contribute to the establishment of a mathematical model of IFN-β induction. This model can be used to further characterize the network in a way that cannot or hardly be performed by laboratory work.

Finally, this work also aimed at designing a synthetic network for stable oscillation in mammalian cells by means of synthetic regulatory modules. By directed interaction of these systems, oscillatory onset and termination of protein production should be monitored on the single cell level.

3 Results

The aim of this work was to develop cells that allow the controlled perturbation of a cellular network by means of synthetic cassettes. The IFN network served as a model network.
The strategy was to use synthetic cassettes that harbor a viral perturbator under the control of a tetracycline-dependent promoter. Viral genes (IAV NS1 and HCV NS3/4A) that are known to specifically interfere with the IFN network should represent different modes of action. It was intended to integrate these constructs into reporter cells that allow the visualization of IFN-β in the case of IFN induction or Mx2 as the outcome of JAK/STAT signaling.
By means of controlled perturbator expression, the response of the respective pathway should be altered and give rise to the spatiotemporal dynamics of the network.

3.1 Design of the perturbator constructs

The first challenge was to design vector constructs which harbor the respective components necessary for controlled expression of the perturbator. The Tet system was exploited to obtain graded expression of the perturbator. High induction levels and low basal expression of NS1 and NS3/4A are necessary for a tightly regulable system. For this purpose, reporter cells need to be stably transfected with two constructs. The one harbors the constitutively expressed rtTA2 and the other one P_{Tet} driving the expression of the respective perturbator (fig. 5). In order to enable detection of NS1 and NS3/4A, they were c-terminally fused to HTV7 (see chapter 1.11 of introduction). These fusions are further on called NS1-H and NS3/4A-H. A specific ligand can persistently bind to HTV7, various fluorescent dyes coupled to the ligand are available (e.g. Oregon Green (green fluorescence) or Coumarin ligand (blue fluorescence)). Since IFN-β TurboGFP reporter cells (see chapter 1.12 of introduction) exhibit green fluorescence, a ligand emitting red fluorescent light (tetramethyl rhodamine = TMR) was used to discriminate NS1-H or NS3/4A-H expression in the following experiments.
The functionality in expressing the fusion protein of the perturbator and HTV7 was determined by flow cytometry analysis after transient transfection into NIH3T3 cells (data not shown). Sustained inducibility of the fusions was obtained for stable clones.

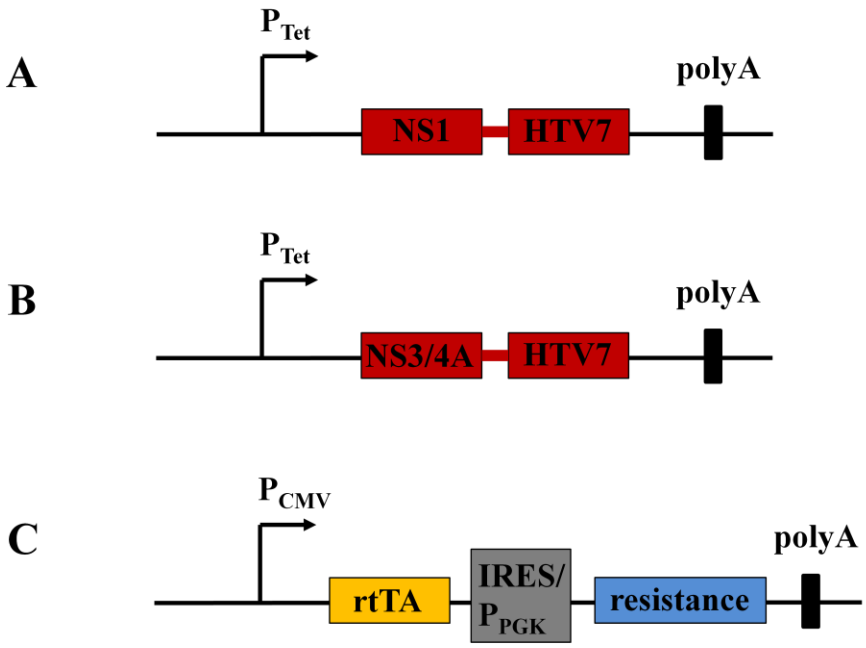

Figure 5: Vectors permitting regulated expression of viral IFN-counteractors.

A: P_{Tet} drives the expression of the NS1-H fusion. B: P_{Tet} drives the expression of the NS3/4A-H fusion. C: The constitutively active Cytomegalo Virus (CMV) promoter drives the expression of rtTA2. The resistance gene is driven by an internal ribosomal entry site (IRES) or the constitutively active phosphoglycerate kinase (PGK) promoter. In all cases, an SV40 polyadenylation signal (polyA) promotes efficient polyadenylation. For later experiments in this work, an improved tetracycline-dependent promoter (P_{Tight}, Clontech) was used to lower basal expression. Either constructs 1A and 1C or 1B and 1C were stably introduced into the reporter cells by co-transfection. If transfection occurred in two steps, constructs which each harbor selection markers were used.

3.2 Reporter cells for monitoring IFN-β and simultaneous IAV NS1-H or HCV NS3/4A-H expression

The induction of NS1-H or NS3/4A-H within the IFN-β TurboGFP reporter cells should lead to an alteration in the outcome, namely IFN-β expression, of this signaling. To measure the alteration of the signaling in single cells, IFN-β expression is visualized by TurboGFP which was integrated into the IFN-β coding region of a BAC that was stably transferred to NIH3T3 cells. Authentic expression of IFN-β was previously confirmed, and a stochastic expression pattern could be observed (Rand, 2010; compare also with figure 6 and chapter 1.12 of the introduction).

3.2.1 The IFN-β TurboGFP reporter cells are suitable for the integration of doxycycline-controlled genes

Since expression of NS1-H and NS3/4A-H should be visualized by exploiting red fluorescence in the following experiments, it was important to initially show that the expression of IFN-β TurboGFP does not lead to undesired fluorescence in the channel reserved for the perturbator. Also, an influence of the perturbator inducer doxycycline on IFN-β TurboGFP expression and intensity should be excluded.
The cells were exposed to NDV for signaling induction to see whether an effect on red fluorescence occurs. Furthermore, IFN-β TurboGFP reporter cells were treated with doxycycline and compared to non-treated cells to see a potential effect of doxycycline on IFN-β TurboGFP expression or mean intensity.

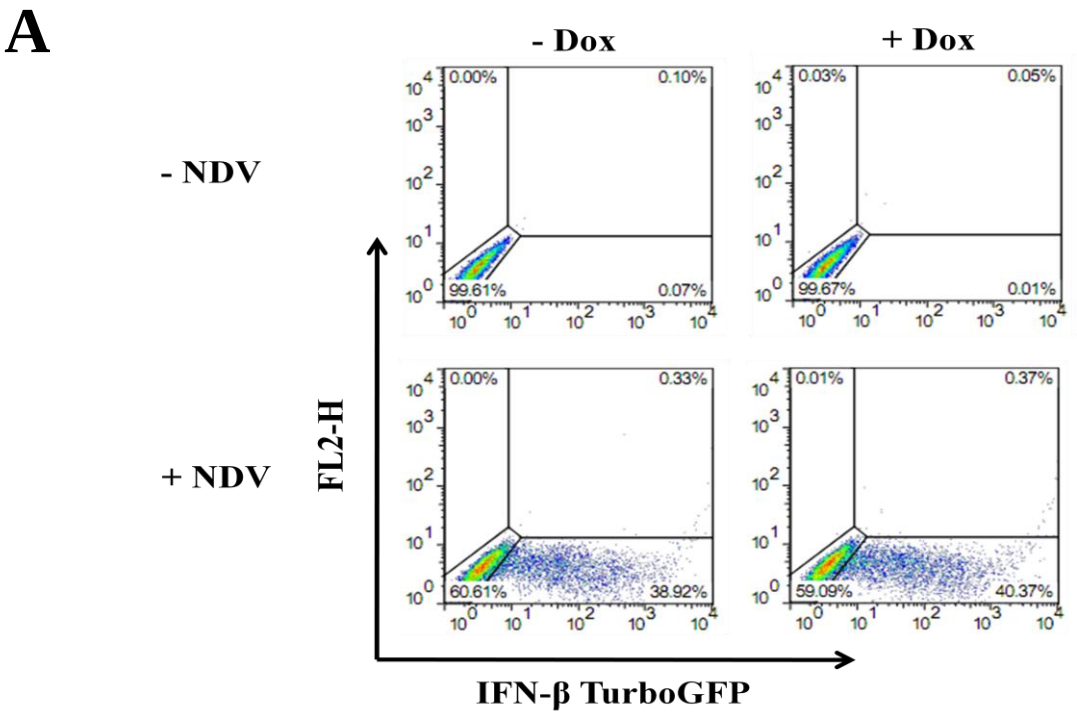

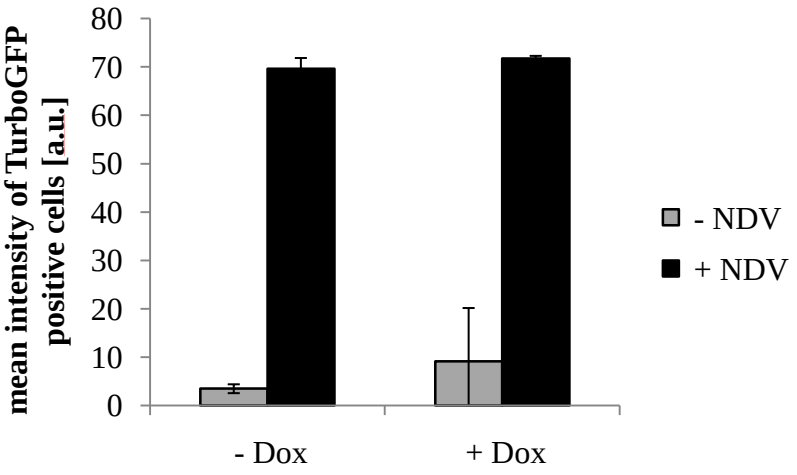

Figure 6: Influence of doxycycline on IFN-β TurboGFP expression.

IFN-β TurboGFP cells were either infected with 80 hemagglutinating units per milliliter (HAU/ml) NDV for 1 h or left uninfected. Cells were measured for the amount of TurboGFP positive cells after 24 h by flow cytometry. A: Density dot plots (red > blue) show fractions of IFN-β TurboGFP expressing cells (lower right gate) and cells with unaltered fluorescence (lower left gate). Strongly IFN-β TurboGFP expressing cells could not be compensated and therefore a low amount appears in the upper right gate. B: Mean intensity of IFN-β TurboGFP positive cells. The data shown represent average values +/- standard deviation of 3 experiments.

In the absence of doxycycline, no fluorescence could be detected in uninfected cells. For the infected cells, proper expression of 39 % of IFN-β TurboGFP positive cells could be visualized in the lower right gate after compensation (fig. 6A). For technical reasons, very high GFP expressing cells could not be fully compensated anymore and appear in the upper right quadrant (0.37%). This has to be taken into account also for later flow cytometry results. Importantly, no signal occurs in the channel displaying red fluorescence, which could thus be used for the visualization of the perturbators NS1-H and NS3/4A-H in the following experiments.
The expression intensity of IFN-β TurboGFP is low in the absence and presence of doxycycline and without NDV infection (fig. 6B). After infection, intensities increased up to 70 a.u..
These results indicate proper and comparable expression of IFN-β TurboGFP in the absence and in the presence of doxycycline and demonstrate that no red fluorescence occurs under these conditions.

3.2.2 Selection and characterization of IFN-β TurboGFP reporter cells harboring the perturbator constructs

The IFN-β TurboGFP cells were shown not to exhibit undesired alteration in response to doxycycline or in the red fluorescence channel. The following chapters show the establishment of cells concomitantly harboring the IFN-β TurboGFP BAC and the vectors for controlled expression of the perturbators.

3.2.2.1 Regulated expression of NS1-H in IFN-β TurboGFP cells

After introduction of the respective constructs into IFN-β TurboGFP cells, regulation of NS1-H in stable clones was determined. Populations of the selected clones were cultivated either in the presence or in the absence of doxycycline and measured for NS1-H basal expression and inducibility. The three best regulated out of 15 measured clones are given in figure 7.

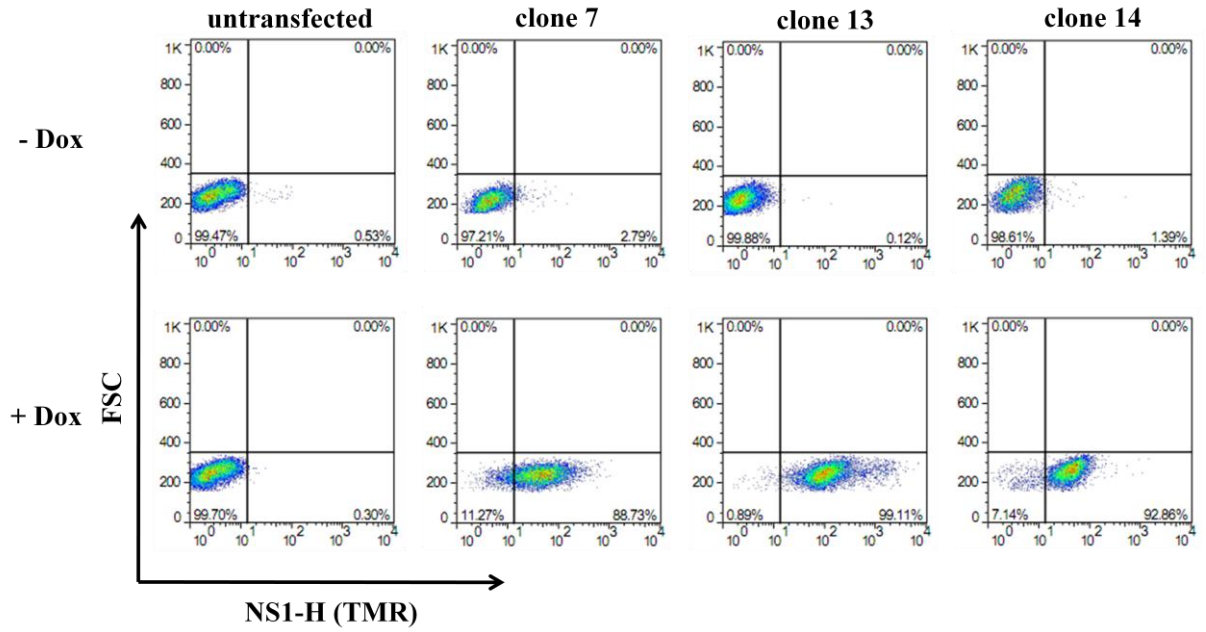

Figure 7: Regulated expression of NS1-H in IFN-β TurboGFP cells.

Cell clones generated upon stable transduction of doxycycline-controlled NS1-H cassettes into IFN-β TurboGFP cells were either treated with 2 µg/ml doxycycline for 3 days (d) or left untreated and stained with TMR ligand. NS1-H expression (TMR) was detected by flow cytometry. Results are shown as density dot plots (red > blue) which show NS1-H expressing cells (lower right quadrant) and cells with unaltered fluorescence (lower left quadrant).

The 3 clones show inducibility upon doxycycline treatment, but they differ in basal and maximal expression. These alterations in the expression pattern can be explained by random integration of NS1-H and the rtTA2 construct which may underlie position effects (chapter 1.12 of introduction).
Clone 13 shows lowest basal expression of the 3 displayed clones. Concerning the induced state, clone 7 exhibits a broad pattern of NS1-H positive cells, whereas clones 13 and 14 show more distinct populations. Maximal NS1-H expression is comparable for clones 7 and 14, but slightly higher in the case of clone 13. Since clone 13 exhibits lowest basal expression, highest maximal expression and therefore best regulation, it was used for further experiments. These cells are consecutively termed IFN-β NS1-H.

3.2.2.2 NS1-H is independently regulable from IFN-β TurboGFP

Since cross-reaction of IFN-β TurboGFP and the doxycycline-dependent NS1-H module could result in misleading results, the cells were characterized concerning this property. In 3.2.1, it was clearly demonstrated that doxycycline has no influence on IFN-β TurboGFP, but clarification is needed for the effect of TMR-stained NS1-H on green fluorescence, where IFN-β TurboGFP occurs if induced. As can be seen in figure 8, the uninduced IFN-β NS1-H population

(lower left quadrant) is comparable to the IFN-β TurboGFP population, indicating no or low leaky expression of NS1-H in the uninduced state. Full induction of NS1-H can be demonstrated upon doxycycline treatment. It does not exert any alteration in IFN-β expression.

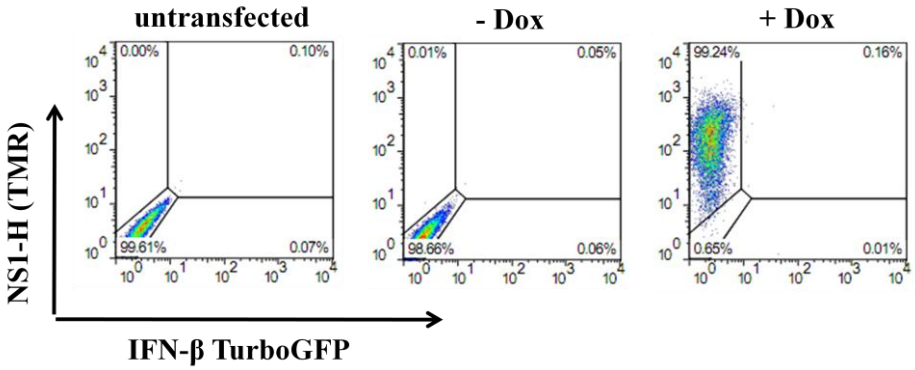

Figure 8: Influence of NS1-H induction on IFN-β TurboGFP expression.

IFN-β NS1-H cells were treated with 2 µg/ml doxycycline for 3 d or left untreated and were stained with TMR ligand. Cells were measured for the amount of NS1-H (TMR) positive cells by flow cytometry. Density dot plots (red > blue) show NS1-H expressing cells (upper left gate) and cells with unaltered fluorescence (lower left gate).

3.2.2.3 IFN-β NS1-H cells show phenotypic alteration to untransfected cells

The previous analyses showed no cross-reaction between the modules. As NS1 is an IFN-β antagonist, basal NS1-H levels in the absence of the inducer doxycycline could cause alteration in IFN-β TurboGFP expression compared to untransfected cells, indeed. To investigate whether undetectable basal activation of NS1-H in the uninduced state would affect the amount or the intensity of IFN-β TurboGFP, the values of untransfected cells were directly compared to the values of IFN-β NS1-H cells.

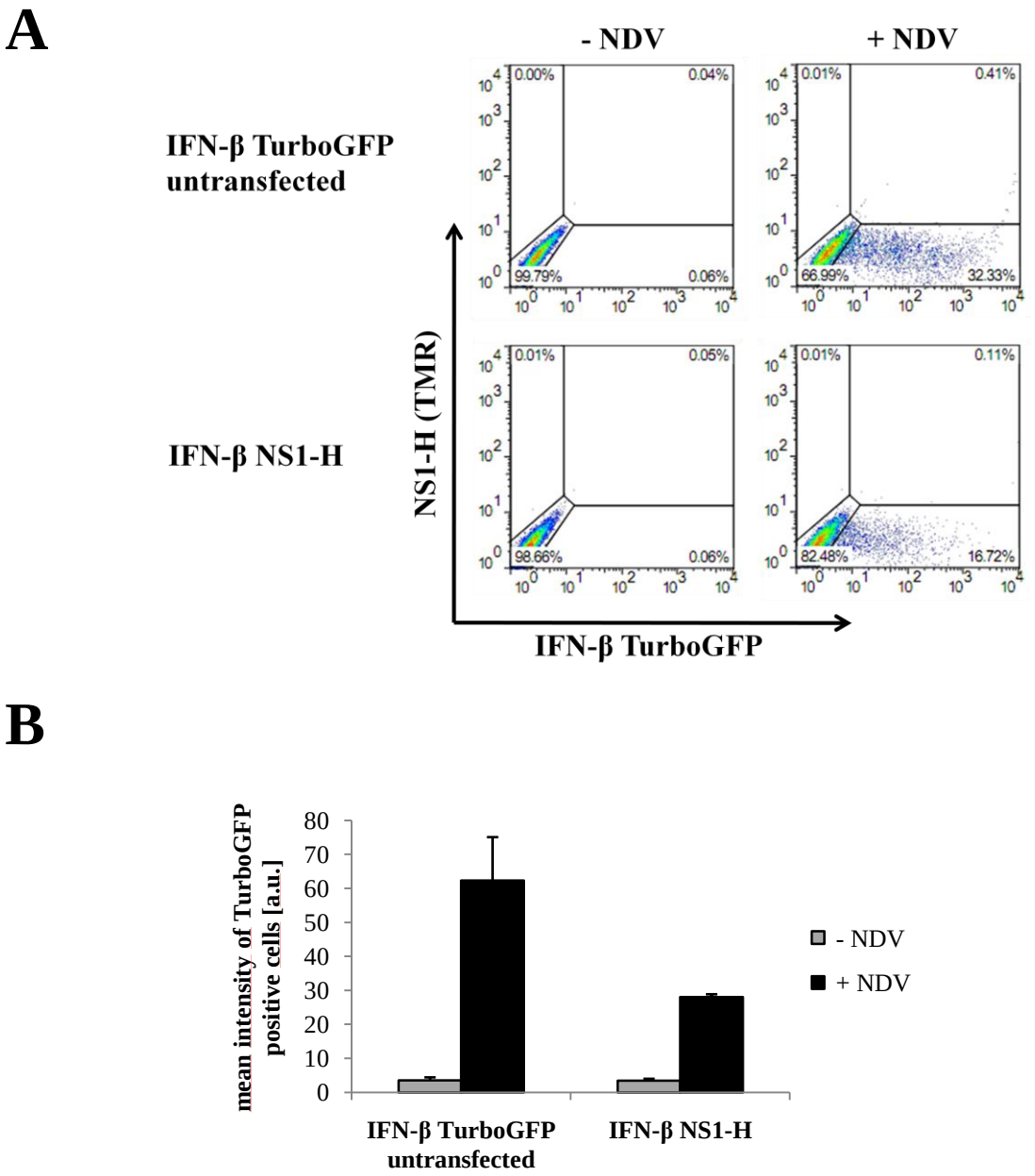

Figure 9: Virus-induced IFN-β TurboGFP expression in uninduced IFN-β NS1-H cells.

IFN-β TurboGFP cells, with or without stably integrated NS1-H, were seeded at equal densities and either infected with 80 HAU/ml NDV for 1 h or left uninfected. Cells were measured for the amount of TurboGFP positive cells after 24 h by flow cytometry. A: Density dot plots (red > blue) show fractions of IFN-β TurboGFP expressing cells (lower right gate) and cells with unaltered fluorescence (lower left gate). Some cells that highly express IFN-β TurboGFP could not be fully compensated and appear in the upper right gate. B: Mean intensity of IFN-β TurboGFP positive cells. The data shown represent average values +/- standard deviation of 3 experiments.

As shown in figure 9, the total number of IFN-β TurboGFP expressing cells differs in the two cell populations. While in the case of untransfected cells, 32 % are positive for TurboGFP after NDV infection, only 17 % show green fluorescence in the cells harboring also NS1-H (fig. 9A). A similar picture could

be demonstrated for the mean intensity of TurboGFP fluorescence which drops to ~50% compared to untransfected cells (fig. 9B). A possible reason is basal expression of NS1-H in the absence of the inducer which could exert an inhibitory effect on IFN-β TurboGFP expression levels. However, this NS1-H expression is below the detection threshold of the flow cytometric device (compare with figs. 7 and 8). Taken together, IFN-β NS1-H cells show alteration in the amount as well as in the intensity of IFN-β TurboGFP positive cells. While this impairs a direct comparison between these cells, IFN-β NS1-H cells still provide substantial inducible expression of IFN-β TurboGFP and thus can be used for the perturbation of IFN-β induction.

3.2.2.4 Ectopically controlled NS1-H expression reflects NS1 levels during early influenza A virus infection

Ectopic expression of a gene is usually performed to gain information about a genes' function. In this work, the NS1 gene from influenza A/PR/8/34 strain (PR8) is ectopically expressed in a regulable manner with the primary aim to specifically perturb the IFN system. In addition, the results can give new insights into the work mechanism of NS1-H. The fact that NS1-H can be controlled by simply administering doxycycline to the medium makes it easy to adjust the level of intracellular NS1-H levels. Thus, perturbation of IFN-β TurboGFP can be controlled. However, it is unclear in how far the ectopically controlled NS1-H expression levels reflect those of NS1 obtained during natural IAV infection. IFN-β NS1-H cells were treated with increasing concentrations of doxycycline for a constant time period or with saturating doxycycline concentrations for differing periods of time. In parallel, untransfected IFN-β TurboGFP cells were infected with the IAV PR8 strain at different multiplicities of infection (MOI). Immunoblotting was performed to compare NS1 values of ectopic versus natural expression.

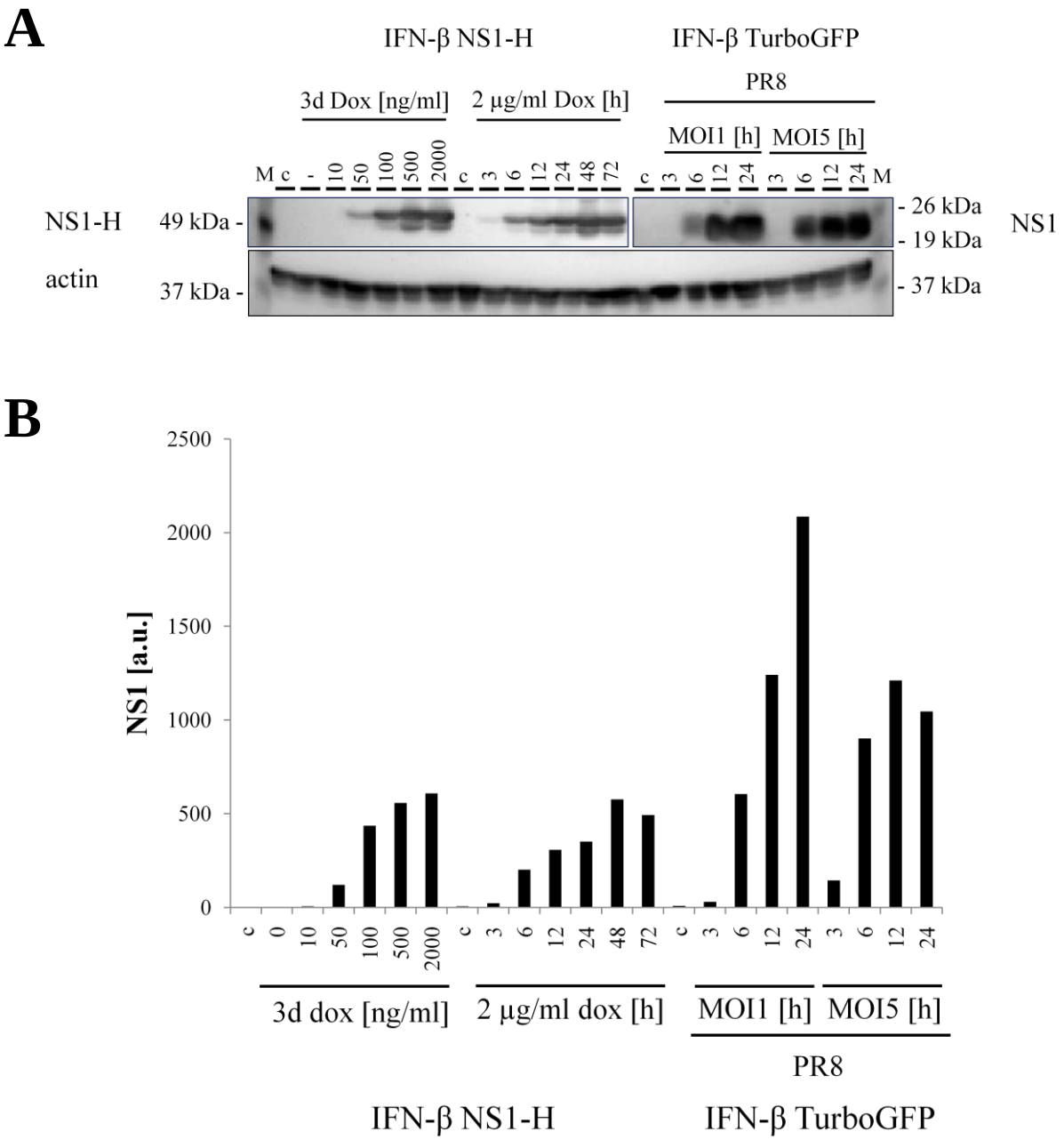

Figure 10: Ectopically induced versus native NS1 levels.

IFN-β NS1-H cells were treated with doxycycline at the indicated concentrations for 3 d or with 2 µg/ml for the indicated time periods and subsequently harvested. IFN-β TurboGFP cells were infected with IAV PR8 for 1 h at an MOI of 1 or 5 and harvested at the indicated time points. Whole cell extracts were prepared and equal amounts of protein were loaded on a gel for SDS-PAGE and subsequently transferred to a membrane. The membrane was treated with an anti-NS1 antibody. After stripping of the membrane, it was treated with an actin-specific antibody. A prestained molecular weight marker is loaded on the left and on the right. The amino acid sequences of ectopically inducible NS1-H and NS1 from viral infection differ in one amino acid (L->E) at position 55. The molecular weight of NS1 is about 26 to 32 kDa pursuant to Santa Cruz Biotechnology. The calculated molecular weight of NS1-H is 61.8 kDa (Vector NTI). A: Western Blot; B: Quantification of the NS1 values (performed with Quantity One program).

Western Blotting shows distinct bands of NS1-H for the whole cell extracts from ectopically NS1-H expressing cells and for the extracts of cells infected with IAV PR8 (fig. 10A). The fusion of ectopically induced NS1 and HTV7 results in higher molecular weight than NS1 from IAV infection.
The quantification of the Western Blot (fig. 10B) shows that ectopically controlled NS1-H levels increase with doxycycline concentrations and over time, as expected. The amount of native IAV NS1 increases until 12 h pi (MOI 5) or 24 h pi (MOI 1). The level of NS1 does not strongly differ between cells infected with an MOI of 1 and an MOI of 5. It is not clear, whether the amount of infectious particles per cell has an impact on viral replication.
The Western Blot and the quantification show that physiological levels of early influenza infection (3 - 6 h pi) can be mimicked by controlled ectopic expression of NS1-H. This underlines the validity of the synthetic NS1-based perturbation model.

3.2.3 Reporter cells for monitoring IFN-β perturbation by hepatitis C virus NS3 protease/NS4A cofactor complex

The IAV NS1 protein is said to inhibit IFN-β induction as well as IFN-induced antiviral effectors by diverse pre- and post-transcriptional mechanisms as well as sequestration of dsRNA. Also, interference with viral ssRNAs possessing 5’ triphosphate groups was demonstrated (reviewed by Ehrhardt et al, 2010). However, some antagonistic functions of NS1 are virus strain specific (Hayman et al, 2006; Kochs et al, 2007). Another IFN antagonist, the non-structural protein 3 and its cofactor 4A from hepatitis C virus, follows a different and more specific way of perturbation. The virus-own protease NS3, whose activity is enhanced by binding its cofactor NS4A, leads to the specific cleavage of IPS-1 *in vitro* and *in vivo* (Loo et al, 2006). This proteolytic reaction makes the IFN cascade lack a factor indispensable for the signaling.

3.2.3.1 Stable expression of NS3/4A-H renders cells unable to induce IFN-β following viral infection

The mechanism of NS3/4A perturbation is different from NS1 and specifically relies on the cleavage of IPS-1. Thus, it was also chosen for perturbation experiments, as it will give additional information on the IFN system's dynamics. For this purpose, HCV NS3/4A genes from JFH-1 strain were set under the control of a tetracycline-inducible promoter and integrated into IFN-β TurboGFP reporter cells. After co-transfection of the cells with this construct and the constitutively expressed rtTA2, isolated clones did not show stable induction, but lost perturbator inducibility over longer cultivation periods (data not shown). One of these clones was subjected to single cell sorting. Resulting clones were expanded and basal expression as well as inducibility was determined.

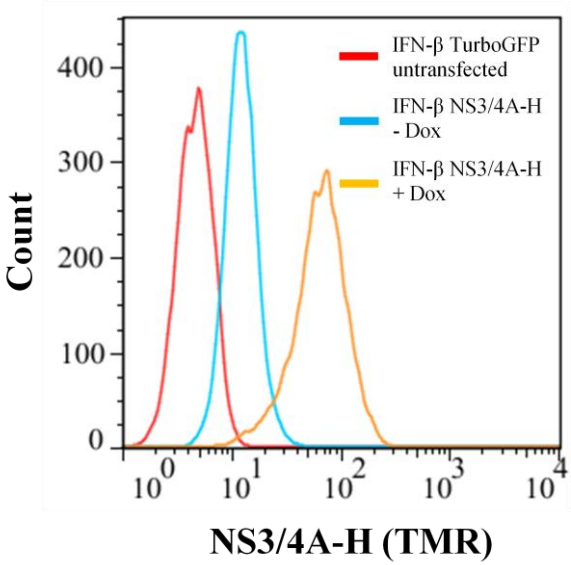

Figure 11: Basal expression and inducibility of stably integrated NS3/4A-H in IFN-β TurboGFP cells.

IFN-β NS3/4A-H cells were treated with 2 µg/ml doxycycline for 3 d or left untreated and stained with TMR ligand. Cells were measured for the amount of NS3/4A-H (TMR) positive cells by flow cytometry. The histogram shows basal expression and inducibility of IFN-β NS3/4A-H cells compared to untransfected cells.

All resulting clones showed comparably high basal expression of NS3/4A-H and were inducible upon doxycycline treatment. The clone displaying lowest basal expression (fig. 11) was chosen for further analyses. These cells were termed IFN-β NS3/4A-H. In order to determine the level of IFN-β TurboGFP inducibility of these cells, it was compared to untransfected cells after viral infection.

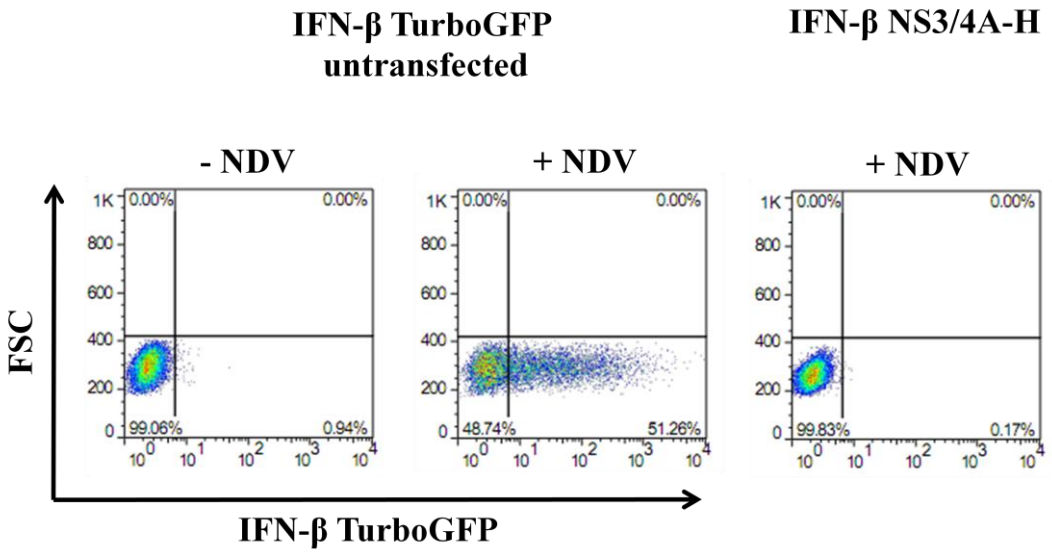

Figure 12: Inducibility of IFN-β in absence of NS3/4A-H induction.

IFN-β TurboGFP cells with or without NS3/4A-H were infected with 80 HAU/ml NDV for 1 h. Cells were measured for the amount of TurboGFP positive cells after 24 h by flow cytometry. Results are displayed as density dot plots (red > blue). IFN-β TurboGFP expressing cells are gated in the lower right quadrant and cells with unaltered fluorescence are gated in the lower left quadrant.

Figure 12 shows that untransfected IFN-β TurboGFP cells that were infected with NDV show proper induction of IFN-β TurboGFP, whereas IFN-β NS3/4A-H cells resemble the uninfected control. This could have several reasons. On the one hand, it could be possible that – for unknown reasons – introduction of NS3/4A-H leads to an alteration of cellular mechanisms that renders the cell no longer responsive to NDV and unable to induce IFN-β TurboGFP. On the other hand, NS3/4A-H could be such a potent IFN antagonist that already basal expression is sufficient to totally block IFN-β induction. To verify this, a plasmid with the constitutively active IRF-3 5D (Lin et al, 1998) was transiently transfected to the IFN-β NS3/4A-H cells. IRF-3 5D is a mutant that carries phosphomimetic aspartic acid substitutions in its C-terminal domain rendering it independent of activational phosphorylation. Thus, it can translocate into the nucleus independent of the IFN-β induction cascade, thereby efficiently inducing IFN-β expression. Figure 13 displays that upon transient transfection with the vector harboring IRF-3 5D, IFN-β NS3/4A-H cells were competent to express IFN-β TurboGFP. Thus, the block of the IFN-β induction cascade is caused by high basal expression of NS3/4A-H. This reveals that NS3/4A in fact seems to be a potent inhibitor of IFN-β induction.

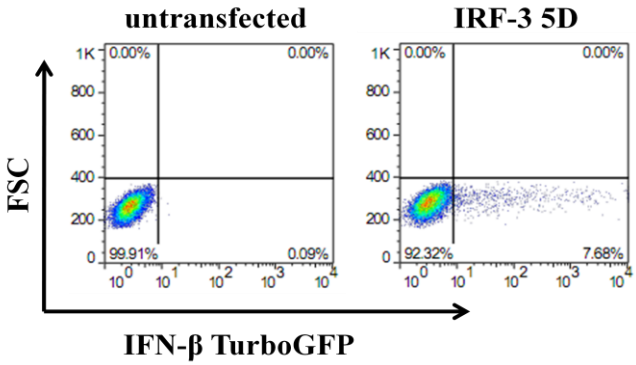

Figure 13: Response of IFN-β NS3/4A-H cells to constitutively active IRF-3 5D.

IFN-β NS3/4A-H cells were transiently transfected with a plasmid harboring IRF-3 5D or were left untreated. Cells were measured for the amount of TurboGFP positive cells after ~ 48 h by flow cytometry. Results are displayed as density dot plots (red > blue) showing IFN-β TurboGFP expressing cells (lower right quadrant) and cells with unaltered fluorescence (lower left quadrant).

3.2.3.2 IFN-β TurboGFP inducibility is rescued by down-regulation of basal NS3/4A-H levels

The just introduced IFN-β NS3/4A-H cells display high basal expression of NS3/4A-H that anticipates IFN-β TurboGFP induction. Consequently, diminution of basal expression needs to be performed by minimizing leaky expression through P_{Tet}. This can be performed by introduction of a transrepressor, the KRAB repressor, which exhibits opposite binding capacities to rtTA2. This activation-repression system should be exploited to reduce basal expression in IFN-β NS3/4A-H cells. For this reason, a plasmid constitutively expressing the KRAB repressor was introduced into the cells and single clones were expanded after selection.

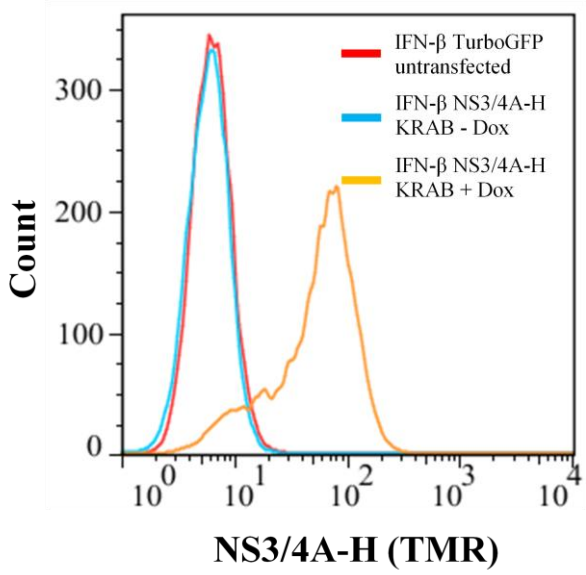

Figure 14: Determination of basal NS3/4A-H levels in a stable IFN-β NS3/4A-H KRAB clone.

IFN-β NS3/4A-H KRAB cells were treated with doxycycline for 3 d or left untreated. The cells were stained with TMR and measured for the amount of NS3/4A-H (TMR) expressing cells by flow cytometry. The histogram shows basal expression and inducibility of IFN-β NS3/4A-H compared to the levels in untransfected cells.

After introduction of KRAB, the obtained clones were measured for basal expression by comparing uninduced with untransfected cells after staining with TMR by a flow cytometric assay. The uninduced, displayed clone does not show significant alteration compared to untransfected cells (fig. 14). After doxycycline treatment, the population shifts to the right indicating that NS3/4A-H can be properly induced.

The important aspect of drastically reducing basal expression in this system is that NS3/4A-H levels are low enough to allow IFN-β TurboGFP induction. This capacity was determined for all obtained IFN-β NS3/4A-H KRAB clones. The most promising clone (also displayed in fig. 14) was directly compared to untransfected cells concerning IFN-β inducibility and mean intensity.

A

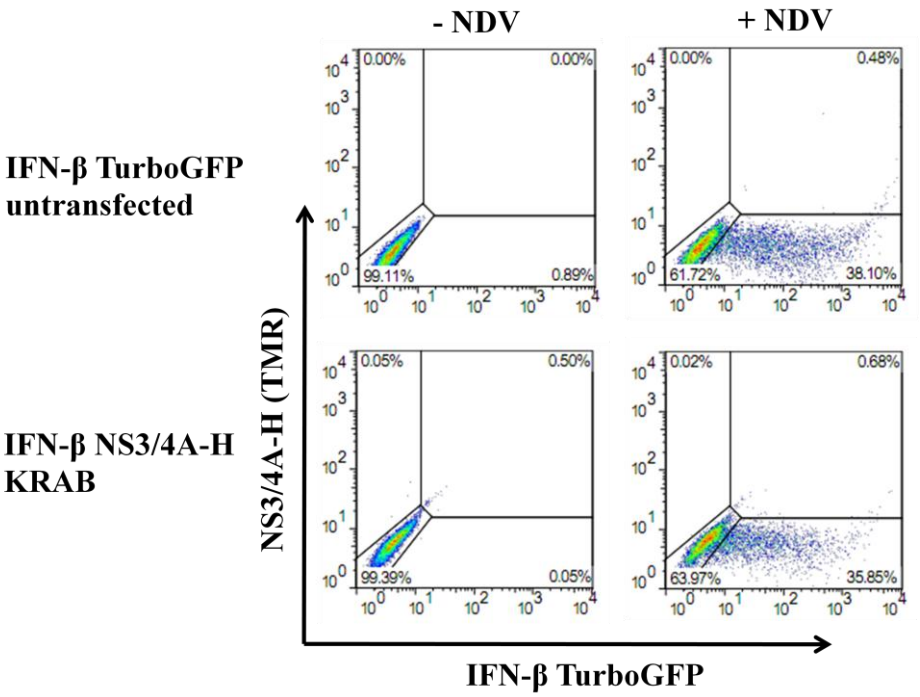

B

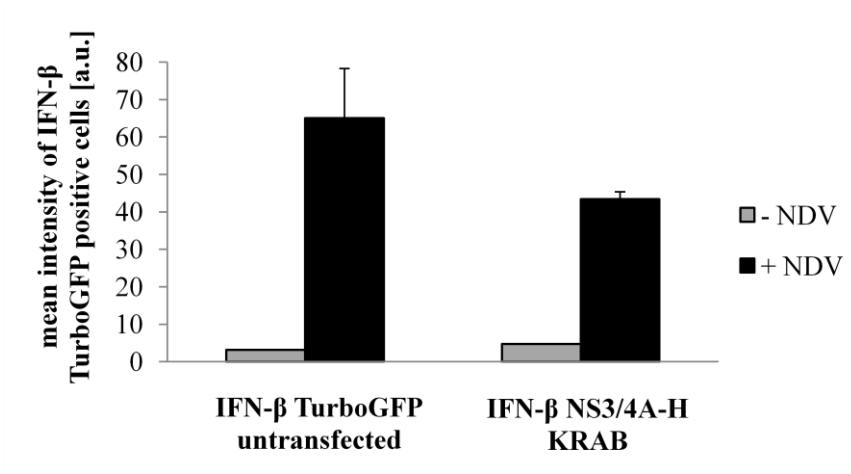

Figure 15: Alterations in the IFN-β TurboGFP expression phenotype of IFN-β NS3/4A-H KRAB cells.

IFN-β TurboGFP cells with or without NS3/4A-H and KRAB were seeded at equal densities and either infected with 80 HAU/ml NDV for 1 h or left uninfected. Cells were measured for the amount of TurboGFP expressing cells after 24 h by flow cytometry. A: Density dot plots (red > blue) show IFN-β TurboGFP expressing cells (lower right gate) and cells with unaltered fluorescence (lower left gate). Cells that highly express IFN-β TurboGFP could not be fully compensated and appear in the upper right gate. B: Mean intensity of IFN-β TurboGFP positive cells. The data shown represent average values +/- standard deviation of 3 experiments.

As already shown for IFN-β NS1-H cells (compare with fig. 9A), also IFN-β expression in the IFN-β NS3/4A-H KRAB cells is not affecting red fluorescence (fig. 15A). Furthermore, IFN-β TurboGFP levels are only slightly diminished compared to untransfected cells. Indeed, IFN-β NS3/4A-H KRAB cells show appropriate IFN-β TurboGFP expression and can be used for further experiments. Figure 15B displays the mean intensity of untransfected IFN-β TurboGFP cells and the cells harboring NS3/4A-H. Comparable to IFN-β NS1-H cells (compare with fig. 9B), uninduced cells with integrated NS3/4A-H show attenuation in IFN-β TurboGFP mean intensity levels. This could give an indication for residual basal expression of NS3/4A-H that causes a constant decrease in IFN-β TurboGFP expression intensity. Certainly, this basal expression would undergo the detection limit of the flow cytometric device. Additionally to these results, NS3/4A-H expression was demonstrated not to exert any effect on IFN-β induction when cells are not infected with NDV (data not shown).

3.3 Doxycycline-induced perturbator expression

Tight regulation of transgene expression is important for the experimental success. In the present case, a strictly controlled, predictable and reliable expression of NS1-H or NS3/4A-H is necessary to later on correlate the expression value of the respective perturbator to IFN-β TurboGFP expression and to know when expression starts and when maximal levels are reached. The following experiments will show how perturbator expression can be controlled and what kind of induction and expression pattern can be obtained. This will be generally evaluated for cells harboring a doxycycline-inducible NS1-H construct, which is similar regulated as the above described cells. These cells, which are also based on IFN-β TurboGFP, are named Tet-NS1-H.

3.3.1 Dynamics of doxycycline-induced perturbator expression

Induction of transgene expression occurs via administration of doxycycline. This inducer can be added to the medium at different concentrations or for differing periods of time to obtain the desired expression of the transgene. To demonstrate in which range of concentration and time an adjustment is possible and to determine at which concentrations or time points post doxycycline administration perturbator induction occurs or maximal levels are reached, Tet-NS1-H cells were analyzed as an example for inducibility in the present systems. Determination was performed for increasing concentrations of doxycycline for a constant time period (fig. 16 A) or for differing time periods in the constant presence of saturating doxycycline concentrations (fig. 16B).

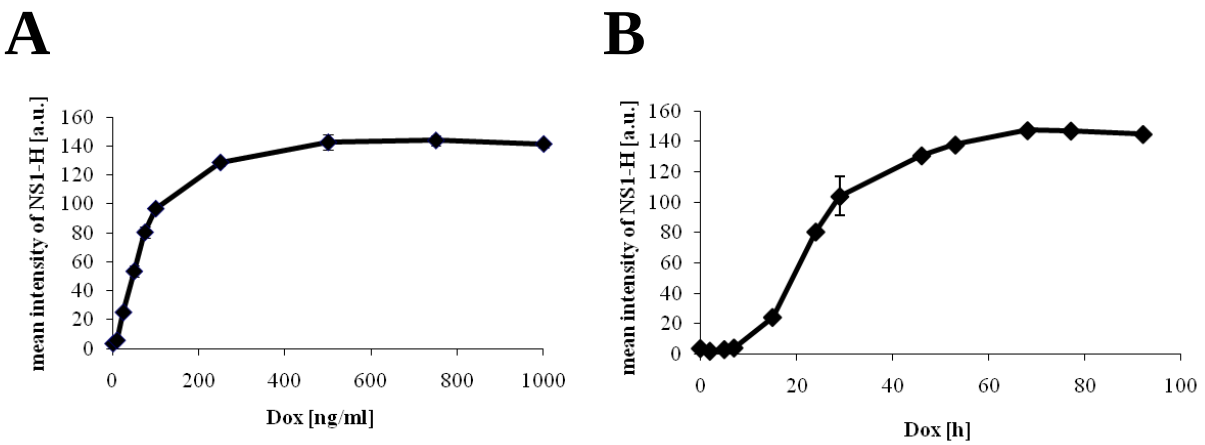

Figure 16: Dynamics of doxycycline-induced NS1-H expression.

Tet-NS1-H cells were treated with (A) increasing concentrations of doxycycline for 3 d or (B) with 2 µg/ml of doxycycline for indicated time spans and were stained with TMR. Cells were measured for the mean fluorescence of NS1-H (TMR) by flow cytometry. The data shown represent average values +/- standard deviation of 3 experiments.

Without doxycycline, no NS1-H is detectable and for 10 ng/ml only minor NS1-H (TMR) intensity can be detected (fig. 16A). However, at concentrations ranging from 25 to 100 ng/ml of doxycycline, NS1-H intensity constantly increases. At 250 ng/ml, cells pass over to plateau phase and no gradual increase can be observed anymore. Maximal intensity, plateau phase, is reached at ~ 500 ng/ml, indicating that this concentration is sufficient to maximally induce NS1-H. At higher concentration, no further increase can be observed.

Figure 16B demonstrates that within the first 7 h of doxycycline administration (2 µg/ml, saturating conditions), no increase of NS1-H (TMR) intensity can be observed. In the range of 15 - 30 h, intensity continuously increases. Plateau phase is reached after constant exposition of the cells to doxycycline for 3 d or longer.

Altogether, perturbator expression shows tight regulation in a dose- and time-dependent manner. Low standard deviation gives rise to predictability and reproducibility of the results.

It was of further interest to determine whether the cell populations' expression increases gradually and homogenously, as it is postulated for this system, in response to increasing concentrations of doxycycline (Schucht et al, 2010).

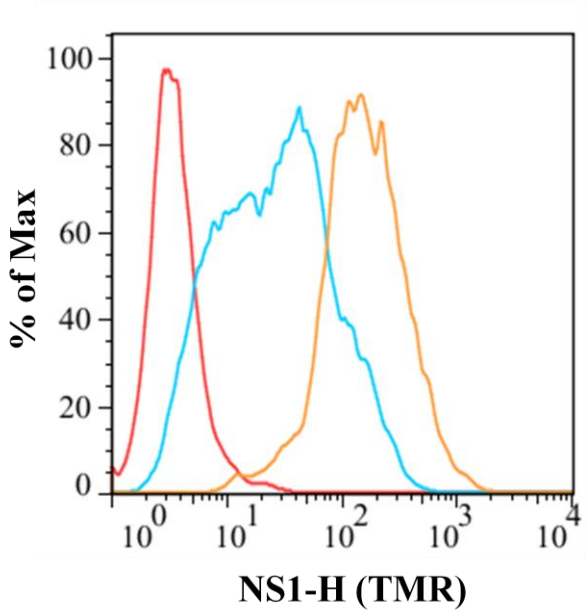

Figure 17: Expression pattern of doxycycline-dependent NS1-H expression.

Tet-NS1-H cells were treated with increasing concentrations of doxycycline for 3 d or left untreated and were stained with TMR. Cells were measured for the amount of NS1-H (TMR) positive cells by flow cytometry. In the histogram, the distribution of NS1-H positive cells for increasing concentrations (0 (red), 25 (blue), 2000 (orange) ng/ml) of doxycycline is shown.

As can be seen in figure 17, a gradual shift of the whole cell population does not occur. Instead, the distribution of NS1-H positive cells is quite broad at intermediate doxycycline concentrations (25 ng/ml). A homogeneous population can finally be monitored for saturating concentrations of doxycycline.
The heterogeneous illustration of NS1-H positive cells at intermediate concentrations of doxycycline displays that the cells do not respond uniformly to doxycycline. This can be validated for living single cells by time-lapse microscopy.

3.3.2 Dynamics of NS1-H induction in single cells

In order to shed light on the induction pattern of the perturbators, single cell analyses are necessary. Those were performed using a time-lapse microscope. In a pre-test, the optimal TMR concentration for these experiments was titrated, because too low concentration of the fluorescent ligand could fail to visualize NS1-H. The other way round, high concentrations of TMR would make even the medium emit the light, letting the resulting pictures appear outshined. The value of 20 nM TMR gave the best results (data not shown). IFN-β TurboGFP cells harboring NS1-H were determined for NS1-H induction in single cells by time-lapse microscopy.

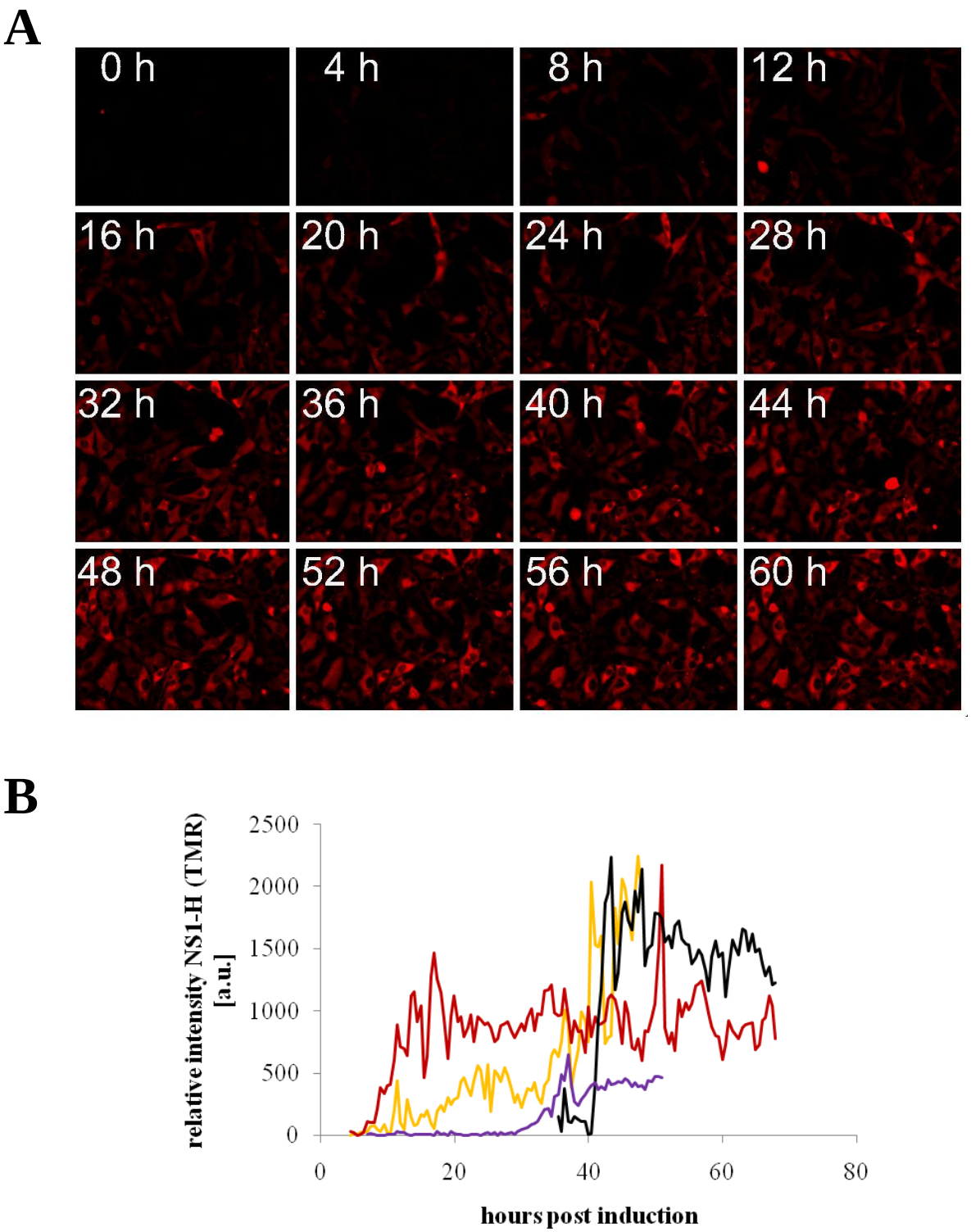

Figure 18: Single cell NS1-H induction in response to doxycycline.

IFN-β TurboGFP cells stably transfected with NS1-H and the KRAB repressor (compare with chapter 3.4.3) were seeded on a collagen-treated chambered microscopy slide at a density of 10^5 cells/ml. Cells were treated with 0.5 µg/ml of doxycycline and stained with TMR. Subsequently, cells were monitored by time-lapse microscopy. Pictures were taken every 30 minutes (min). A: Fluorescence pictures of the indicated time points. B: Fluorescence profiles of representative single cells showing onset and course of NS1-H (TMR).

The fluorescence pictures in figure 18A show the onset of NS1-H overtime in a batch of cells. At early time points of induction (8 - 16 h pi), obviously not all cells behave equally, because only few cells have turned on NS1-H expression. Indeed, the strength of the cells expressing NS1-H strongly differs. A direct comparison of the induction curves of single cells illustrates that NS1-H induction between the cells differs at three levels (fig. 18B). i) The time point of NS1-H induction. ii) Maximal expression levels. iii) The course of NS1-H onset. In fact, the onset in some cells happens slowly, while others are quickly induced. These data indicate that doxycycline-dependent expression shows heterogeneity at multiple levels, while the overall pattern of gradual induction within single cells is maintained. For later experiments, these results indicate that single cells need to be monitored under distinct conditions, as NS1-H and IFN-β TurboGFP are both stochastically induced.

The time point of NS1-H induction was shown to strongly vary between single cells and it was of interest to see whether the concentration of doxycycline can affect it. For this reason, doxycycline-induced expression onset time points were counted for intermediate and high concentrations of doxycycline. As demonstrated in figure 19, under intermediate concentrations of doxycycline (0.1 µg/ml) most cells turn on NS1-H expression between 3 and 12 h with a maximum at 6 – 9 h (40% of all measured cells). Under saturating conditions (0.5 µg/ml), cells respond more pronounced to the inducer and show almost 60% of the cells inducing NS1-H between 3 and 6 h post doxycycline administration.
Together, these data show that different doxycycline concentrations affect the time point of NS1-H onset. The induction time point at lower concentrations varies in a greater range as for higher concentrations, where earlier and more homogeneous induction occurs. Also, the mean time point for the lower doxycycline concentration is higher (mean value: 8.4 h; SD: 3.6 h) than for saturating conditions (mean value: 6.9; SD: 5.3 h). This underlines the hypothesis of earlier induction for higher doxycycline concentrations.

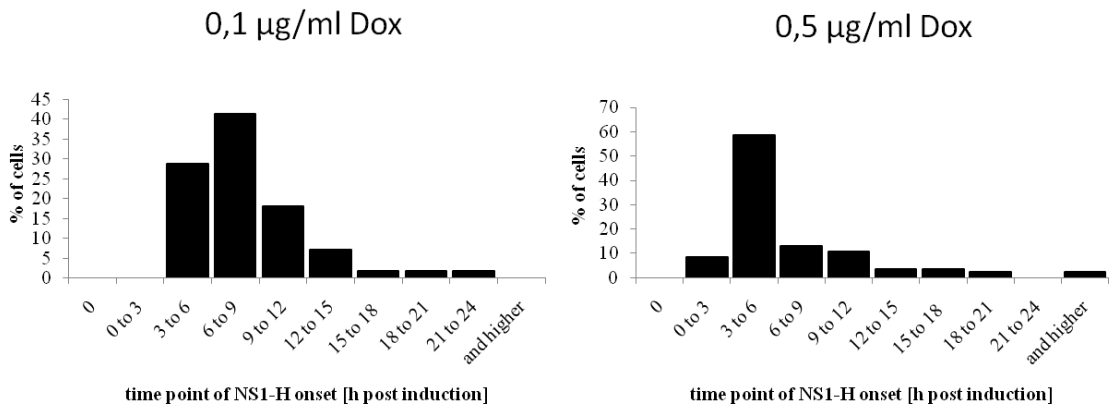

Figure 19: NS1-H induction in response to different concentrations of doxycycline.

NIH3T3 based cells stably transfected with NS1-H (compare with chapter 3.5.3) were seeded on a collagen-treated chambered microscopy slide at a density of 10^5 cells/ml. Cells were treated with 0.1 (left diagram) or 0.5 (right diagram) µg/ml of doxycycline and stained with 20 nM TMR. These cells were monitored by time-lapse microscopy taking pictures every 30 min. The bars demonstrate the distribution of NS1-H inducing cells at different time points post induction. n=56 for 0.1 µg/ml doxycycline (mean value: 8.4 h; SD: 3.6 h); n=86 for 0.5 µg/ml doxycycline (mean value: 6.9; SD: 5.3 h).

3.4 Timing of NS1-H or NS3/4A-H induction has an impact on efficiency of IFN-β TurboGFP perturbation

Regarding pathway progression on the single cell level is a very modern tool to get insight into the spatiotemporal dynamics of cellular networks. So far, IFN induction as well as its repression by NS1-H or NS3/4A-H has been mostly investigated on the mRNA or protein level by bulk assays like Western/Northern Blot or by RT-PCR. Thereby, the influence on single cells can give detailed information about the temporal course of perturbation as well as the dynamics and efficiency of the perturbator itself. Via flow cytometry, a high number of single cells can be quantitatively analyzed for a certain time point. By means of such measurements, the impact of NS1-H or NS3/4A-H levels and induction time point relative to infection on IFN-β TurboGFP levels and intensity were determined.

3.4.1 NS3/4A-H and NS1-H counteract IFN-β induction with different efficiencies

The determination of the effect of perturbator induction at different time points can give rise to the moment when the action of a perturbator is most sufficient. This, in turn, indicates which moment or step of the IFN network is crucial for ongoing signaling. To find this out, the overall distribution of NS1-H or NS3/4A-H positive cells after induction at certain time points relative to NDV infection was observed with regard to IFN-β TurboGFP expression. Representative density dot plots of some of the determined time points are given in figure 20A and B.

A NS1-H

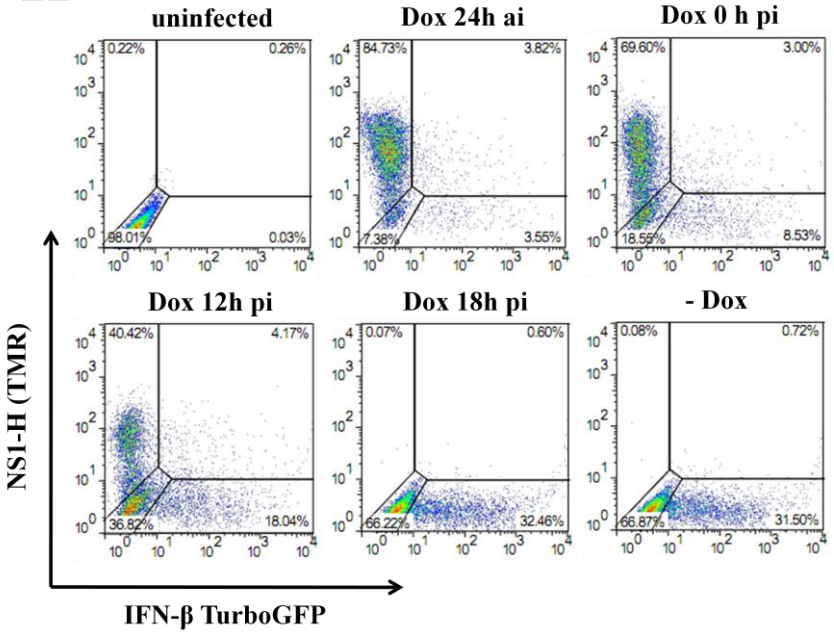

B NS3/4A-H

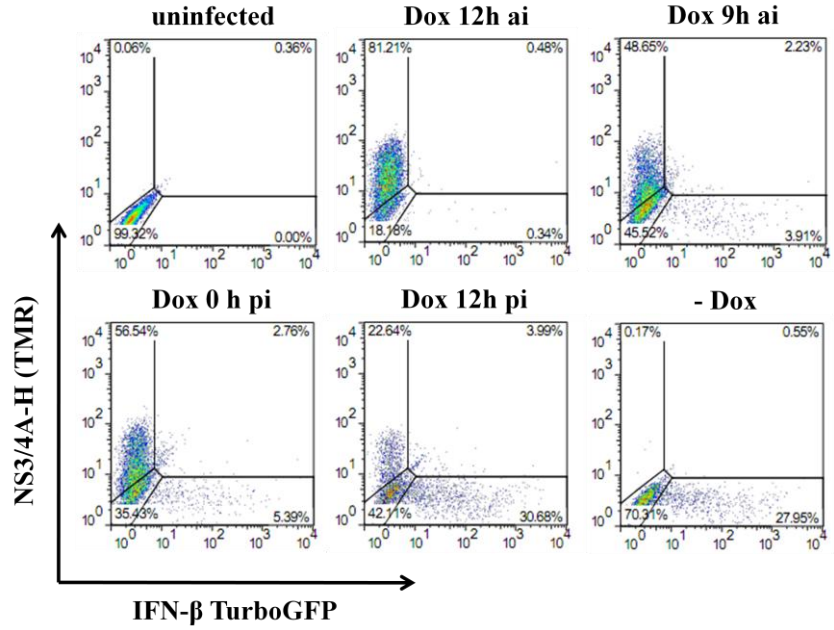

Figure 20: Influence of the perturbation time point on IFN-β TurboGFP expression.

Equal densities of IFN-β NS1-H or IFN-β NS3/4A-H KRAB cells were treated with 2 µg/ml doxycycline at different time points relative to NDV infection (80 HAU/ml; 1 h). Cells were stained with TMR and measured 24 h pi. IFN-β NS1-H (A) or IFN-β NS3/4A-H KRAB (B) cells were measured for the amount of IFN-β TurboGFP and NS1-H or NS3/4A-H (TMR) positive cells by flow cytometry. The results are displayed as density dot plots (red > blue) showing IFN-β expressing cells in the lower right gate and NS1-H or NS3/4A-H positive cells in the upper left gate. Cells positive for IFN-β TurboGFP and NS1-H or NS3/4A-H are gated in the upper right and cells with unaltered fluorescence in the lower left. Representative examples of the tested time points of perturbator induction relative to NDV infection are shown.

The dot plots in figures 20A and B display the distribution of NS1-H or NS3/4A-H and IFN-β TurboGFP in a cell population after doxycycline treatment at different time points relative to infection.
Without doxycycline, cells are just positive for IFN-β TurboGFP. It is obvious that NS1-H or NS3/4A-H expression increases the earlier the cells were treated with doxycycline. In parallel, IFN-β TurboGFP levels decrease. This clearly demonstrates that NS1-H as well as NS3/4A-H exerts an IFN-β TurboGFP antagonizing effect. According to this, the fusions of the viral perturbators to HaloTag have retained their perturbing function.
Especially in the case of NS1-H, cells positive for both markers could be visualized. This is a minor but significant amount of cells. For NS3/4A-H, those cells only exerted low intensities of IFN-β TurboGFP. The existence of these cells indicates that a state of the cells exists in which they are able to express both, the perturbator and IFN-β TurboGFP. Indeed, further experiments on these cells are given in chapter 3.5.
It is further obvious that differences between the perturbation via NS1-H and NS3/4A-H exist. While cells harboring NS1-H still show a significant amount of cells positive for IFN-β TurboGFP or both markers even though treated with doxycycline for 24 h before infection, IFN-β TurboGFP expression is already fully interrupted when the NS3/4A-H cells were kept under doxycycline from 12 h ai on. In fact, the levels of NS1-H and NS3/4A-H cannot be directly compared with each other, but since NS3/4A-H intensities in the induced state are also lower than those of NS1-H, this indicates a faster perturbation behavior by NS3/4A-H.

3.4.1.1 NS1-H or NS3/4A-H induction shortly after infection causes a drastic decrease in IFN-β TurboGFP levels

The dot plots could already give information about the distribution of NS1-H or NS3/4A-H and IFN-β TurboGFP, also with regard to the co-expression of both markers. However, by means of a correlation of NS1-H or NS3/4A-H versus IFN-β TurboGFP expression for all measured time points, their antithetic expression can be highlighted. For this reason, the amount of positive cells for the mean values of 3 experiments for both parameters were applied the one against the other for all measured time points. Cells positive for both markers are not shown. They will be further analyzed in chapter 3.4.1.2.

A NS1-H

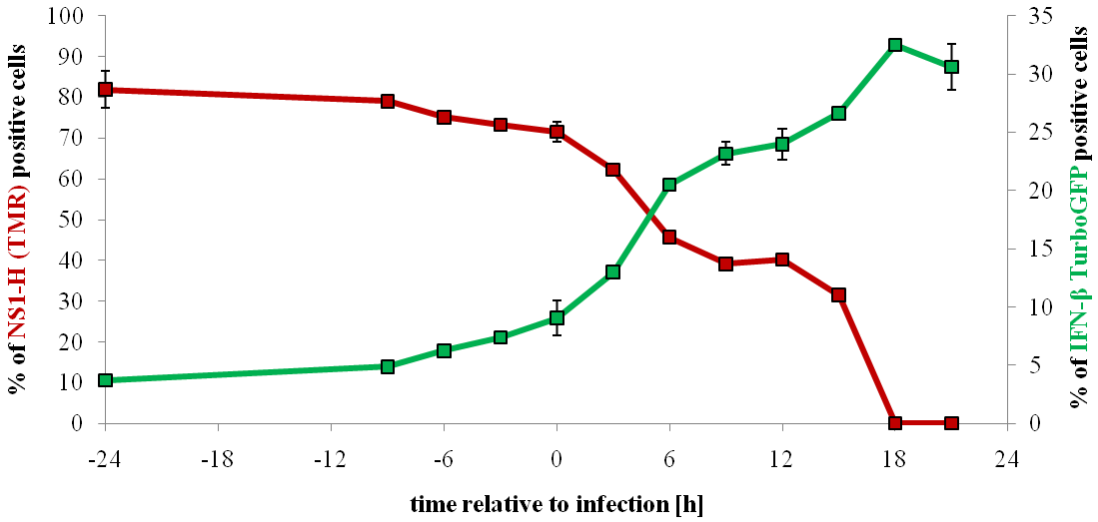

B NS3/4A-H

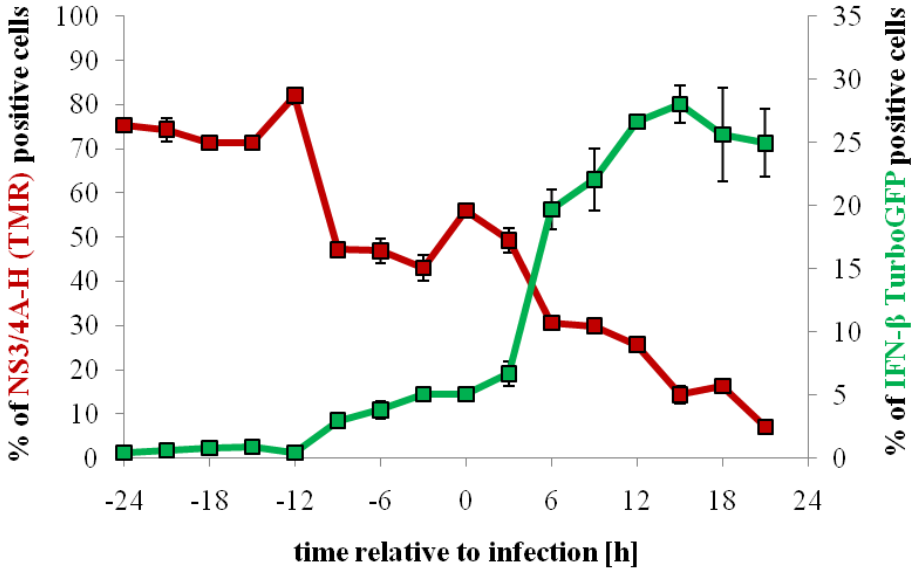

Figure 21: Correlation of NS1-H or NS3/4A-H expression with IFN-β TurboGFP expression.

IFN-β NS1-H (A) or IFN-β NS3/4A-H KRAB (B) cells were treated with 2 µg/ml of doxycycline at different time points relative to infection. Cells were infected with 80 HAU/ml NDV for 1 h at time point "0" and stained with TMR. Cells were measured for the amount of IFN-β TurboGFP and NS1-H or NS3/4A-H (TMR) positive cells 24 h pi by flow cytometry. The data shown represent average values +/- standard deviation of 3 experiments. In figure B, the values for the time point 12 h pi were determined from duplicates. Standard deviation is not given in this case. Cells positive for both IFN-β TurboGFP and NS1-H or NS3/4A-H were skipped in these figures. If the measurements were arranged at different time points, the amount of positive cells was equalized by using NDV-infected IFN-β TurboGFP cells or the cells harboring NS1-H.

In figures 21A and B, the correlations of NS1-H or NS3/4A-H onset versus the decrease/arrest in IFN-β TurboGFP are given. In addition to the results visualized by the dot plots, it is eye-catching that the amount of IFN-β TurboGFP positive cells only drops to 5 % in the case of NS1-H, but a complete block of IFN-β expression does not occur. This block could be demonstrated for NS3/4A-H expressing cells at similar time points. Indeed, a stronger perturbation via NS1-H could be detected when the cells were kept under doxycycline for a longer time period (e.g. 7 days, data not shown), although no complete block was possible. This could be due to the fact that NS1-H usually is higher expressed in IAV-infected cells than in maximally induced cells of this work (compare with fig. 10).

It is eye-catching that the levels of IFN-β TurboGFP continuously decrease overtime in the case of NS1-H with a slightly higher effect shortly after infection. However, this effect is much more drastic for the cells expressing NS3/4A-H, which show a strong effect of NS3/4A-H on IFN-β TurboGFP levels in a small time window between 3 and 6 h pi. This effect can be related to the fact that in natural infection, the virus needs some time to let the cellular machinery express its genome. Consequently, NS1 or NS3/4A is just present after infection and probably is most efficient at this time point.

The differences in the perturbation patterns of NS1-H and NS3/4A-H can be explained by their different types of interference with the IFN network. The proteolytic cleavage which occurs via NS3/4A-H is very efficient, since one NS3/4A-H complex is able to cleave several IPS-1 molecules. In contrast, certain NS1-H dimers are necessary to bind the same amount of RIG-I or TRIM25. Accordingly, the stoichiometry for the factors would be very different and significantly more NS1-H molecules would be needed for the counteraction of IFN-β TurboGFP.

3.4.1.2 Cells positive for both IFN-β TurboGFP and NS1-H or NS3/4A-H turn up after IFN-β and perturbator induction

In the previous analyses, cells positive for the perturbator and IFN-β TurboGFP could be visualized. These cells are of exceptional interest, because they indicate that the perturbation is not an all-or nothing event, but intermediate steps occur. This is probably caused by a belated induction of the perturbator occurring after IFN-β TurboGFP induction. Another reason could be that perturbator levels are too low to suffice for perturbation.
The number of cells expressing both markers is constant overtime and ranges from 2 – 4 % in the case of NS1-H and from 1 – 4 % for NS3/4A-H (data not shown). This could indicate a continuous onset and termination of IFN-β TurboGFP expressing cells which has to be clarified by single cell microscopic analyses (see chapter 3.5).
Perturbator induction at various time points could affect IFN-β TurboGFP mean intensity since already constant basal levels of the perturbators give rise to this behavior (compare fig. 9B and 15B). Such an effect would indicate that i) the distribution of IFN-β TurboGFP positive cells is altered due to perturbator expression or ii) ongoing IFN-β TurboGFP expression can be blocked or inverted. Determination of the mean intensities of cells positive for the respective perturbator and IFN-β TurboGFP could give insight into the mechanism. However, flow cytometry analyses on the mean intensity of these cells were limited due to highly expressing IFN-β TurboGFP that could not be compensated. For this reason, the course of perturbator increase compared to a possible IFN-β TurboGFP arrest in single cells is addressed later in this work (chapter 3.5).

3.4.2. Influence of increasing NS1-H or NS3/4A-H levels on IFN-β TurboGFP induction

After the analysis of the influence of the perturbators' induction time point on IFN-β expression, it was of interest to analyze which effect a dose-dependent increase of the perturbators (displayed in chapter 3.3.1) would have on IFN-β TurboGFP expression. For this examination, IFN-β NS1-H and IFN-β NS3/4A-H KRAB cells were kept under a certain concentration of doxycycline for a constant period of time. The dot plots in figure 22 monitor the influence of the respective amount of NS1-H or NS3/4A-H which can be equated with a certain concentration of doxycycline that was administered to the cells. Representative dot plots of several concentrations are shown.

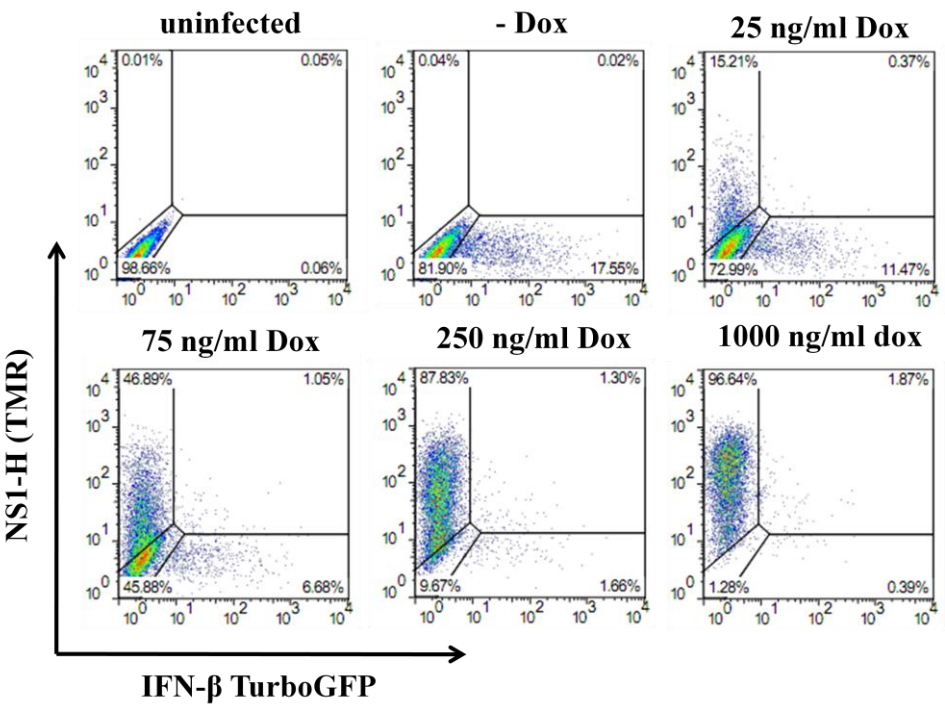

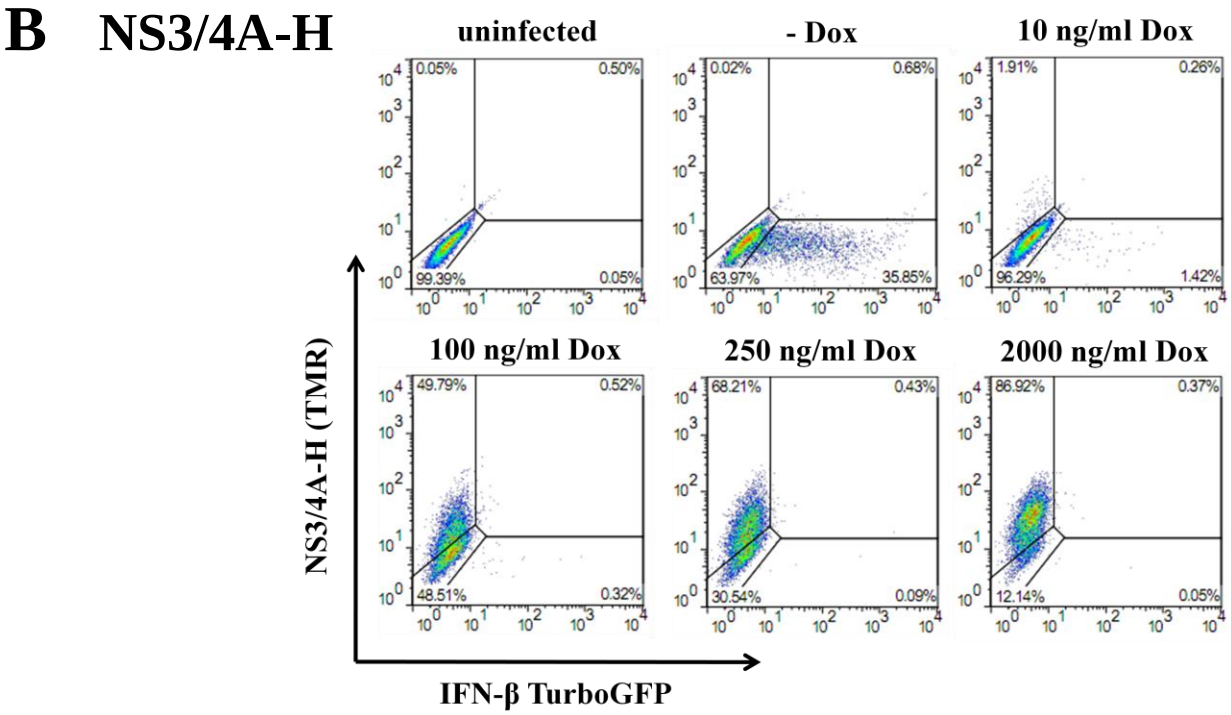

Figure 22: Influence of increasing perturbator levels on IFN-β TurboGFP expression.

IFN-β NS1-H (A) or IFN-β NS3/4A-H KRAB (B) cells were pre-treated with increasing amounts of doxycycline for 3 d. Then, cells were infected with 80 HAU/ml NDV for 1 h and stained with TMR. Cells were measured for the amount of IFN-β TurboGFP and for NS1-H e.g. NS3/4A-H (TMR) positive cells 24 h pi by flow cytometry. The results are displayed as density dot plots (red > blue) showing IFN-β expressing cells in the lower right gate and NS1-H or NS3/4A-H (TMR) positive cells in the upper left gate. Cells positive for IFN-β TurboGFP and NS1-H e.g. NS3/4A-H are gated in the upper right and cells with unaltered fluorescence in the lower left. Examples of the tested concentrations are shown here.

As expected and as shown before, the uninfected and uninduced IFN-β NS1-H and IFN-β NS3/4A-H KRAB cells do not show expression in the channels for NS1-H or NS3/4A-H (TMR) and IFN-β TurboGFP.

The infected, uninduced IFN-β NS1-H cells exhibit strict IFN-β TurboGFP expression (17.5 %). At low doxycycline concentrations (25 ng/ml), 15 % of NS1-H positive cells shift to the upper left gate, whereas the amount of IFN-β TurboGFP positive cells (lower right channel) is decreasing to 11.5 % (fig. 22A). Only very few cells (0.37 %) express both reporters. With increasing concentrations of the inducer, NS1-H positive cells increase and the amount of IFN-β TurboGFP positive cells decreases. At the same time, the amount of cells expressing both reporters is constantly low.

The NDV-infected, uninduced cells stably harboring NS3/4A-H show 36 % of IFN-β TurboGFP positive cells (fig. 22B). However, when 10 µg/ml doxycycline were administered to the cells for 3 d, the corresponding NS3/4A-H levels suffice to almost block IFN-β TurboGFP expression (only 1.42 % left

behind). Also, it is remarkable that at this concentration, only 1.9 % of the cells actually shifted to the upper left channel where the NS3/4A-H positive cells should be monitored. As already mentioned before, low amounts of protein tagged to HTV-7 cannot be visualized by the flow cytometric device. This underlines the theory that very low levels of NS3/4A-H are sufficient to efficiently perturb IFN-β TurboGFP expression. At higher concentrations of doxycycline, NS3/4A-H expressing cells can be visualized, but concomitantly, almost no IFN-β positive cells can be determined.

These data clearly demonstrate that the perturbator cassettes can be used to interfere with IFN induction in a dose-dependent manner. However, IFN-β TurboGFP is much more sensitive to NS3/4A-H perturbation and regulation can be obtained only at very low doxycycline concentrations.

For a better overview of the results for all tested concentrations of doxycycline, a correlation of the dot plots from figure 22 was realized in figure 23.

A NS1-H

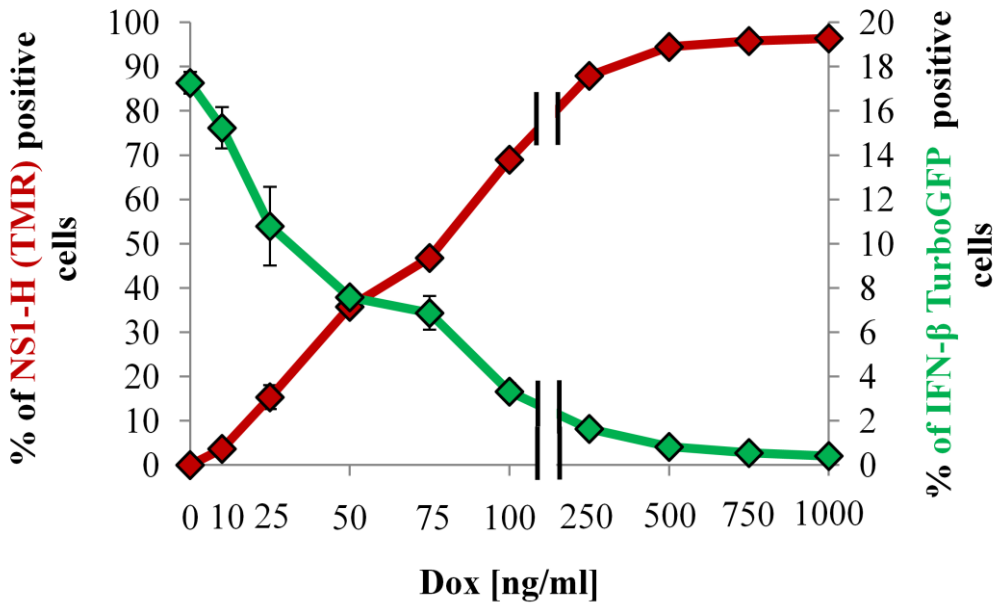

B NS3/4A-H

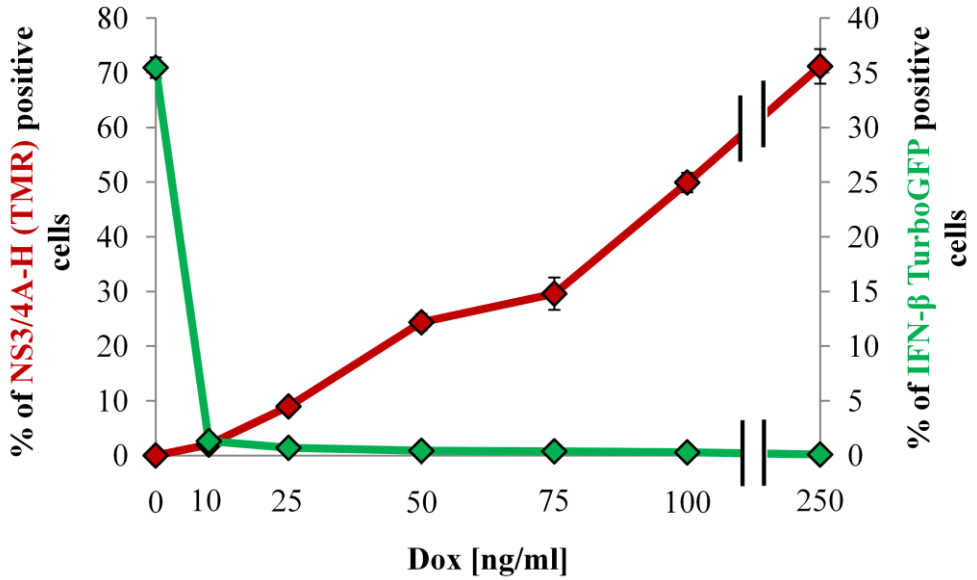

Figure 23: Correlation of NS1-H and NS3/4A-H with IFN-β TurboGFP expression.

IFN-β NS1-H (A) or IFN-β NS3/4A-H KRAB (B) cells were pre-treated with increasing amounts of doxycycline for 3 d. Then, cells were infected with 80 HAU/ml NDV for 1 h and stained with TMR. Cells were measured for the amount of IFN-β TurboGFP and for NS1-H or NS3/4A-H (TMR) positive cells 24 h pi by flow cytometry. The data shown represent average values +/- standard deviation of 3 experiments.

IFN-β NS1-H cells that were treated with increasing concentrations of doxycycline show a constant increase of NS1-H positive cells until maximal levels are reached at a concentration of 500 ng/ml (fig. 23A). As a consequence, IFN-β TurboGFP gradually decreases and nearly reaches the base line.
For the IFN-β NS3/4A-H KRAB cells, a completely different perturbation pattern was obtained (fig. 23B). NS3/4A-H also constantly increases the higher the doxycycline concentration is, but administration of only 10 ng/ml doxycycline leads to a drastic decrease of IFN-β TurboGFP expression. After addition of 50 ng/ml of the inducer, the base line is reached and for higher concentrations only minor effects can be visualized.
These data clearly demonstrate the differences, and thereby probably the advantages, of the perturbation mode for the respective virus. The abrupt perturbation at low levels of NS3/4A-H might contribute to the persistence of HCV within a host. In contrast, NS1-H interference occurs creeping whereby at least low levels of IFN-β can be produced to induce an antiviral state of the cells in the end.

3.4.2.1 Co-expression of IFN-β TurboGFP and the perturbator

Cells positive for both reporters could be visualized especially for time-dependent doxycycline administration, but also in the dose-dependent experiments they turned up. The number of these cells (compare with the upper right gate of fig. 22A and B) was determined for IFN-β NS1-H as well as for IFN-β NS3/4A-H cells (data not shown). For NS1-H, the amount slightly increases with rising concentrations of doxycycline until 75 ng/ml. Afterwards, a constant level of 1 – 1.5 % appears. For NS3/4A-H, a constant level of 0.5 % of these cells could be visualized. These low levels indicate the presence of a state, where almost no IFN-β TurboGFP can be induced as a result of pre-treatment of the cells with the perturbators.
Analyses on the course of IFN-β TurboGFP mean intensity of these cell populations are not given here for the reasons described in chapter 3.4.1.2. Also, the levels of cells expressing both reporters are, especially in the case of NS3/4A-H, too low to display significant alterations. The question of a possible interruption of IFN-β TurboGFP expression by the perturbators will be addressed in chapter 3.5.

3.4.3 IFN-β NS1-H reporter cells show improved inducibility after integration of KRAB

IFN-β NS1-H cells did not show significant basal levels of NS1-H, but proper inducibility upon doxycycline administration. However, the amount and intensity of IFN-β TurboGFP compared to untransfected cells was altered. To obtain IFN-β NS1-H cells displaying comparable values in IFN-β TurboGFP expression and intensity, an improvement of the cells was performed. Such cells which do not show significant differences to untransfected cells can be taken for single cell analyses without respect to untransfected cells. For NS3/4A-H, this improvement has previously been done (chapter 3.2.3.2).
For IFN-β NS1-H cells, a corresponding improvement was performed by stably integrating the KRAB repressor. After selection, several clones were evaluated. The characteristics of the most promising one are given in figure 24 (IFN-β NS1-H KRAB). In the uninduced state, this clone displays red fluorescence comparable to the one of untransfected cells. Further on, it is properly induced upon doxycycline treatment.

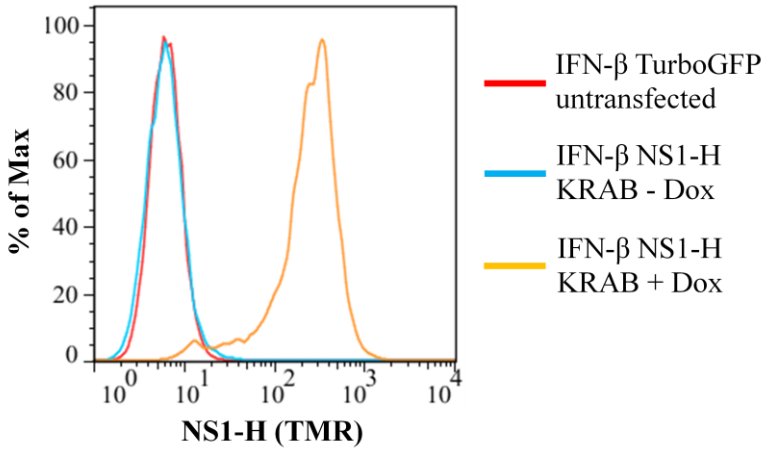

Figure 24: Expression characteristics of an IFN-β TurboGFP clone expressing NS1-H and KRAB.

IFN-β NS1-H KRAB cells were either treated with doxycycline for 3 d or left untreated and stained with TMR. Cells were measured for the amount of NS1-H (TMR) positive cells by flow cytometry. In the histogram, the fluorescence of untransfected IFN-β TurboGFP cells is compared to the fluorescence of uninduced and induced IFN-β NS1-H KRAB cells.

Basal levels of IFN-β NS1-H KRAB cells can hardly be distinguished from untransfected cells. However, this was expected since IFN-β NS1-H cells also resembled the untransfected cells for this criterion. To exclude whether undetectable basal levels influence IFN-β TurboGFP inducibility and intensity these and untransfected IFN-β TurboGFP cells were determined for these parameters.

A

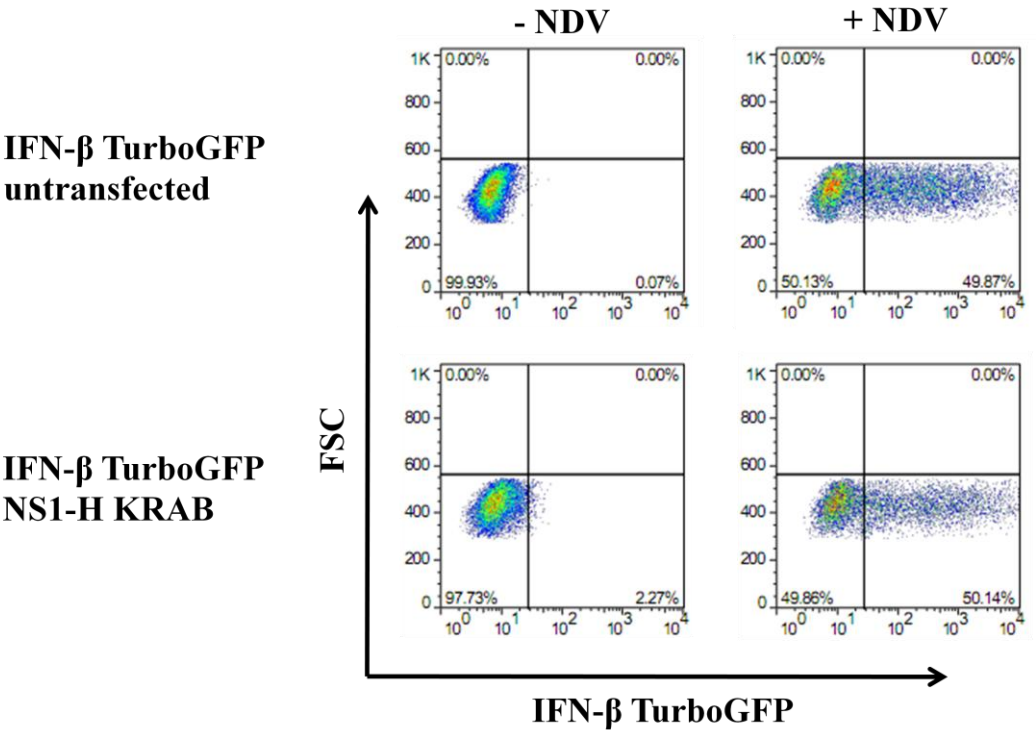

B

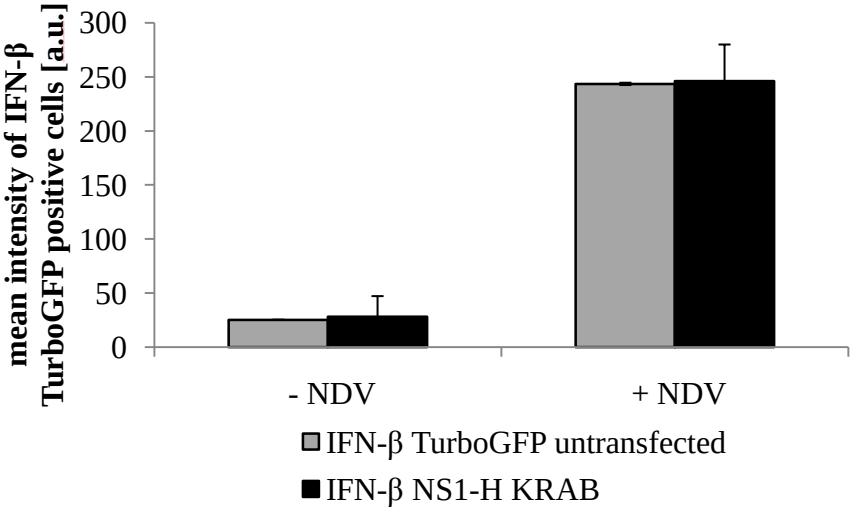

Figure 25: Comparison of IFN-β TurboGFP cells harboring NS1-H and KRAB with untransfected cells.

Untransfected cells or IFN-β NS1-H KRAB cells were seeded at equal densities and were either infected with 80 HAU/ml NDV for 1 h or left uninfected. Cells were measured for the amount of TurboGFP positive cells after 24 h by flow cytometry. A: Density dot plots (red > blue) show IFN-β TurboGFP expressing cells (lower right gate) and cells with unaltered fluorescence (lower left gate). B: Mean intensity of IFN-β TurboGFP positive cells. The data shown represent average values +/- standard deviation of 3 experiments.

Before introduction of KRAB, the amount of IFN-β TurboGFP expressing cells was strikingly diminished in IFN-β NS1-H cells compared to untransfected cells (compare with fig. 9A). In figure 25A, inducibility of IFN-β NS1-H KRAB cells compared with untransfected cells is given. Both exhibit around 50 % of the cells expressing IFN-β TurboGFP under the present conditions. The values for the IFN-β NS1-H KRAB cells, indeed, are directly comparable with the ones of untransfected IFN-β TurboGFP cells.

Before the introduction of the KRAB repressor, also the intensity of IFN-β TurboGFP was reduced in the cells harboring the NS1-H construct (compare with fig. 9B). The mean intensity of IFN-β TurboGFP positive cells was also determined for the IFN-β NS1-H KRAB cells compared to untransfected cells and is given in figure 25B. In the uninfected state, IFN-β NS1-H KRAB and untransfected cells exhibit mean intensities of ~ 25a.u.. After infection, levels increased 10-fold in both cases. For the uninfected as well as the infected state, cells show comparable values, indicating that the obtained IFN-β NS1-H KRAB clone does not show alteration concerning the important parameters for this work. For this reason, the IFN-β NS1-H KRAB clone was used for time-lapse experiments of this work.

3.5 Single cell analysis of IFN-β perturbation by NS1-H and NS3/4A-H

Perturbation experiments of cellular networks are usually performed for cell populations. However, important aspects like the temporal course and the localization of both, signaling target and perturbator cannot be followed in detail by those methods. Also the alteration of the outcome after perturbation can only be given quantitatively, but not qualitatively. Those results can only give mean values of a batch of cells, but this is hardly transferable to a single cell. Since cells usually do not behave equally, single cell analyses via live-cell imaging is an emerging tool.
For this work, it was of particular importance to perform this analysis, since all determined factors, IFN-β TurboGFP and NS1-H or NS3/4A-H, display stochastic behavior on several levels. However, high-throughput computational analysis programs were not available and hampered an automatic analysis of large numbers of individual cells. For this reason, in this study, a representative amount of cells was evaluated by mechanical tracking.

3.5.1 Perturbation of IFN-β induction by NS1-H in single living cells

Flow cytometry analyses already gave a lot of indications for the behavior of the cells during IFN-β perturbation. They demonstrated that cells that were pre-treated with doxycycline (compare with fig. 22) exhibited strong counteraction against IFN induction, indicating that pre-treatment leads to an “anti-IFN state” of the cells. Also, the amount of cells positive for both, IFN-β TurboGFP and the respective perturbator are low in this experimental setup. For NS1-H or NS3/4A-H induction at the time point of infection or later, an increase in cells positive for both reporters could be demonstrated until a decrease occurred at late times of induction (compare with fig. 20). However, single cells cannot be measured over time in this approach.
The appearance of cells positive for both, IFN-β TurboGFP and NS1-H or NS3/4A-H, indicates that the perturbation of IFN-β induction is a dynamic process causing intermediate states of perturbator and IFN-β TurboGFP expression. To verify what the matter is with single living cells emitting green and red fluorescence, time-lapse experiments were performed. Treatment of the cells for all following time-lapse experiments was performed according to a standard protocol: After adherence on a micro-slide, the cells were infected with 80 HAU/ml for 1h and subsequently treated with 0.5 µg/ml doxycycline and 20 nM TMR. Pictures were taken every 15 or 30 min. Since NS1 is known to shuttle between the cytoplasm and the nucleus, measurement of the cells was

standardized on cytosolic tracking (Han et al, 2010). Differences and intricacies are depicted in the figure legends.

A

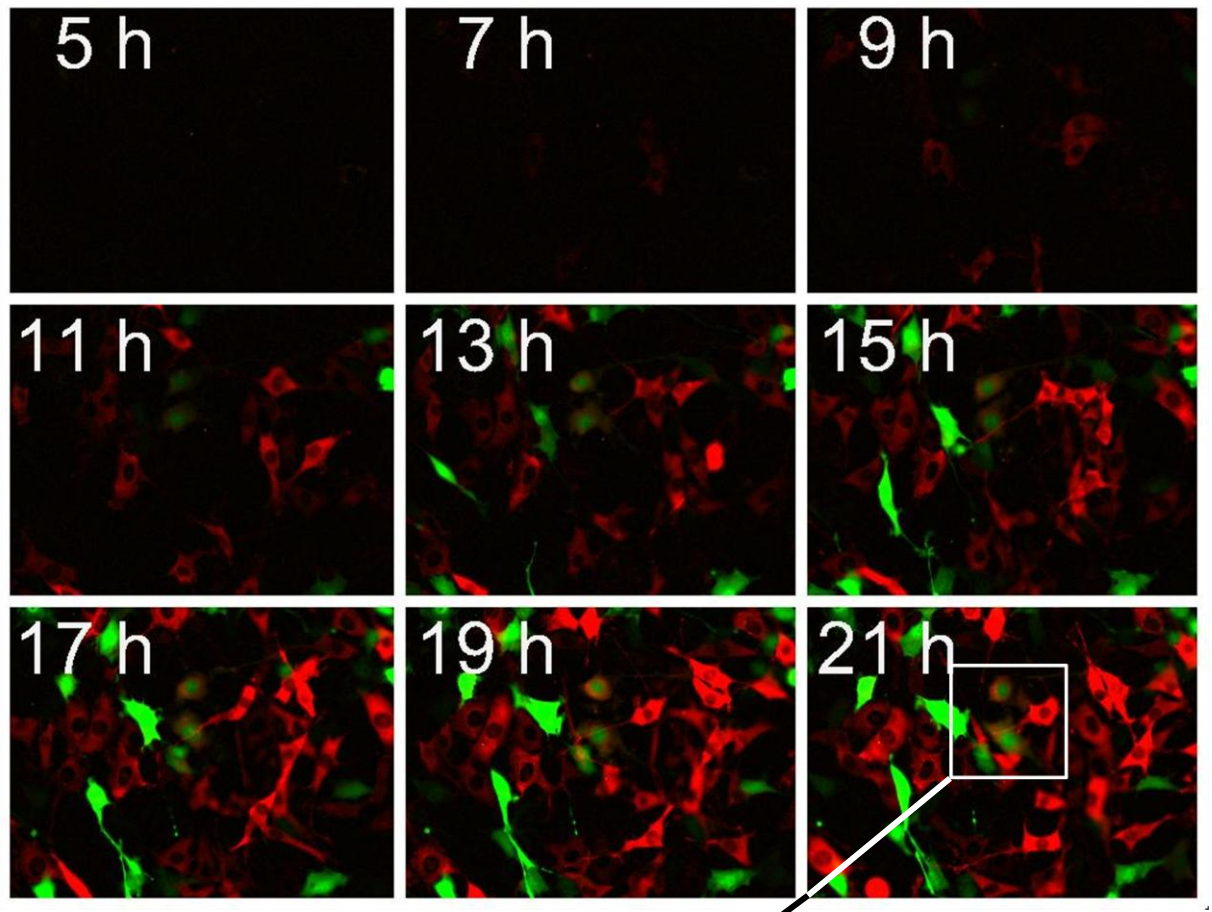

B

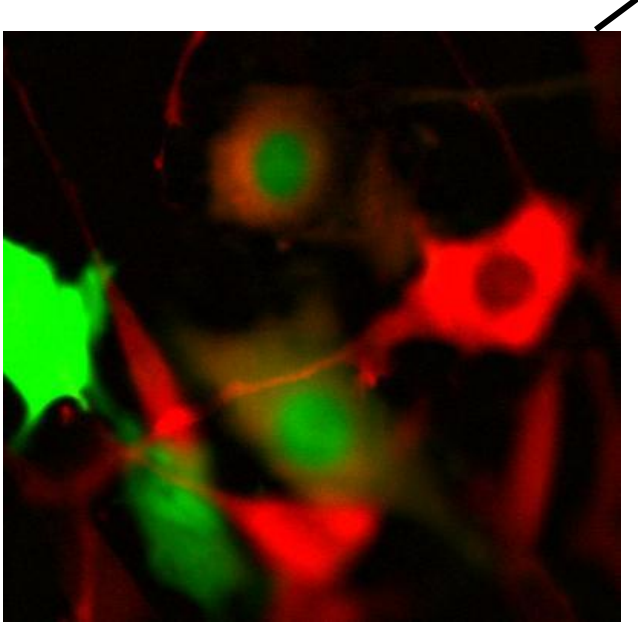

Figure 26: Concomitant IFN-β TurboGFP and NS1-H induction.

IFN-β NS1-H KRAB cells were infected with 80 HAU/ml NDV for 1 h. 4 h post infection, new medium was added including 0.5 µg/ml doxycycline and 20 nM TMR. Subsequently, cells were monitored by time-lapse microscopy taking images every 15 min. A: Fluorescence pictures of the indicated time points pi are shown. B: Cut of fig 27A 21 h pi showing cells double positive for both, IFN-β TurboGFP and NS1-H (TMR).

In figure 26A, the onset of IFN-β TurboGFP and NS1-H within a population of cells is given for the indicated time points. In this experiment, first NS1-H expressing cells appear at approximately 7 - 9 h pi, meaning 3 – 5 h post induction via doxycycline, since it was administered to the cells 4 h pi. In the flow cytometry experiments these cells appear a little belated (compare with fig. 16B) indicating that time-lapse microscopy is more sensitive. Indeed, these results fit to the induction of NS1-H in single cells of a different origin (compare with figure 19B).
First cells positive for IFN-β TurboGFP can be visualized in this particular cutting at 9 – 11 h pi, what is in agreement with the results for untransfected cells (Rand, 2010). From this time on, cells positive for both, green and red fluorescence, can also be visualized (see magnification of time point 21 h pi in fig. 26B). At late time points pi, many cells positive for either IFN-β TurboGFP or NS1-H and only a minor number of cells positive for both reporters can be visualized. These cells co-expressed both reporters for around 10 h before the observation was stopped. Three hypotheses can be suggested from ongoing GFP expression in the presence of NS1-H:

i) NS1-H expression does not show an effect on cells that do already express IFN-β TurboGFP.
ii) NS1-H slowly down-regulates IFN-β TurboGFP expression.
iii) NS1-H stops the increase of IFN-β TurboGFP causing a premature plateau phase.

In untransfected IFN-β TurboGFP cells, GFP expression gradually increases after NDV infection, suddenly reaching a maximum of expression and staying at this level (plateau phase). However, maximal expression of IFN-β TurboGFP strongly varies between single cells (Rand, 2010). It would be interesting to determine whether a premature plateau is reached or whether IFN-β TurboGFP expression can even be inverted after perturbation of IFN-β induction. A disruption of ongoing RIG-I-mediated signaling causing arrest or inversion of IFN-β induction has not been demonstrated, yet. However, it cannot be distinguished between a “natural” and a “perturbed” plateau. For this reason, the relation between the time point of perturbator induction and the time point when IFN-β TurboGFP expression stops increasing need to be analyzed. This can be performed by correlating these two parameters with each other after following single cells over time. Indeed, IFN-β TurboGFP and perturbator induction vary strongly in the intensity of their courses, which consequently can lead to a certain variation in the correlation.

In fact, not all cells that are positive for both markers can be used for this measurement. Perturbator onset should occur a certain time before IFN-β TurboGFP arrest or inversion in order to increase the probability that a "perturbed" plateau or even inversion is analyzed. The time period, in which IFN-β TurboGFP and NS1-H have to come up, is small and consequently, only a low frequency of cells shows this pattern. Single cells corresponding to these demands were measured for green and red fluorescence overtime (see the fluorescence profile of a single cell in fig. 27A) and a correlation was performed in the described manner (fig. 27B).

A

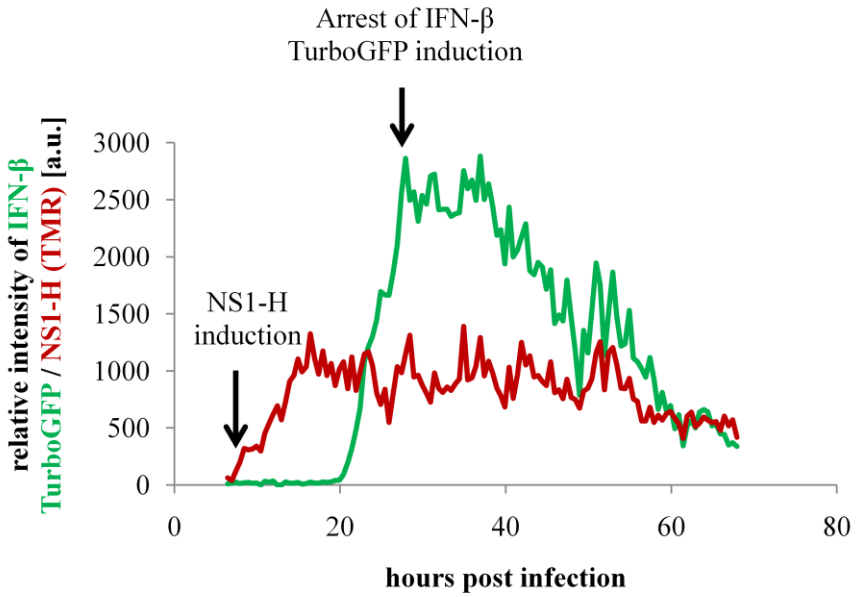

B

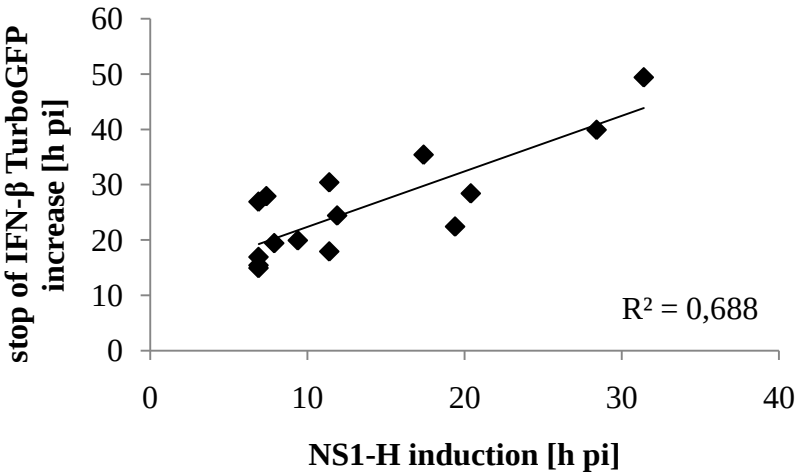

Figure 27: Correlation of NS1-H onset with the termination of IFN-β TurboGFP induction.

IFN-β NS1-H KRAB cells were infected with 80 HAU/ml NDV for 1 h. 4 h pi, a medium exchange was performed for medium containing 0.5 µg/ml doxycycline and 20 nM TMR. Subsequently, cells were monitored by time-lapse microscopy taking images every 30 min. A: Fluorescence profile of a single cell showing onset and course of IFN-β TurboGFP (green line) and NS1-H (TMR, red line). Cells were tracked within the cytoplasm. B: Onset of NS1-H (TMR) induction plotted against the time point of IFN-β TurboGFP induction arrest. 15 single cells were found in this experimental run, measured and related to a linear trend line.

In figure 27A, the course of IFN-β TurboGFP and NS1-H expression of a single cell is given. NS1-H relative intensity starts to come up at ~ 7 h pi and quickly increases until a maximum (plateau phase) is reached at ~ 17 h pi. Meanwhile, IFN-β TurboGFP expression is set on at ~ 20 h pi increasing in intensity until 25 h pi. From 38 h pi on, IFN-β TurboGFP intensity drops continuously.

15 cells which fulfill the above described demands for the correlation were found in this experimental run. 39 % of them showed an inverted phenotype and 61 % of the determined cells went to plateau phase. To demonstrate whether the establishment of an IFN-β TurboGFP plateau or its inversion can be related to NS1-H expression, the arrest of IFN-β TurboGFP increase was plotted against NS1-H induction (fig. 27B). A linear trend line was drawn to compare the events with each other. It is obvious that the determined events reflecting single cells do not strongly deflect from the trend line ($R^2 = 0.69$), indicating that the time between NS1-H increase and IFN-β TurboGFP arrest is constant. Indeed, the time span between NS1-H increase and IFN-β TurboGFP arrest or inversion is 12 h with a standard deviation of 5.4 h. For most cells, NS1-H increases in the range of 7 to 12 h pi with few strong outliers (mean value 13.6 h, SD 8 h) whereas the maximum of IFN-β TurboGFP is reached between 15 and 29 h pi (mean value 26 h, SD 9.8 h). The difference in the time point of NS1-H increase to previous results can be explained by the fact that in this experiment here, cells were chosen which fulfill specific demands. Probably, early NS1-H expressing cells would not be able to additionally induce IFN-β TurboGFP, because the NS1-H value in these cells does not allow it.

These results indicate that the arrest of IFN-β TurboGFP increase and the induction of NS1-H are related to each other and that belated interruption of IFN-β induction is possible via perturbation by NS1-H.

In this experimental setup, cells could also be observed in which NS1-H expression decreases and IFN-β TurboGFP was subsequently induced even though doxycycline was present, what was not expected (data not shown). Also, it could be observed that IFN-β TurboGFP expression is not affected if only low

levels of NS1-H are expressed, giving rise to a certain threshold that needs to be reached by NS1-H to affect IFN-β TurboGFP expression.

3.5.2 Interference of NS3/4A-H and IFN-β TurboGFP expression in living single cells

The perturbation mechanism of NS3/4A differs significantly from the perturbation via NS1. Some discrepancies in the corresponding perturbation patterns could already be shown by flow cytometry analyses. Single cell analyses can shed light on further differences between the two perturbators as well as on the dynamics of IFN induction. Single cell analyses were already shown for NS1-H. In the following, live cell imaging of IFN-β perturbation via NS3/4A-H will be performed.

Concerning the onset of IFN-β TurboGFP and NS3/4A-H in a population of cells, a similar picture could be observed after time-lapse performance as for NS1-H (compare with fig. 26A); hence this is not shown again. Indeed, single cells expressing both, IFN-β TurboGFP and NS3/4A-H were measured for the ability of NS3/4A-H to arrest or invert IFN-β TurboGFP expression. For this reason, time-lapse microscopy was performed for IFN-β NS3/4A-H KRAB cells infected with NDV. Since flow cytometry analyses displayed highest amounts of cells positive for IFN-β TurboGFP as well as for NS3/4A-H at 6 to 12 h pi, doxycycline was administered 10 h pi. In this run, 14 cells fulfilled the demands which were already described for the correlation of NS1-H induction with the arrest of IFN-β TurboGFP increase.

A

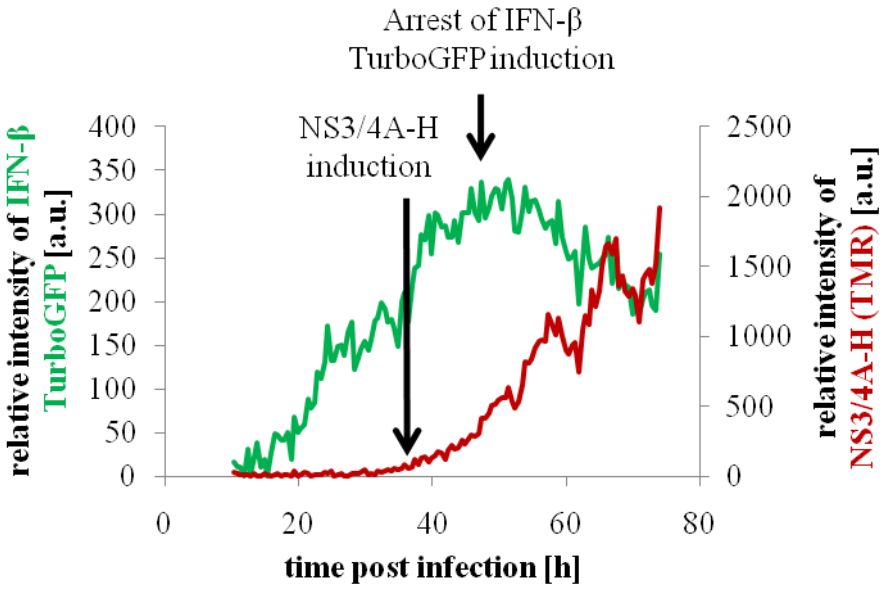

B

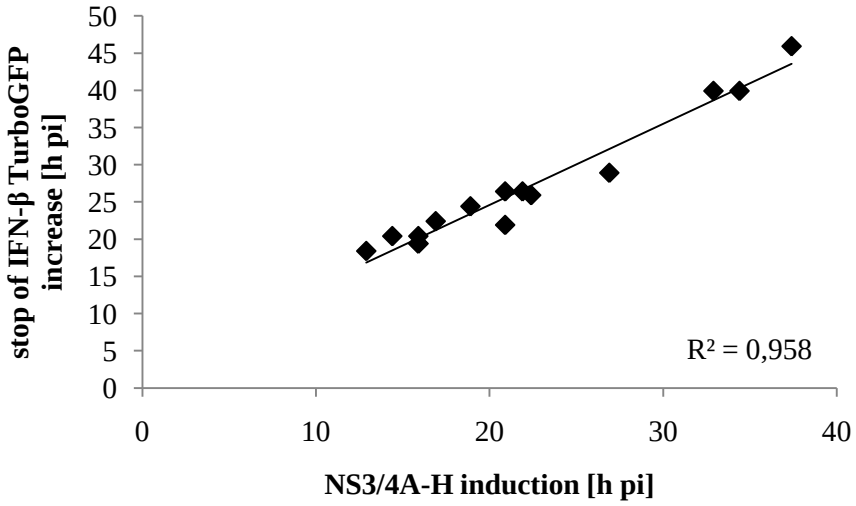

Figure 28: Correlation of NS3/4A-H onset with arrest or inversion of IFN-β TurboGFP induction.

IFN-β TurboGFP cells harboring NS3/4A-H and KRAB were infected with 80 HAU/ml NDV for 1 h. A medium exchange was performed for medium containing 0.5 µg/ml doxycycline and 20 nM TMR 10 h pi. Subsequently, cells were monitored by time-lapse microscopy taking images every 30 min. The subsequent measurement of fluorescence intensities was done in the cytoplasm of the cells. A: Fluorescence profile of a single cell showing onset and course of IFN-β TurboGFP (green line) and NS3/4A-H (TMR, red line). B: Onset of NS3/4A-H (TMR) induction plotted against time point of IFN-β TurboGFP arrest or inversion. 14 single cells could be measured from this run and were related to a linear trend line.

For this experiment, 33 % of the cells showed an inverted phenotype, whereas 67 % terminated IFN-β TurboGFP increase and went over to plateau phase. The fluorescent profile of one cell of the first group is demonstrated in figure 28A. For this cell, IFN-β TurboGFP is induced around 16 h pi and maximally expressed at ~ 46 h. Afterwards, IFN-β TurboGFP intensity decreases again. NS3/4A-H is induced at ~ 37.5 h and continuously increases until the end of the measurement. The graphs attract attention concerning the transition point of IFN-β TurboGFP expression, because slightly before (~8.5 h pi) NS3/4A-H starts to intensify. This gives an indication that these mechanisms are coupled with each other. To verify this, a correlation of the induction arrest of IFN-β TurboGFP versus the onset of NS3/4A-H was performed. The result is given in figure 28B. A linear trend line was drawn for better comparability of the individual events with each other. This figure shows that all events hardly deflect from the linear trend line, indicating a strong relation between NS3/4A-H induction and the arrest of IFN-β TurboGFP increase (R^2 = 0.958). This is also underlined by a constant mean value of the time span between NS3/4A-H onset and IFN-β TurboGFP arrest/inversion (4.8 h; SD 1.9 h). NS3/4A-H increase appeared lately, at a mean time point of 21.9 h (SD 7.7) and IFN-β TurboGFP arrest occurs short time later (mean: 26.7; SD 8.6).
These data indicate a strict, time-dependent perturbation of IFN-β TurboGFP expression in the case of NS3/4A-H. The time period between NS3/4A-H onset is shorter and has a lower SD as in the case of NS1-H. This might result from a faster action of NS3/4A-H or could be caused by the perturbation mechanism or the point of action within the IFN-β induction cascade which are multiple for NS1-H. Another reason could be stochasticity within pathway progression.

3.5.3 Inversion of IRF-7 nuclear translocation by NS1-H expression

It was demonstrated that IRF-3, which is necessary for the induction of early type I IFNs, is activated by TBK-1 and IKKε. Also, it was shown that IRF-7, the transcription factor inducing the second, stronger wave of the IFN response, is activated by the same batch of kinases (Sharma et al, 2003). Since IRF-7 shares great homology with IRF-3 it could work as an IRF-3 surrogate in this work.
In the previous experiments it was shown that ongoing IFN-β TurboGFP expression can be interrupted by the viral perturbators. The use of reporter cells stably expressing fluorescently labeled IRF-7 and the doxycycline-dependent NS1-H cassette would allow answering the question whether translocation of activated IRF-7, which is an event upstream of IFN-β induction, can also be inverted by perturbation of the cascade. The temporal dynamics between NS1-H

onset and the relocation of IRF-7 will be of interest and can be compared to previous results for IFN-β TurboGFP perturbation.
For the further perturbation experiments, NIH3T3-based reporter cells stably expressing IRF-7 fused to the cyan fluorescence protein (CFP) were used (Rand, 2010). These reporter cells are further called IRF-7-C. By means of these cells, U. Rand could show that virus-induced IRF-7 translocation is a stochastic process ranging from 6 to 22 h pi. He could also demonstrate that a very consistent delay of 2 - 6 h occurs between IRF-7 translocation to the nucleus and IFN-β TurboGFP onset. This indicates a relation between the two events.

3.5.3.1 Characterization of IRF-7-C reporter cells expressing NS1-H

IRF-7-C reporter cells were stably transfected with the rtTA2 construct and, in a second transfection step, with the construct harboring NS1-H under control of P_{Tight}, an improved variant of P_{Tet} which demonstrates lower basal leakiness and higher inducibility due to reduction of potential transcription factor binding sites in the spacer region between the *tet*Os (Clontech, 2003). With this promoter, the additional integration of KRAB could be lapsed.
24 single clones were measured for leaky expression and for inducibility of NS1-H. Most of them displayed low basal expression (data not shown), but one clone displayed exceptional low levels. Indeed, this clone (fig. 29) shows proper regulation of NS1-H upon doxycycline administration. For these reasons, it was used for further experiments and termed IRF-7 NS1-H.

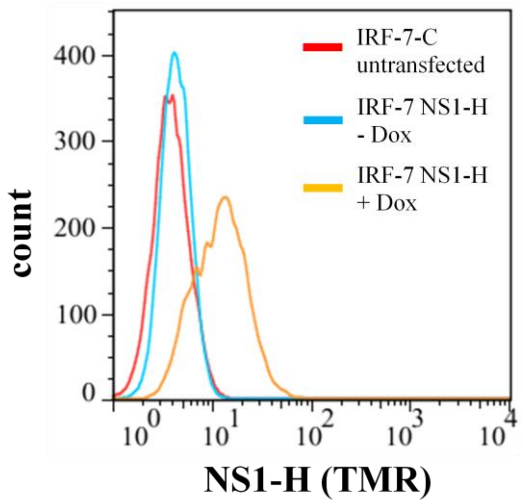

Figure 29: Regulation of NS1-H in IRF-7-C cells.

IRF-7 NS1-H cells were either treated with doxycycline for 3 d or left untreated and stained with TMR. Cells were measured for the amount of NS1-H (TMR) positive cells by flow cytometry. The histogram shows an overlay of untransfected IRF-7-C reporter cells with uninduced and induced IRF-7 NS1-H cells.

Since NS1-H is known to at least partially block the IFN induction pathway upstream of the kinases TBK-1 and IKKε, it is unclear whether marginal NS1-H basal expression could block translocation of the IRF-7 CFP fusion.

Consequently, the IRF-7-C reporter cells harboring NS1-H were measured for the ability of IRF-7-C to translocate in the presence of potential basal NS1-H expression. The cells were infected with NDV and time-lapse recording was performed (figs. 30A and B).

A

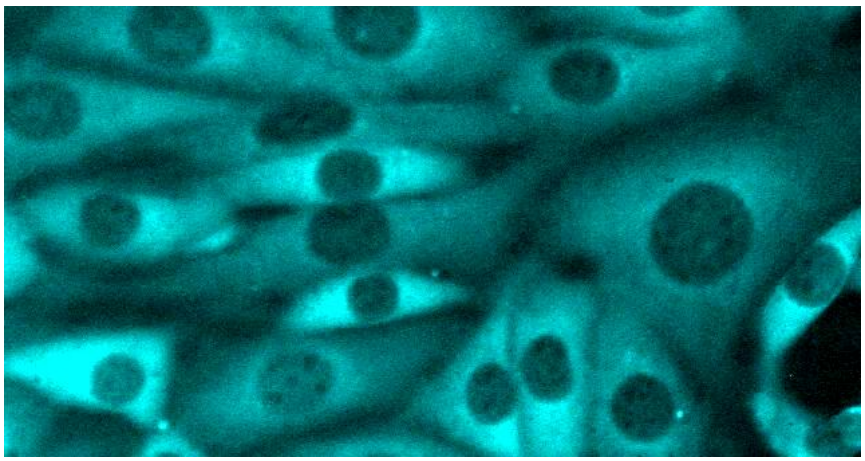

B

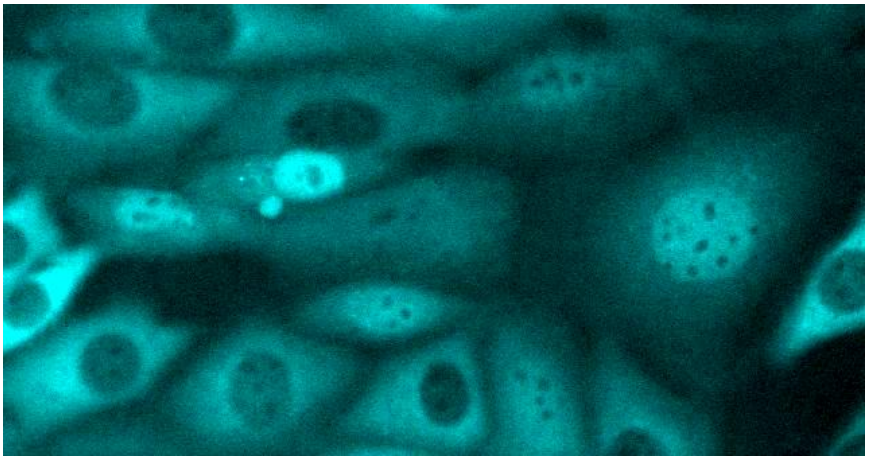

Figure 30: Nuclear accumulation of IRF-7 CFP in IRF-7 NS1-H cells.

IRF-7 NS1-H cells were seeded on a collagen-treated chambered microscopy slide at a density of 2.5 * 10^4 cells/well. Adherent cells were infected with 80 HAU/ml NDV for 1 h and subsequently monitored by time-lapse microscopy. A: Cells before nuclear accumulation of IRF-7 CFP (12:35 h pi). B: Cells showing nuclear accumulation of IRF-7 CFP (20:05 h pi).

Uninduced IRF-7 NS1-H cells do not show nuclear accumulation of IRF-7-C at early time points after infection (12:35 h pi), which is expected (fig. 30A). However, translocation can clearly be monitored at later time points pi (20:05 h

pi; fig. 30B). This indicates that even though minor levels of NS1-H could constantly be present in the cells, the translocation of IRF-7 CFP is still possible. Certainly, these pictures do not show whether the translocation efficiency is somehow altered. For this reason, the number of IRF-7 CFP translocation events in equally treated untransfected IRF-7-C cells and IRF-7 NS1-H cells was measured. As a proof for the perturbing effect of NS1-H on the level of RIG-I-mediated signaling, a third batch of IRF-7 NS1-H cells, which were pre-treated with doxycycline from 24 h pi on, was also counted for translocation events.
As expected, in the case of doxycycline treatment, only a minor part of cells shows translocation (~13 %). For the uninduced IRF-7 NS1-H cells, 30 % of the cells translocate. 47 % of the untransfected cells are displaying translocation events (fig. 31).
These results demonstrate that potential basal levels of NS1-H cause decreased translocation events in the described cells, even though basal expression could hardly be measured by flow cytometry. This is probably due to the limited sensitivity of this assay, as mentioned before. Indeed, this effect was shown to be caused by NS1-H, since induction of NS1-H leads to a further decrease.

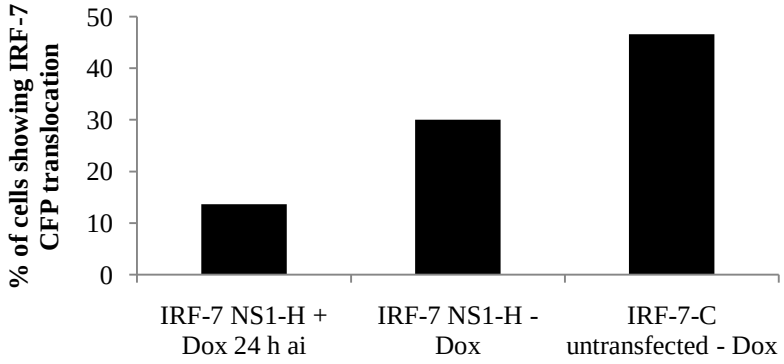

Figure 31: Comparison of translocation events in IRF-7-C and IRF-7 NS1-H cells.

IRF-7-C and IRF-7 NS1-H cells were seeded on a collagen-treated chambered microscopy slide at a density of 2.5 * 10^4 cells/well. Adherent cells were infected with 80 HAU/ml NDV for 1 h and subsequently monitored by time-lapse microscopy. The percentage of translocating cells within the analyzed sections is given. The first bar demonstrates IRF-7 NS1-H cells that were pre-treated with doxycycline from 24h ai on (n = 153). The second bar shows uninduced IRF-7 NS1-H cells (n = 227). The third bar displays untransfected cells (n = 119).

Even though IRF-7 NS1-H cells display attenuation compared to untransfected cells, these cells were used for further perturbation experiments, since a respective amount of cells still responds to NDV infection.

3.5.4 Inversion of IRF-7 CFP translocation after perturbation with NS1-H

In this work, it was shown that the appearance of IFN-β TurboGFP protein is strongly altered in response to the presence of NS1-H and that ongoing expression can be blocked or even inverted. It was of interest to find out whether the relocation of IRF-7 CFP into the cytoplasm can be initiated by NS1-H. Indeed, nucleus to cytoplasm relocation is a naturally occurring event, which has to be further elucidated. For this reason, a correlation between the time point of NS1-H induction and IRF-7 CFP relocation was chosen to display a possible relation between the two events.

For the determination, cells were monitored using time-lapse microscopy. Single cells were tracked for NS1-H relative intensity in the cytoplasm and tracks for IRF-7 CFP were taken for the relative intensity in the cytoplasm and in the nucleus. The nucleus/cytoplasm ratio of IRF-7 CFP was determined and values higher than "1" indicate nuclear translocation.

A

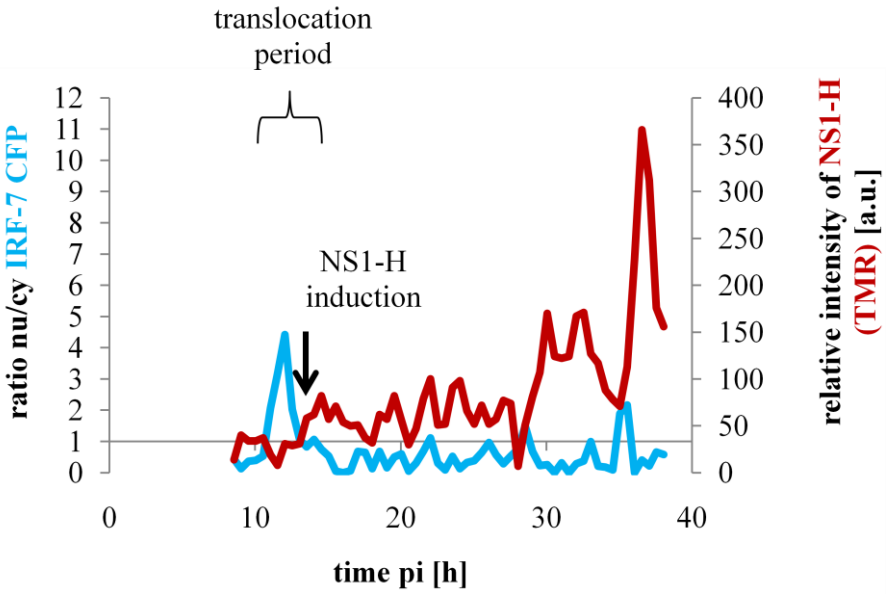

B

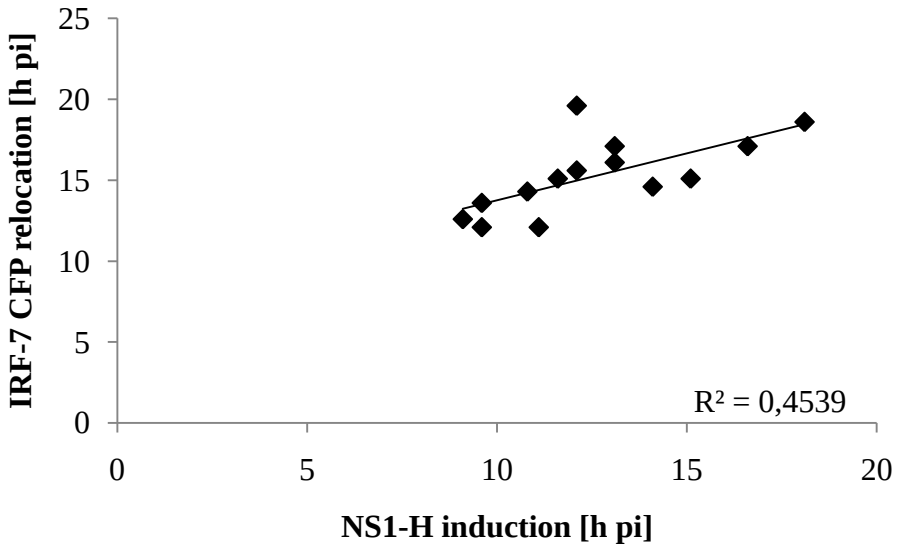

Figure 32: Correlation of NS1-H induction with IRF-7 CFP nuclear-cytoplasmic relocation.

IRF-7 NS1-H cells were infected with 80 HAU/ml NDV for 1 h. 8 h pi, a medium exchange was performed for medium containing 0.5 µg/ml doxycycline and 20 nM TMR. Subsequently, cells were monitored by time-lapse microscopy taking images every 30 min. A: Fluorescence profile of a single cell showing onset and course of NS1-H (TMR, red line) and IRF-7 CFP ratio of nucleus/cytoplasm (blue line). Values higher than "1" indicate nuclear translocation. B: NS1-H (TMR) induction plotted against time point of IRF-7 CFP nuclear-cytoplasmic relocation of 14 single cells (related to a linear trend line).

The NS1-H induction graph versus nucleus/cytoplasm ratio of IRF-7 CFP is shown in figure 32A. NS1-H expression is induced around 12 h pi in this single cell. Translocation appears 10 h pi and persists for 4.5 h with a maximum at the same time point of NS1-H induction. Inversion of translocation shortly after NS1-H induction could indicate an influence of the perturbator on this behavior. Since relocation also occurs in untransfected cells, it was of interest to determine the relation between NS1-H induction and IRF-7 CFP relocation by means of a correlation (fig. 32B). For this correlation, cells were chosen which show relocation of IRF-7 CFP after NS1-H onset. 14 cells in this experiment fitted to the demands. One of these cells showed a slightly higher aberration than the others and caused a drop of the correlation coefficient from 0.7 to 0.45, what needs to be mentioned since the other 13 cells show much higher consistency. Anyway, this correlation clearly demonstrates that NS1-H induction is related to IRF-7 CFP relocation showing that NS1-H can indeed cause shuttling of IRF-7 CFP from the nucleus to the cytoplasm what is probably coupled with the earlier

demonstrated interruption of IFN-β TurboGFP induction. Indeed, the mean period between pathway induction (NDV infection) and IRF-7 CFP relocation is 15.3 h (SD 2.3 h). The time span between NS1-H onset and IRF-7 CFP relocation was determined to be low for all tested cells (mean: 2.7 h; SD: 2 h) which is expected since IRF-7 relocation occurs upstream of IFN-β TurboGFP arrest. The short time frame also demonstrates the influence of NS1-H on a factor closely related to IRF-7. Interruption in this case is assumed to appear fast.

As demonstrated for the cell in figure 32A, IRF-7-C cells expressing NS1-H show a relatively short retention time of IRF-7 CFP within the nucleus. It was previously demonstrated that IRF-7 CFP has a retention time of 12.6 h (SD: 7.2 h) within the nucleus of IRF-7-C cells (Rand, 2010). However, for cells expressing NS1-H after doxycycline treatment, this time span is significantly decreased to 5 h (SD: 2.4; fig. 33). Untreated IRF-7 NS1-H cells do not show significantly different nuclear accumulation of IRF-7 CFP (4 h; SD: 3.7). This might indicate a lack in significance due to small sample numbers (n=12 for untreated and n=8 for doxycycline-treated IRF-7 NS1-H cells). Procentual standard deviation shows highest variation in case of untreated IRF-7 NS1-H cells (94 %). For the doxycycline-treated cells, this value is about 47 % and 57% for untransfected cells, indicating more pronounced effects for the cells expressing NS1-H.

These data also give a hint that a premature relocation occurs through NS1-H, because retention time within the nucleus is drastically decreased for cells that undergo relocation of IRF-7 CFP.

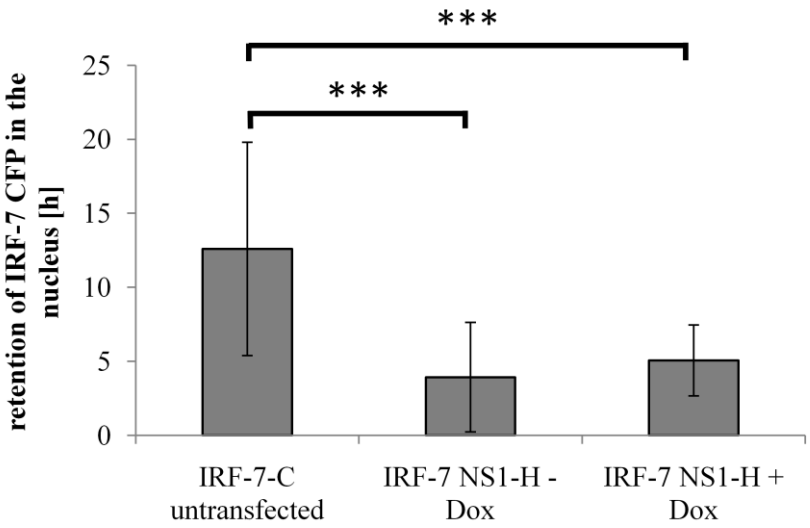

Figure 33: IRF-7 CFP retention in the nucleus of untransfected and IRF-7 NS1-H cells.

IRF-7-C and IRF-7 NS1-H cells were seeded onto a collagen-treated chambered microscopy slide at a density of 2.5 * 10^4 cells/well. Adherent cells were infected with 80 HAU/ml NDV for 1 h and treated with 0.5 µg/ml doxycycline 4 – 8 h pi, if necessary. Subsequently, cells were monitored by time-lapse microscopy taking pictures every 30 min. The retention time of IRF-7 CFP is given in the figure. The first bar demonstrates IRF-7 CFP retention in IRF-7-C cells. These data were kindly provided by U. Rand (2010; n = 55). The second bar demonstrates the retention time of IRF-7 CFP in IRF-7 NS1-H cells (n = 12) and the third bar shows these cells exposed to doxycycline (n = 8). The p-value between the untransfected cells and IRF-7 NS1-H cells without doxycycline is $1.17 * 10^{-6}$. Untransfected cells compared to doxycycline-treated IRF-7 NS1-H cells have a p-value of $2.3 * 10^{-6}$. P-values were calculated by student's t test.

3.6 Specificity of NS1-H and NS3/4A-H for the perturbation of early IFN induction

In the previous experiments it was shown that as well NS1-H as NS3/4A-H are potently interfering with IFN-β TurboGFP induction. Furthermore, it was clearly demonstrated that NS3/4A-H is a much stronger IFN antagonist, of which already low levels are sufficient to interrupt IFN-β induction. In the introduction it was said that both factors are specifically interacting with this cascade, whereas NS1-H acts at multiple steps and NS3/4A-H cleaves one important factor of the pathway (chapters 1.9 – 1.10). However, publications for both, NS1 and NS3/4A affirm a potential influence of the factors on IFN-induced signaling (Helbig et al, 2008; Jia et al, 2010). At least for NS1 could be shown that the anti-IFN mechanisms are strain-and cell type-specific (Han et al, 2010; Hayman et al, 2006; Melén et al, 2007). To clarify these assumptions about an effect of NS1 or NS3/4A on JAK/STAT signaling and therefore the induction of ISGs, an experiment was performed using two further reporter cells. They are based on NIH3T3 and harbor a BAC with the locus for an ISG, the murine *Mx2* gene. In one of them luciferase and in the other tdTomato is driven by the Mx2 promoter (Pulverer, 2008; Pulverer et al, 2010). These cells show high induction of the reporters upon induction of the IFN signaling cascade and exhibit basal levels of luciferase or tdTomato in the uninduced state.

3.6.1 Mx2 reporter cells harboring NS1-H

The constructs coding for doxycycline-dependent NS1-H and the construct harboring the constitutively expressed rtTA2 were stably introduced into the cells displaying Mx2 induction by luciferase expression (Mx2Luc). The best clone was stably transduced with a lentivirus harboring the constitutively expressed KRAB repressor to lower basal NS1-H expression. After selection, 5 regulated clones were characterized for low basal expression and high inducibility of NS1-H. The most promising clone (Mx2Luc NS1-H) was used for further experiments (fig. 34). Proper luciferase inducibility was also assumed (data not shown).

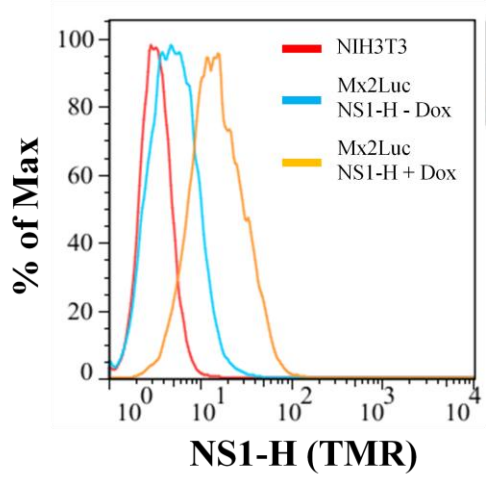

Figure 34: Expression characteristics of the Mx2Luc NS1-H clone.

Mx2Luc NS1-H cells were either treated with doxycycline for 3 d or left untreated and stained with TMR. Cells were measured for the amount of NS1-H (TMR) positive cells by flow cytometry. In the histogram, the fluorescence of untransfected NIH3T3 cells is compared with the fluorescence of uninduced and induced Mx2Luc NS1-H cells. As a control for these cells serve NIH3T3 wt cells.

For untransfected Mx2Luc cells, it was shown that maximal luciferase amounts after stimulation with 500 Units (U) of IFN-β can be obtained 24 h post induction (Pulverer, 2008). For this purpose, this time point was elected for further determinations. Since measurements will also be performed after NDV infection, it was necessary to analyze the time point of maximal luciferase induction after NDV infection in order to obtain comparable results. For this purpose, equal amounts of Mx2Luc NS1-H cells were seeded and infected with 80 HAU/ml NDV. Cells were harvested at the indicated time points pi (fig. 35) and measured for luciferase activity.

Mx2Luc expression already shows an increase 24 h pi. The climax of the reporter cells was measured 48 h pi and for later time points, a decrease in Mx2 promoter activity was realized. Luciferase levels that come close to basal expression were obtained 5 d pi.

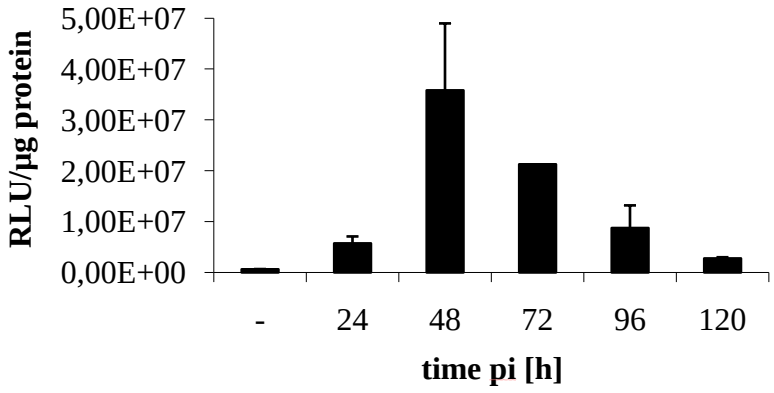

Figure 35: Mx2 induction in response to NDV infection.

Mx2Luc NS1-H cells were infected with 80 HAU/ml NDV for 1 h. At the indicated time points pi, cells were harvested and whole cell extracts were prepared. Luciferase activity was measured (as described in Materials and Methods). The data shown represent average values +/- SD of 3 experiments. For the 72 h value, no SD is given, since only one experiment was performed.

3.6.2 NS1-H does not affect interferon stimulated gene expression

As previously described in this work, early IFN induction in response to viral infection could be efficiently perturbed. However, a second, even stronger wave of IFN induction follows when secreted IFN-α/β molecules bind to the IFNAR receptor which induces JAK/STAT signaling (see introduction chapter 1.7.5 and fig. 2) and targets in the induction of ISGs.
H5N1 NS1 interferes with JAK/STAT signaling in HeLa cells by inhibiting STAT phosphorylation due to restriction of IFNAR and induction of SOCS protein expression (Jia et al, 2010). Furthermore, it is known that NS1 acts at the post-transcriptional level by blocking host cell mRNA processing and nuclear export (Hale et al, 2008). It was investigated whether the influenza strain PR8 encoded NS1 protein (as used in this study) influences IFN signaling and therefore might also affect the induction of ISGs like IRF-7 or Mx2. This will show whether PR8 NS1 perturbation is specific for IFN induction and whether NS1-H also acts on the post-transcriptional level.
In the present case, JAK/STAT signaling was either directly induced by administration of 500 U/ml IFN-β into the medium of cells or by NDV infection. The latter method leads to the secretion of early IFNs which subsequently bind to the IFNAR receptor causing JAK/STAT signaling. By these methods the direct and indirect effect of the perturbator on this pathway can be shown.
NS1-H expression was induced at varying time points relative to IFN-β induction or NDV infection. After harvesting, cells were measured for luciferase activity.

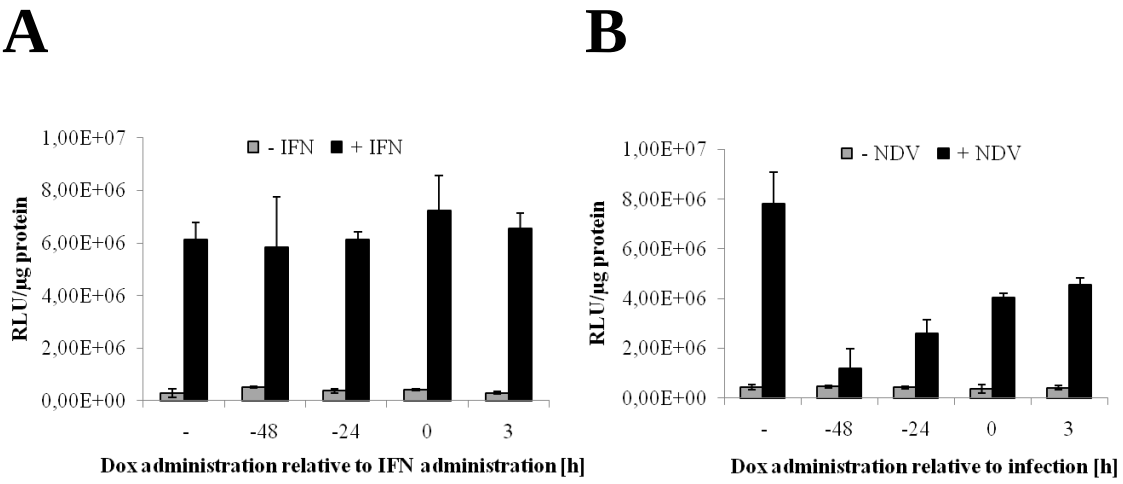

Figure 36: Influence of NS1-H on JAK/STAT signaling.

Mx2Luc NS1-H cells were treated with 2 µg/ml doxycycline at certain time points relative to IFN-β induction/NDV infection. A: Cells were exposed to 500 U of IFN-β. B: Cells were infected with 80 HAU/ml NDV for 1 h. 48 h pi or rather 24 h post induction via IFN-β, cells were harvested for analysis of luciferase activity (as described in Materials and Methods). The data shown represent average values +/- SD of 3 experiments.

In figure 36A, it is clearly visualized that the NS1 variant used in this work does not directly influence IFN-β-mediated signaling, since no alteration of luciferase could be detected for any time point of NS1-H induction. Levels are constant at approximately 6 million RLU/µg protein.
Indeed, when cells were infected with NDV, a time-dependent decrease of luciferase can be observed. Since JAK/STAT signaling is not influenced by NS1-H expression, this effect fully reflects the influence of NS1-H on IFN induction. Also doxycycline administration pi still leads to a decrease in the Mx2 response. Similar results could be seen for flow cytometry analyses (fig. 21A). Consequently, the results for Mx2 support the results gained for IFN-β NS1-H cells.
The fact that NS1-H does not influence IFN-β-induced luciferase expression also shows that neither post-transcriptional nor –translational mechanisms of NS1-H occur.

3.6.3 Reporter cells for monitoring the influence of NS3/4A-H on Mx2 induction

For the NS1 variant used in this work, no direct influence on JAK/STAT signaling could be measured. It was of further interest to see whether NS3/4A-H of JFH-1 strain directly affects this pathway.

So far, contradictory results were obtained by independent groups. For instance, Cheng et al. (2006) declared that NS3/4A leaves IFN signaling intact, whereas two other groups claimed a perturbing effect (Helbig et al, 2008; Lin et al, 2005).
In order to be able to clarify this, an NS3/4A-H expressing clone of Mx2Tom reporter cells was established. Regulation of NS3/4A-H upon doxycycline administration is displayed in figure 37. Low basal expression of NS3/4A-H could also be detected. Mx2Tom NS3/4A-H cells as depicted in figure 37 were used for further analyses.

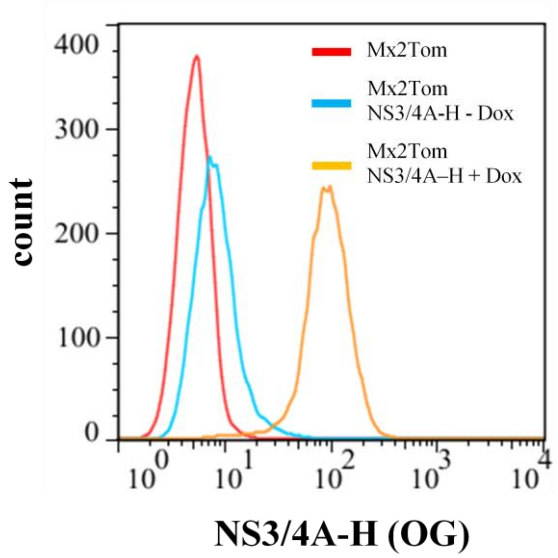

Figure 37: Expression characteristics of NS3/4A-H in Mx2Tom cells.

Mx2Tom NS3/4A-H cells were either treated with doxycycline for 3 d or left untreated and stained with Oregon Green (OG). Cells were measured for the amount of NS3/4A-H (OG) positive cells by flow cytometry. In the histogram, the fluorescence of untransfected NIH3T3 cells is compared to the fluorescence of uninduced and induced Mx2Tom NS3/4A-H cells.

The direct influence of NS3/4A-H on JAK/STAT signaling was to be determined in Mx2Tom NS3/4A-H cells. For this purpose, it was necessary to induce this pathway via IFN-β administration to the medium. In this case, pre-treatment with doxycycline does not alter Mx2Tom expression (fig. 38A) indicating that NS3/4A-H does not affect JAK/STAT signaling. Since the question arises, whether Mx2Tom alteration via NS3/4A-H can be visualized in these cells, Mx2Tom induction was also measured 48 h after NDV infection. In untransfected Mx2Tom cells, proper induction after NDV infection was measured by this method (data not shown). Cells were also pre-treated with or without doxycycline, but Mx2Tom induction could neither be shown in the presence nor in the absence of doxycycline (fig. 38B). This indicates that NS3/4A-H basal expression totally blocks IFN induction and does not allow IFN-β secretion and binding to IFNAR. Together with the previous findings, these results demonstrate that NS3/4A-H effectively acts on IFN induction, but not on JAK/STAT signaling.

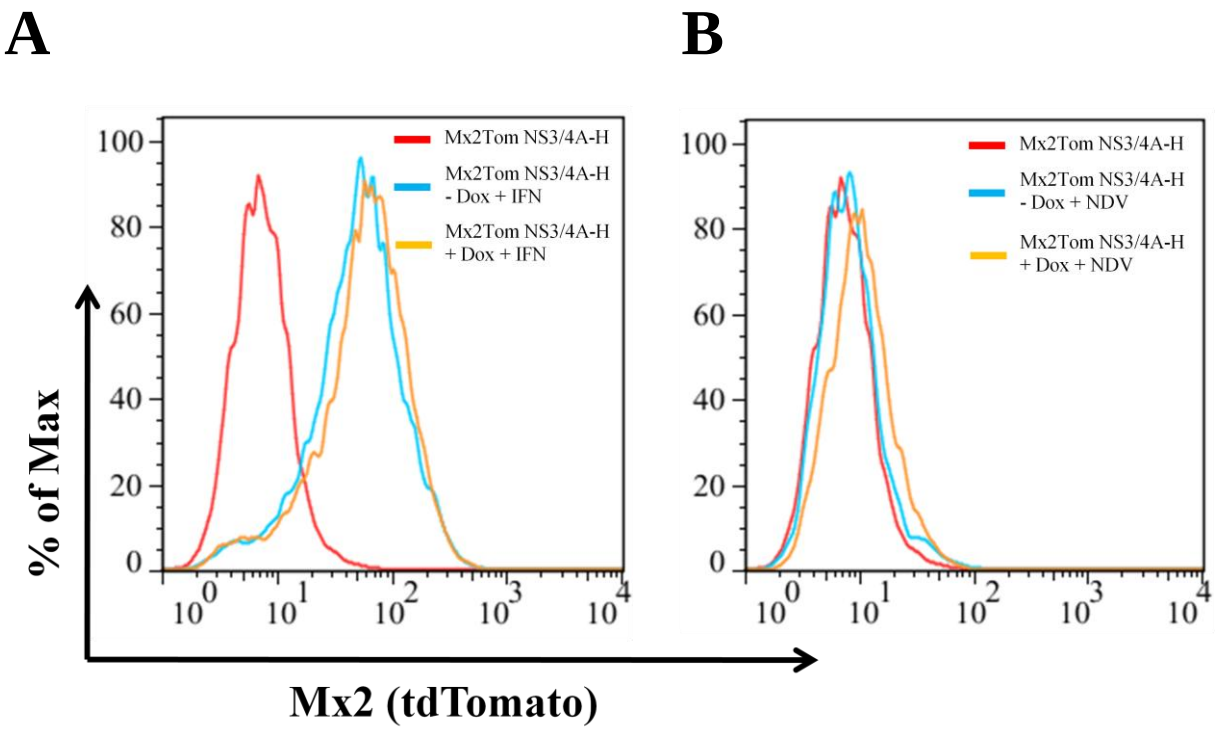

Figure 38: Influence of NS3/4A-H on JAK/STAT signaling.

Mx2Tom NS3/4A-H cells were treated with 2 µg/ml doxycycline. A: Cells were exposed to 500 U of IFN-β. B: Cells were infected with 80 HAU/ml NDV for 1 h. 24 h pi or rather 48 h post IFN-β induction, cells were measured for the amount of Mx2Tom positive cells by flow cytometry. In the histogram, the fluorescence of uninfected Mx2Tom NS3/4A-H cells is compared to the fluorescence of uninduced and induced Mx2Tom NS3/4A-H cells 48 h post NDV infection.

3.7 A synthetic mammalian oscillator

In the previous experiments, a successful, synthetic biology approach for the perturbation of a cellular network was shown. However, synthetic biology also aims at rebuilding biological circuits and designing components and networks that do not yet exist in nature. These factors or networks should give predictable function and be inert to the cellular machinery.
A very recent synthetic biology approach is the establishment of oscillatory circuits in mammalian cells. First synthetic oscillators were demonstrated to work in prokaryotes and lower eukaryotes. In 2009, the first oscillator was shown in mammalian cells (Tigges et al, 2009). However, this approach was only successful in transient experiments (see chapter 1.6 of introduction).

3.7.1 Towards a stable, synthetic mammalian oscillator

The aim of this part of the work was to establish a stable oscillator in mammalian cells. The oscillator should consist of one positive and one time-delayed negative feedback loop that are reciprocally regulated. Important is that the negative feedback loop does not totally block the expression of the positive part, because otherwise, expression of both would be interrupted in a delayed manner. To visualize oscillation, at least these loops were coupled to the expression of a fluorescence reporter. The onset as well as the amplitude of oscillation should be regulated by an external inducer.
Our approach is based on two mammalian expression systems, the Tet-(Off) and the Cou system (see chapter 1.4 - 1.5 of introduction), that are independently regulable from each other (Kästner, 2007). The coumermycin-dependent promoter (P_{Cou}) drives the expression of the KRAB repressor and a destabilized variant of the marker protein TurboRFP (tRFP, Evrogen). The CouTA, tTA and a destabilized TurboGFP (tGFP, Evrogen) are expressed from P_{Tet}. TurboRFP and TurboGFP are fused to the destabilizing sequence PEST (Li et al, 1998; Rogers et al, 1986). For simplicity, the markers which indicate the state of the respective proteins driven by the same promoter are not mentioned further. The mechanism of oscillation is described in figure 39.

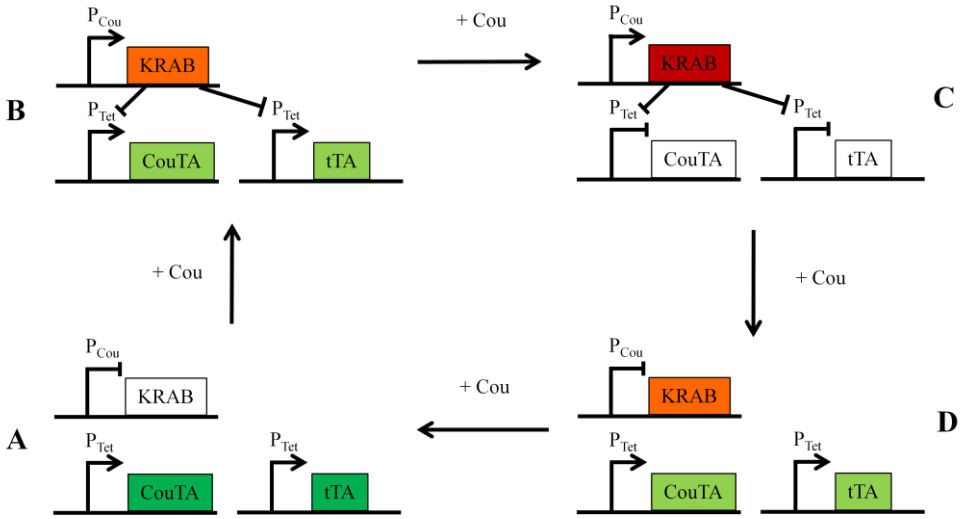

Figure 39: Design of the synthetic oscillator.

In the absence of doxycycline, the tTA and the CouTA are continuously expressed (A). When coumermycin is present, the CouTA dimerizes and binds to P_{Cou} where it induces KRAB expression (B). The KRAB repressor binds to P_{Tet} and represses expression from this promoter (C). tTA and CouTA are not built until the CouTA in the cell is depleted. Then, expression of KRAB terminates and because of the autoregulated tTA expression, tTA and CouTA come up again and the circuit starts anew (D). An approximate state of tGFP and tRFP expression is indicated by light and dark coloring of the components. Fine-tuning of the network occurs via control of transactivator expression by the administration of doxycycline.

The components that are necessary for this oscillator are assembled on two vectors which harbor each a different selection marker. The composition of these vectors is demonstrated in figure 40.

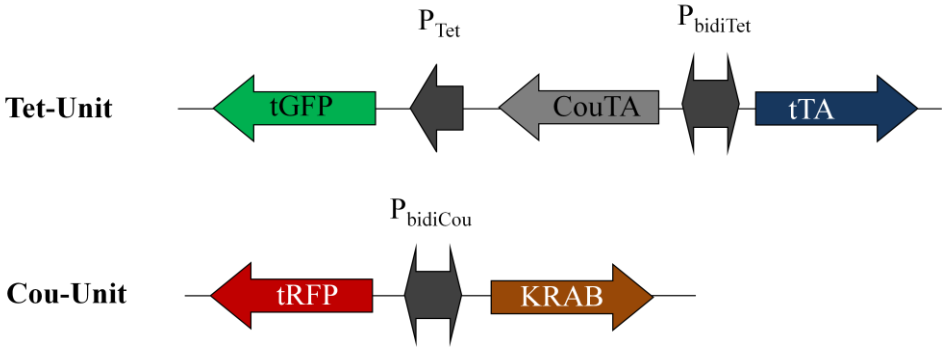

Figure 40: Composition of the oscillator vectors.

Two vectors with different selection markers harboring all necessary components for the oscillator were constructed. The so-called Tet-Unit is composed of a bidirectional tetracycline-dependent promoter ($P_{bidiTet}$) driving the expression of the Tet-Off tTA on the one hand and the CouTA on the other hand. A second, unidirectional P_{Tet} controls the expression of tGFP. The second construct, the Cou-Unit, is composed of a bidirectional coumermycin-dependent promoter ($P_{bidiCou}$) driving the expression of the KRAB repressor and tRFP to monitor the intracellular levels of the KRAB repressor.

3.7.2 Doxycycline-dependent expression upon stable implementation of the Tet-Unit

After verification of the function of all Tet-Unit components in transient (data not shown), it was stably integrated into human embryonic kidney cells stably harboring the SV40 large T-antigen (HEK-293T). 19 stable clones were checked for tGFP expression. Since the Tet-Off system is used for the oscillator, tGFP is expected to be induced in the absence of doxycycline, whereas reduced levels are expected in the presence of doxycycline.
Unfortunately, none of the clones showed strong expression and especially none showed reliable regulation (fig. 41A). However, the co-transfection of the Tet-Unit and another vector expressing eGFP under the control of P_{Tet} showed by far more expression of GFP (fig. 41B). While almost 100 % of the cells shift to the lower right quadrant in the absence of doxycycline, only 39 % do this in the presence of doxycycline.
Taken together, this means that low levels of tGFP in the induced state are caused by the GFP variant, perhaps by the short half-life. Since the Cou-Unit also contains a marker to describe the state of the components and therefore indicates oscillations, the visualization via tGFP is not mandatory for verification of the oscillator.

A

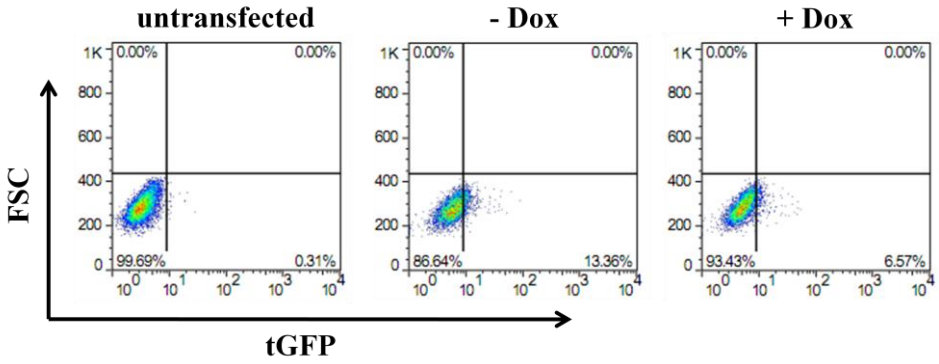

B

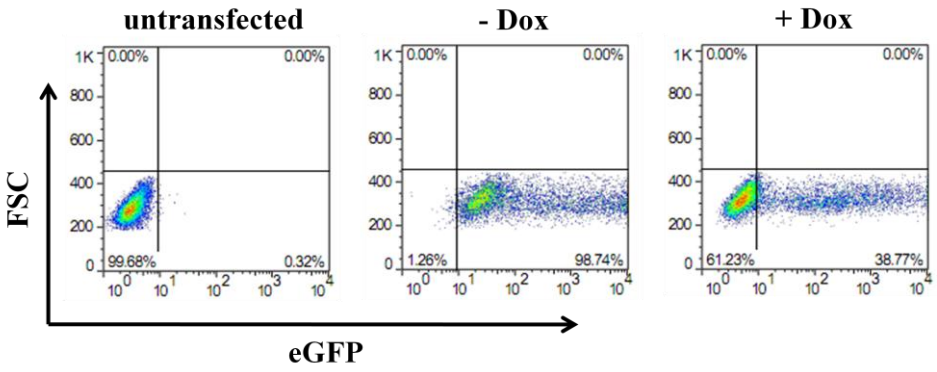

Figure 41: tGFP expression in a stable Tet-Unit expressing clone.

HEK-293T cells stably transfected with the Tet-Unit (A) or stably transfected with the Tet-Unit and transiently transfected with a construct driving eGFP from P_{Tet} (B) were treated with 2 µg/ml doxycycline or left untreated. Flow cytometry measurement was done for the amount of tGFP positive cells ~ 48 h post transfection. Results are displayed as density dot plots (red > blue) showing GFP expressing cells in the lower right quadrant and cells with unchanged fluorescence in the lower left quadrant.

3.7.3 Functionality of the Cou-Unit in stably transfected cells

The Cou-system, a mammalian expression system which is induced upon coumermycin administration, consists of the coumermycin-dependent promoter and the respective transactivator (Zhao et al, 2003). However, the concomitant expression of two genes was not possible due to a lack in a bidirectional promoter. Especially for the herein described oscillator, such a promoter was established. Functionality of the promoter was verified by expressing tRFP from the one and tGFP from the other side (data not shown). With this tool, concomitant expression of tRFP and KRAB from the same promoter is feasible.
The functionality of tRFP in the Cou-Unit was first determined by a transient co-expression with the constitutively expressed CouTA, demonstrating functionality, but high basal levels of the Cou-Unit (data not shown).
Afterwards, HEK-293T cells were stably transfected with the Cou-Unit. Functionality was measured for 23 clones after transient transfection with the constitutively expressed CouTA with or without coumermycin. The best clone shows only slight levels of tRFP positive cells in the absence of coumermycin. However, only low induction was demonstrated to occur in the presence of coumermycin (data not shown).
It was demonstrated that the Cou-Unit is stably integrated into the cells, but it exhibits low tRFP expression. This might be due to the short half-life of this

protein which affects stability during the preparation of the cells for the measurement. However, during live-cell imaging this should not exhibit a problem.

3.7.4 Combination of both units in one cell

After verification of their stable function in HEK-293T cells, the constructs were both stably integrated into the same cells and clonal populations were expanded. Time-lapse microscopy was performed with the resulting clones.
As in the flow cytometry data, visualization of the reporters was not possible. Consequently, oscillations could not be measured. Indeed, this does not mean that no oscillations of the respective factors in the circuit occur, but it lacks in the visualization of the destabilized reporters. A reason for this could be a too short half-life of the reporters. This needs to be further examined.

4 Discussion

In this work, regulable perturbation of an intracellular signal transduction cascade, namely IFN-β induction, was performed by means of synthetic expression cassettes. In these cassettes, viral genes that are known to interfere with this particular pathway were expressed from a tetracycline-inducible promoter. The HCV NS3/4A gene or the IAV NS1 gene was fused to HaloTag V7, which could be visualized by the use of specific fluorescent ligands in single living cells.
By means of these cassettes, information about the efficiency and the temporal dynamics of NS1-H and NS3/4A-H perturbation as well as IFN-β induction could be yielded. Invertibility of ongoing IFN-β induction was demonstrated. Besides, an influence of NS1-H and NS3/4A-H on IFN stimulated signaling (JAK/STAT signaling) could be excluded. Quantitative and qualitative data were gained by the perturbation experiments which will serve as a base to create a mathematical model of early type I IFN induction.
Furthermore, synthetic modules were explored for the generation of a stable, synthetic oscillator in mammalian cells. Expression in the respective cells is based on two mammalian expression systems that are independently controllable.

4.1 Influence of HaloTag V7 fusion on the perturbators

To gain information about the expression characteristics of a gene product, fusion of the protein to a reporter is generally performed. In the present work, the viral perturbators NS1 and the NS3 cofactor NS4A were C-terminally fused to HTV7 to enable their visualization. However, the fusion of a reporter protein to a certain protein can be delicate and cause drastic changes in the protein's characteristics.
The fusion could cause a partial or full loss of functionality of the native protein. This could be due to a change in the secondary structure of the gene product. Thus, in this work functionality concerning the perturbation activity of NS1-H and NS3/4A-H was investigated and could be demonstrated (fig. 20).
Also, the localization of the protein within the cell can be affected by e.g. structural changes or the size of the fusion protein. Potential binding sites or hiding of localization signals can result from this. IAV NS1 proteins shuttle between the cytoplasm and the nucleus in a strain-, time- and cell type specific manner (Han et al, 2010; Hayman et al, 2006; Melén et al, 2007). In the present

case, NS1 from PR8 was used and it was still able to localize in both, the cytoplasm and the nucleus (data not shown). NS3/4A has been shown to act in the cytoplasm and also the fusion protein was found in this cellular compartment (data not shown).
Besides, transcriptional regulation or/and degradation of RNA or the mature gene product can also differ compared to the single, native gene products (perturbator or reporter). As a consequence, lower or higher steady state levels and turnover of the protein fusion can occur.
Such influences were hypothesized to be responsible for the lack of visualization of low amounts of the respective fusion protein, which could be observed at early time points after induction (fig. 16B, 20A). Certainly, gene expression needs some time to be induced, but additional factors might cause this.
Differential maturation of the components of the fusion proteins might be responsible for a potential delay in action and visualization of the proteins. For instance, maturation of HTV7 might take longer than that of the perturbator moiety and consequently, binding of and visualization via the reactive ligand occurs delayed. However, if present, this is a minor effect since constant low levels of the perturbators as basal levels (figs. 9A and 15A) or NS3/4A-H levels at low doxycycline concentrations (fig. 22B and 23B) cannot be visualized either. In the case of flow cytometry analyses, a detection limit of the cytometric device causes delayed visualization (fig. 16B) as time-lapse results displayed earlier visualization of the reporter in multiple cell clones (fig. 19, 26).
Taken together, the fusion protein reflects the basic properties of the native protein, but differences in the efficiency and the turnover of the perturbator-HTV7 fusions compared to the single native gene products cannot be excluded and need to be considered for the results obtained in this work.

4.2 Controlled perturbation of IFN-β induction by the influenza A virus NS1 protein

NS1-H expression levels within IFN-β NS1-H cells

The IAV NS1 protein counteracts early IFN induction at multiple levels. The intensity of this interfering effect and therefore the pathogenicity is strain-specific. This behavior of IAV relies on the respective NS1 sequence which also differs between influenza strains (Geiss et al, 2002). In this study, the NS1 protein of influenza A virus PR8 strain was used and all experiments were performed in reporter cells based on the NIH3T3 cell line. So far, no data exist for the controlled expression of NS1 and consequently, the values of ectopically

controlled NS1-H compared to the amount occurring during native IAV infection could not be estimated. In this work, the respective NS1 values in NIH3T3 cells were compared to the levels of NS1 produced upon infection of NIH3T3 cells with influenza A virus PR8. Quantification was done after Western Blotting (fig. 10). These data reveal that NS1 levels during early stages of infection (up to 6 h pi) can be mimicked by ectopically expressed NS1-H in the cell clone analyzed. However, levels during later stages of infection (12 – 24 h pi) are 2.5 - to 4-fold higher than for ectopically controlled NS1-H, indicating that ectopic NS1-H levels might not be sufficient to totally block IFN-β TurboGFP expression in this cell clone.
In the uninduced state, IFN-β TurboGFP reporter cells ectopically expressing NS1-H, IFN-β NS1-H, do not display leaky expression of NS1-H neither in flow cytometry analyses (fig. 8) nor in the Western Blot (fig. 10). Nevertheless, the amount and the intensity of IFN-β TurboGFP expressing cells is decreased (fig. 9). This gives the indication that basal expression under the detection limit of the flow cytometric device occurs in uninduced cells. Indeed, these cells are adequately expressing IFN-β TurboGFP and could be used for the perturbation experiments as long as total IFN-β TurboGFP values of IFN-β NS1-H and related cells were not compared to each other.

The influence of NS1-H on IFN-β TurboGFP expression

The effect of NS1-H on IFN-β TurboGFP expression was determined for a population of IFN-β NS1-H cells. NS1-H expression was induced at different time points relative to induction of the IFN-β induction cascade via NDV to determine the effect of pre-induced NS1-H and to find out whether and in how far belated NS1-H induction still affects IFN-β TurboGFP expression.
The effect of NS1-H induction at different time points relative to infection reveals a continuous decrease in the amount of IFN-β TurboGFP positive cells (figs. 20A and 21A). A little stricter perturbation occurs between time points 3 and 6 h pi. Perhaps, NS1-H affects ongoing signaling quite fast at this time point for unknown reasons. Indeed, this time frame approximately correlates with the expression of influenza virus genes after natural infection. Indeed, the amount of NS1-H 3h pi is comparable to the amount of native NS1 after natural infection at an MOI of 1 (fig. 10). In fact, viral mRNA is synthesized in the early stages of infection about 0.6 h pi (Vester et al, 2010). A delay occurs for translation and to obtain a respective amount of NS1 within the cell. Altogether, this time window could fit to the declared hypothesis.

A similar experiment was performed by tuning intracellular NS1-H levels by the administration of differing doxycycline concentrations. With this, the amount of NS1-H which is required for the block of IFN-β TurboGFP could be determined or it could be demonstrated whether a certain level (threshold) exerts an exceptional effect on IFN-β TurboGFP.
When a certain level of NS1-H was constantly induced overtime, a strong perturbing effect was measured already at intermediate doxycycline concentrations (25 – 100 µg/ml; figs. 22A and 23A). Accordingly, a pre-treatment gives highest perturbation efficiency. These results indicate that the amount of NS1-H primarily seems to be important for perturbation and not the time point of induction.
The dot plots from these perturbation experiments (figs. 20A and 22A) demonstrate that IFN-β TurboGFP cannot be totally blocked in the established reporter cells. This can have multiple reasons. First, PR8 NS1-H IFN counteracting abilities are not strong enough. Second, maximally inducible NS1-H levels (fig. 10) are not sufficient to totally block IFN-β TurboGFP expression. To reach these high levels appearing during native infection by inducible expression of NS1-H, other cell clones would have to be generated in which inducibility is significantly increased. In this respect, a rational design of a chromosomal locus to achieve minimal basal expression and maximal inducibility would be advantageous. Such strategies have become feasible exploiting strategies for site directed integration of expression cassettes into predefined chromosomal sites. It would be interesting to analyze whether the shielding of the expression cassette from surrounding influences by e.g. insulators would cause higher inducibility (Gaszner & Felsenfeld, 2006).
A total block of IFN-β TurboGFP expression might be reached, when native levels of NS1-H can be adjusted within a cell. On the other hand, this effect might be cell-type or strain-specific and a total block cannot be achieved even at higher NS1-H levels.

4.2.1 Influence of NS1-H on JAK/STAT signaling

NS1 from some IAV strains obtains regulatory functions by interacting with components that are necessary for the transcription, splicing and translation of cellular RNAs. The cleavage and polyadenylation specific factor 30 (CPSF-30) is bound by NS1 and therefore polyadenylation of cellular mRNAs is inhibited (Noah et al, 2003). Also, NS1 interacts with the poly(A)-binding protein II (PABPII) inhibiting its function and nuclear export of the protein and host cell mRNAs (Chen et al, 1999). Further, nuclear-cytoplasmic transport of cellular

mRNAs is inhibited by interaction of NS1 with factors of the nuclear export machinery (Satterly et al, 2007). These mechanisms can have strong effects on the induction of ISGs. H5N1 avian influenza NS1 was even demonstrated to directly interfere with JAK/STAT signaling by inhibiting STAT phosphorylation (Jia et al, 2010).
To verify whether NS1-H derived from IAV PR8 affects the induction of ISGs, its effect on Mx2 induction was determined in Mx2Luc NS1-H reporter cells (fig. 34). The results suggest that NS1-H does not exert any effect on JAK/STAT signaling (fig. 36A). The fact that Mx2 is properly induced without showing any reduction in the presence of NS1-H upon IFN-β induction also demonstrates that the mRNA was properly processed. These results are supported by the findings of Hayman et al. (2006) and Kochs et al. (2007) who demonstrated that PR8 NS1 efficiently perturbs IFN-β induction, but it does not work on the post-transcriptional level or on secondary signaling.

4.3 Dynamics of IFN-β TurboGFP perturbation by HCV NS3/4A-H

TLR-3 dependent signaling does not occur in NIH3T3 cells

The early IFN antagonistic functions of HCV NS3/4A are quite distinct. It was demonstrated to proteolytically cleave IPS-1. Cleavage of the TLR-3 adaptor protein TRIF is controversially discussed (Dansako et al, 2007; Li et al, 2005). This might be due to the fact that HCV is, as IAV also, underlying strong genetic drifting and subtypes might show different behavior, especially in variation of the cell type. In this study, NIH3T3 cells were used and analysis for the presence of TLR-3 was performed by direct administration of poly I:C, a dsRNA analogon, to the supernatant of NIH3T3 IFN-β reporter cells. Under these conditions, only a marginal induction of IFN-β expression could be measured (data not shown) confirming the absence of TLR-3 signaling pathway. Consequently, a potential effect of NS3/4A-H on TRIF can be ignored and NS3/4A-H is extremely specific for cleaving IPS-1 of RIG-I-mediated signaling.

Establishment of IFN-β NS3/4A-H KRAB cells

The establishment of IFN-β TurboGFP cells with inducible NS3/4A-H was challenging (compare with chapter 3.2.3), but clonal populations of cells exhibiting inducibility of both NS3/4A-H and IFN-β TurboGFP were lately obtained after introduction of KRAB caused by down-regulation of basal NS3/4A-H expression (figs. 14 and 15A).

IFN-β NS3/4A-H KRAB cells show slightly lower IFN-β TurboGFP induction compared to untransfected cells (fig. 15A). As for the IFN-β NS1-H cells, a decrease in the mean intensity of IFN-β TurboGFP occurred (fig. 15B) which might indicate that cells are still marginally expressing NS3/4A-H. Indeed, the cells express adequate values of IFN-β TurboGFP. As no comparison for total IFN-β TurboGFP amounts between IFN-β NS3/4A-H KRAB cells and cells related to untransfected cells should be performed, these cells were used for subsequent perturbation experiments.

The influence of NS3/4A-H and core on IFN-β TurboGFP expression

With respect to the experiment for NS1-H, also the influence of NS3/4A-H on IFN-β TurboGFP expression was determined. NS3/4A-H expression was induced at different time points relative to NDV infection to determine, whether a time point exists at which NS3/4A-H has an exceptional influence on IFN-β TurboGFP expression.

The data for this experiment demonstrate an abrupt decrease in IFN-β TurboGFP expression 3-6 h pi (figs. 20B and 21B). In the case of NS1-H stronger perturbation occurs at the same time point, but this effect is more drastic for perturbation via NS3/4A-H. So far, the reason for enhanced perturbation at these time points remains unclear, but it might be advantageous for the virus to early perturb IFN-β TurboGFP expression in a highly efficient manner. Further, this time point might fit to NS3/4A expression after native infection. However, data for this were not obtained in this work, but are a future perspective.

In the case of NS3/4A-H, a total block of IFN-β TurboGFP expression can be visualized from 12 h ai on or earlier (fig. 20B). In the case of NS1-H (fig. 20A), a total block of IFN-β TurboGFP expression could not be shown for any time point (24 h or earlier, fig. 20; data not shown). This indicates a stronger perturbing effect for NS3/4A-H than for NS1-H, which has not been shown so far. Indeed, this was expected since strong IFN antagonistic properties can be related to the persistence of a virus within the host which efficiently happens in the case of HCV.

mRNA and protein levels of NS1-H and NS3/4A-H cannot be directly compared with each other, since NS1-H and NS3/4A-H show different expression intensities for equal culture conditions. This becomes obvious when flow cytometry data for both factors are compared (e.g. figs. 20 and 22). Nevertheless, approximate declaration can be done especially when significant fluctuations occur as for the perturbation patterns. Also, maximal NS1-H

intensity is much higher than for NS3/4A-H, but concomitantly the effects of NS3/4A-H are stronger.
When IFN-β NS3/4A-H KRAB cells were monitored for the effect of different, constant NS3/4A-H levels on IFN-β TurboGFP expression, the significant difference in the perturbation mechanisms and consequently in the perturbation patterns between NS1-H and NS3/4A-H became even more obvious (figs. 22 and 23). For the latter, the lowest concentration tested (10 ng/ml doxycycline) was sufficient to almost fully block IFN-β TurboGFP expression. This demonstrates that few NS3/4A-H molecules are sufficient to cleave the IPS-1 proteins within the cell. In contrast, NS1-H needs to build dimers and to bind its interaction partners in a stoichiometric manner. Consequently, much more molecules of NS1-H seem necessary for a similar effect.
Taken together, these results demonstrate that NS3/4A-H very efficiently perturbs IFN induction leaving no residual IFN-β TurboGFP expressing cells. This might contribute to persistence of the virus within a host. However, further experiments would be needed to show that ectopically induced NS3/4A-H levels contribute to levels comparable to natural infection conditions.
Fine-tuned perturbation is only possible for very low concentrations of the perturbator. The tuning could be more efficient if NS3/4A-H would exert a shortened half-life which would also affect basal levels within the cell. Consequently, the usage of destabilizing tags could cause tighter regulation of the perturbation.

4.3.1 Influence of HCV NS3/4A-H on JAK/STAT signaling

NS3/4A-H as expressed from the synthetic expression cassettes was demonstrated to strongly interfere with IFN-β TurboGFP induction and to give reproducible data concerning perturbation intensity (figs. 20B and 22B). The fact that perturbation via NS3/4A-H just relies on the interaction with RIG-I-mediated signaling makes this system very specific. Though, it has not been clarified yet whether NS3/4A-H affects the induction of ISGs after JAK/STAT signaling. Helbig et al. (2008) demonstrated an inhibitory effect on STAT1 phosphorylation. Controversially, Cheng and co-workers (2006) could not display any effect of NS3/4A on IFN-induced signaling. By means of synthetic reporter cassettes, this question was addressed to at least demonstrate the specificity of our system. In figure 38A, it is clearly demonstrated that the presence of NS3/4A-H does not affect IFN-β-induced Mx2 expression, but Mx2Tom expression is completely abolished when NS3/4A-H perturbs IFN-β induction after NDV infection (fig. 38B). This again demonstrates the

impenetrable block of RIG-I signaling via NS3/4A-H and also underlines the specificity of NS3/4A-H to affect IFN-β induction

Combination of IFN-β and JAK/STAT perturbation in single cells

Both, NS1-H and NS3/4A-H were demonstrated to specifically perturb IFN-β TurboGFP expression. The combination with a second synthetic perturbation cassette for the interference with JAK/STAT signaling in one cell would be challenging. By this, interference of early type I IFN induction and subsequent JAK/STAT signaling could be performed in one cell. Thereby, information about the influences of both pathways on each other as well as data about the spatiotemporal dynamics between both pathways could be gained.
For this purpose, a factor known to interfere with JAK/STAT signaling would be expressed in the context of a second inducible system like the coumermycin system. This system was demonstrated not to interact with the Tet system (Kästner, 2007).
Various viruses have evolved strategies to interrupt JAK/STAT signaling as reviewed in Randall & Goodburn (2008). One appropriate candidate for JAK/STAT perturbation could be the HCV structural protein core which was demonstrated to interfere with JAK/STAT signaling at the level of STAT-1 phosphorylation (Lin et al, 2006) as well as SOCS-1 and SOCS-3 regulation, even though these results were contradictory (Bode et al, 2003; Miyoshi et al, 2005; Walsh et al, 2006).
The establishment of stable reporter cells for perturbation of these two pathways was initiated during this project, but clones that express core over time could not be established for unknown reasons (data not shown). Indeed, loss of expression during cell passaging/expansion could neither be overcome by single cell sorting nor by integration of KRAB. Actually, the attributes of core to participate in proliferation and carcinogenesis should be regarded as beneficial for the establishment of a stable cell clone (reviewed by Irshad & Dhar, 2006). Indeed, several groups were able to establish stable cell clones for tetracycline-repressible core in UTH cells or the osteosarcoma cell line U2-OS (Berg et al, 2009; Moradpour et al, 1996). Constitutive expression of core could be performed in HepG2 and Chang Liver cells, respectively (Ruggieri et al, 2007). Also in NIH3T3 cells, stable overexpression of core was demonstrated (Han et al, 2002; Kim et al, 2004).
The reason for the failure of stable core expression in this work is unclear. It can be hypothesized that HTV7 detection is not sensitive enough to allow visualization of potential low levels of core which might be sufficient for the

observed effects demonstrated by other groups. Indeed, when combined with the perturbation module for IFN-β interference a different reporter would have to be chosen for the detection of core. A more sensitive reporter could be used in this case, which might lead to visualization of core.
Also, mutations within core according to the HCV strain (JFH-1 in this case) could influence integration and stable expression of core. The corresponding protein might harm the cells and cause cell death. Non- or low-expressing cells would benefit from that and outcompete potential high-expressing cells. Thus, changing the core variant could be of benefit. Another way to overcome this problem could be further screening for strictly regulated clones or shortening of half-life to circumvent potentially harmful intracellular accumulation of the core protein. The half-life of core (~ 9 h for the protein; Moradpour et al, 1996) could be shortened by the usage of a destabilization tag.

4.4 Interference with ongoing IFN-β expression by viral counteractors deciphers cellular signaling dynamics

Signal transduction pathways are delicate mechanisms which are strictly regulated at multiple levels. Once initiated, they are able to continuously fix this state as long as the conditions are not changed. Also, IFN-β expression was demonstrated to maintain a certain expression level after reaching plateau phase (Rand, 2010).
In the present work, an observation attracted attention upon exploring the question whether ongoing IFN-β TurboGFP expression can be interrupted by perturbation via NS1-H or NS3/4A-H. This observation was the appearance of cells that were positive for both, IFN-β TurboGFP and the perturbator. This was especially obvious in the time-dependent perturbation experiments (fig. 20), but, at a lower extent, also in the dose-dependent experiments (fig. 22). In the latter experiments, pre-treatment with doxycycline induced an “anti-IFN state” due to the constant presence of the IFN-antagonist within the cells. It was further eye-catching that more cells were positive for NS1-H and IFN-β TurboGFP than for NS3/4A-H and IFN-β TurboGFP in the dose-dependent experimental setup. For time-dependence, cells expressing NS3/4A-H and IFN-β TurboGFP were either low in the one or in the other fluorescence, whereas a wide broader distribution of cells expressing both reporters could be visualized for NS1-H. This supports the above discussed indication for a stricter perturbation mechanism via NS3/4A-H or/and a fast shut-down of IFN-β TurboGFP after NS3/4A-H onset.
The existence of cells expressing both markers is very intriguingly since it indicates that the perturbation is not a strict all-or-nothing event, but has a

certain dynamic. Cells are able to express both, even though interference is expected to occur. It is conceivable that this is a transient state of the cell between perturbator onset and IFN-β TurboGFP termination; alternatively, this state might persist. The latter would suggest that ongoing activation of IFN-β induction pathway is not needed for maintenance of expression. Indeed, there are no data which show that RIG-I signaling needs to be continuously running for causing sustained IFN-β TurboGFP expression. Thus, it could be that only an initial trigger of RIG-I-mediated signaling is needed to establish continuous IFN-β expression. The methods set-up in this thesis allowed studying this question.

Withdrawal of the activation signal is sufficient to interrupt IFN-β expression indicating a "dead man's switch"-like mechanism

To clarify whether ongoing IFN-β TurboGFP expression can be disrupted, single cell analyses needed to be performed. For this approach, an improvement of IFN-β NS1-H cells was ventured by introduction of KRAB, which can reduce the basal activity of rtTA-dependent promoters. Tight induction of NS1-H was maintained and the amount and intensity of IFN-β TurboGFP within the responding cells were comparable to untransfected cells (fig. 25). Obviously, the small, undetectable amount of NS1-H in IFN-β NS1-H cells was sufficient to cause alteration in the frequency and intensity of IFN-β TurboGFP expression.
Accordingly, the IFN-β NS1-H KRAB and the already improved IFN-β NS3/4A-H KRAB cells were used to follow living cells that express both reporters overtime. As could be visualized, cells positive for both, NS1-H and IFN-β TurboGFP, stay in this state constantly in the displayed cell and IFN-β TurboGFP expression does not seem to decrease apparently (fig. 26). Indeed, determination of the fluorescence profiles for both markers of a representative number of single cells revealed that IFN-β TurboGFP goes to a premature plateau phase or inverts expression in response to perturbator induction (see examples in figs. 27A and 28A). A correlation of perturbator onset versus IFN-β TurboGFP plateau/inversion further points out that these events are related to each other in the case of NS1-H (fig. 27B). This result was even more stringent for NS3/4A-H (fig. 28B) since lower standard deviation from the regression line could be visualized in this case.
In the flow cytometry experiments it was demonstrated that IFN-β TurboGFP expressing cells still appear even though NS1-H is fully induced (compare with figs. 22A and 23A, doxycycline concentrations 0.5 – 2 µg/ml).

On the single cell level, it could also be visualized that the cells do not necessarily express NS1-H continuously, but expression decreases for unknown reasons; then IFN-β TurboGFP turns on (data not shown). The reason could be a lack in doxycycline, since medium cannot be exchanged during a time-lapse microscopy run. Certainly, other cells remained switched on at this time point which could again be related to the stochastic expression behavior of the cells.
However, this and other effects cannot be visualized in cell populations what makes the tool of single cell analysis over time an indispensable tool for questions like this.
Together, these data show that IFN-β TurboGFP expression needs a constant trigger to maintain expression. Perturbation causes an interruption of the signaling. This behavior resembles a "dead man's switch", where a signal is transmitted as long as a button is pushed and turns off when the button is released. Thus, interruption of the induction pathway at cytosolic stages can subsequently block or invert IFN-β expression. This finding has important implication for an infected host. In particular, this means that after induction of viral perturbator expression, IFN-β expression can be arrested or even down-regulated which disrupts the establishment of an antiviral state within the host and neighboring cells. Consequently, counteraction of infection cannot or only alleviated be performed anymore.

Mechanisms upstream of IFN-β TurboGFP induction are perturbed by NS1-H

The perturbation of IFN-β induction by NS1-H was demonstrated in this work. A relation in the dynamics between the translocation of IRF-7 into the nucleus and IFN-β TurboGFP induction was demonstrated before (Rand, 2010). Here, IRF-7 could act as a substitute for IRF-3 which is activated by the same kinases. By means of IRF-7 translocation, perturbation via NS1-H could be demonstrated on a different level of RIG-I-mediated signaling.
Reporter cells constitutively expressing a fusion protein of IRF-7 and CFP as well as doxycycline-inducible NS1-H were characterized and did not show significant basal expression of NS1-H (fig. 29). However, the translocation potential of IRF-7 CFP in these cells was slightly attenuated (fig. 31). This can be caused by basal NS1-H expression if relocation indeed occurs after perturbation.
To verify this mechanism, single cells were analyzed for the ability of IRF-7 CFP to relocate from the nucleus to the cytoplasm according to NS1-H induction. Since relocation is a natural incident, a correlation of NS1-H onset

with the relocation time point of IRF-7 CFP was performed (fig. 32). Indeed, a striking correlation was confirmed by mathematical regression, even though a certain deviation is obvious. This indicates that the two events are related to each other by a constant time frame between them.
Together, the data show that IRF-7 shuttling to the nucleus is reversible upon pathway interference – a new finding which has not been demonstrated before. Along with these results, it could also be shown that the mean retention of IRF-7 CFP in the nucleus (12.6 h) was decreased after doxycycline treatment compared to untransfected cells (5 h; fig. 33).
In total, these data show that relocation of IRF-7 CFP is coupled to NS1-H onset and consequently RIG-I-mediated signaling is interrupted also on this level, what makes the hypothesis of a "dead man's switch" more valid.

4.5 Dynamics of IFN-β induction with respect to the perturbation via NS1-H and NS3/4A-H

Even though the mechanisms of the diverse interacting components of the IFN system are known, only minor information could be gained yet for its spatiotemporal dynamics. The data shown in this thesis demonstrate that perturbation of the network via NS3/4A-H results in a total block of IFN-β TurboGFP induction (figs. 21 B and 23B). Since NS3/4A-H was shown to work specifically on IPS-1 in these cells (fig. 38A) and no TLR-3 dependent pathway can be induced (data not shown), the strong block indicates that no bypass to the IFN-β TurboGFP induction via IPS-1 exists. The loss of IPS-1 cannot be circumvented; this probably makes the NS3/4A protease that efficient.
It was further shown in this work that NS1-H and especially NS3/4A-H cause a drastic decrease in IFN-β TurboGFP expression when induced 3 - 6 h pi (fig. 21). This result was already previously discussed (chapter 4.3). Additionally, one could speculate whether at this time point where most efficient perturbation is displayed, NS3/4A-H is just induced before signaling has reached the relevant stages. Therefore no IFN-β TurboGFP induction occurs. Later perturbation does not have such strong effects, because the downstream signaling of IPS-1 was already started and the above described patterns of IFN-β TurboGFP transition to plateau phase or inversion occur, which are less effective than pre-treatment.
Since a less efficient but still apparent decrease at this time point also occurs for NS1-H (fig. 21A), it is likely that the same or a closely related factor is exceptionally influenced via NS1-H. In fact, NS1 was already demonstrated to build a complex with RIG-I, thereby inhibiting further signaling (Pichlmair et al, 2006). Despite of this aberration, NS1-H constantly perturbs IFN-β TurboGFP

induction in a time- and dose-dependent manner. This further indicates that NS1-H acts on multiple levels and does not show specific perturbation at a certain time point.
U. Rand (2010) demonstrated that the process of nuclear accumulation of IRF-7 CFP takes 30 – 60 min. He further showed that IRF-7 accumulates inside the nucleus for 12.6 h in average (SD 7.2 h). In this work, it was demonstrated that IRF-7 NS1-H cells display shortened retention of IRF-7 CFP in the nucleus (fig. 33). This, together with the correlation on relocation and NS1-H induction (fig. 32), indicates premature relocation and consequent interruption of the signaling via NS1-H. Unexpectedly, induction of NS1-H expression did not lead to significant changes in IRF-7 nuclear accumulation periods. Due to the strong variability of these events, lack of significance might originate from too small sample numbers (n = 12 for uninduced cells; n=8 for induced cells).
U. Rand further demonstrated that between IRF-7 CFP translocation and IFN-β TurboGFP onset, a relative constant time span of 2 to 6 h is maintained.
In this work, it was demonstrated that the time span between NS1-H induction and IRF-7 CFP relocation is quite short (2.7 h; SD: 2 h). The period between NS1-H onset and IFN-β TurboGFP arrest is about 12 h (SD 5.4 h). Consequently, the time period between IRF-7 relocation and IFN-β TurboGFP arrest could be about 9.3 h. However, it would be interesting to observe these events upon NS1-H perturbation in a single cell clone to verify this value.
These obtained data give further information about the temporal dynamics of RIG-I-mediated IFN-β induction and data that are necessary for the establishment of a reliable mathematical model.

4.6 Challenges in the establishment of cells displaying doxycycline-dependent transgene expression

Within this work, control of perturbator expression was realized upon transcriptional control via synthetic regulatory cassettes/modules. Indeed, the establishment of cells with tightly regulated expression was challenging since only few clones provided good inducibility and absence of relevant basal activity. This limitation is frequently encountered upon establishment of tightly regulated clones.
In fact, differences in the inducibility of single clones were demonstrated (fig. 7). Also, varying levels of basal expression were observed between cells (figs. 7 and e.g. 11 and 29). In the case of IFN-β NS3/4A-H cells, basal expression was too high to allow IFN-β TurboGFP induction (fig. 12). These differences in the expression of a transgene after random integration into a host can be explained

by position effect meaning that the new, neighboring sequences and effectors can influence the expression of the integrated transgene or from an integrated promoter (West & Fraser, 2005). For the latter, promoter crosstalk between the integrated and surrounding promoters can happen (Hampf & Gossen, 2007). Inducible promoters are exceptionally susceptible to this effect. Thereby, the outcome of downstream transgene expression can be strongly altered in basal expression or/and maximal induction as it could be observed for P_{Tet} in this work. Also, the constitutively active promoter driving rtTA2 could affect P_{Tet} when expressed from the same construct. To avoid at least the latter effect, the two units were provided on two separate plasmids.
A different approach to overcome this effect is the use of previously defined and potentially modified chromosomal loci. One modification could be the integration of two insulators which shield DNA segments between them from neighboring influences (reviewed by Gaszner & Felsenfeld, 2006; also described in chapter 4.2).

4.7 Expression and stochasticity of the doxycycline-dependent constructs

Doxycycline-dependent regulation of the reporters was demonstrated in chapter 3.3 for cells stably harboring NS1-H under control of P_{Tet}. Even though differences in regulation can occur within individual cell clones, the overall induction pattern stays comparable. The cells displayed reproducible time- and dose-dependent regulation of NS1-H (fig. 16). Indeed, a gradual expression response should be given using the classical Tet system, relying on constitutive expression of the transactivator (Schucht et al, 2010).
However, Hop et al (1997) demonstrated with the classical Tet-Off system that doxycycline affected the number of expressing cells rather than the expression level. Such a pattern would be expected for an on/off-type (bimodal) rather than the expected graded expression pattern (compare with chapter 1.6 of the introduction). In flow cytometry experiments it was later shown that a broad peak of differentially induced cells occurs in this system with increasing concentrations of doxycycline indicating heterogenous expression within single cells (Bornkamm et al, 2005).

The data on the single cell level shown here clearly demonstrate that this issue is more complex and differs between single cells (fig. 18). Indeed, heterogeneity of doxycycline-induced expression was observed at multiple levels:

- Time point of NS1-H induction
- Maximal level of expression
- Differential course of NS1-H induction

In this work, it was demonstrated that genetically identical cells do not respond uniformly to doxycycline stimulation as concluded from flow cytometry based data (Schucht et al, 2010). Thus, the potential of a cell to be induced seems to be governed by stochasticity.
Importantly, the overall expression pattern obtained by the design of the expression cassettes in this study is distinct from the clear bimodal expression pattern described for cassette designs in which the tetracycline transactivator drives its own expression via a feedback mechanism. In this case, only two distinct populations occur (on/off), since expression is always distinct if turned on (May et al, 2008).
Definitely, this complex expression pattern remains to be elucidated in further detail; microscopic monitoring as used in this study could contribute.
For single cell analyses of this work, only cells were chosen which fulfill the requirements of perturbator induction on the verge of IFN-β TurboGFP arrest or rather IRF-7 relocation, making the data valid. For flow cytometry experiments, a certain error emerges, since cell populations are not synchronized. Indeed, this error is expected to be moderate since analysis in comparable settings showed that most cells respond to doxycycline early after administration and only a minor population does not immediately respond (Behme and Wirth, unpublished).

4.8 Synthetic perturbation

Advantages of synthetic expression modules for perturbation of cellular networks

In this work, a synthetic perturbation approach was performed. Here, synthetic perturbations are defined as the expression of an ectopic perturbator-reporter fusion by an externally regulable mammalian expression system, the Tet system. So far, no comparable approach has been performed and consequently, information concerning this area is rare. Certainly, the herein described method will be discussed with some other methods to cause perturbation.

Perturbation is generally achieved by the use of chemicals, RNAi or by gene knock-out to gain insight into a proteins' function (chapter 1.3).
In the present work, two different mechanisms of perturbation were performed. One causes a knock-down of the desired signaling (NS1-H; figs. 22A and 23A) by working on multiple factors. The effect of knocking down, but rarely knocking-out gene expression is in common with RNAi approaches. siRNA-mediated interference can also be coupled to the Tet system (Berger et al, 2010). This method can also be used to specifically knock-down gene expression in a regulated manner with even higher specificity as for NS1-H.
The second approach described herein principally leads to a knock-out of IPS-1 and consequently to a total block of the signaling (NS3/4A-H; figs. 22B and 23B). Such an effect can be achieved by the deletion or disruption of a GOI causing a knock-out as it was shown for IRF-3 and IRF-7 (Sato et al, 2000). By this method, first evidences for the work mechanisms of IRF-3 and IRF-7 were gained after analyses of IFN-α and –β outcome in IRF-3 -/- or both IRF-3 -/- and IRF-7 -/- mouse embryonic fibroblasts. However, such a perturbation is time-consuming and irreversible. Furthermore, the deletion or disruption of a gene can cause lethality.
Chemical perturbation can probably be regulated by the administration of a certain dosage of the inducer. Indeed, it is often unspecific and can cause the knock-down of groups of proteins. Also, it cannot be ruled out that the respective chemical affects the host cell metabolism leading to false results. Tetracycline or doxycycline as inducer for the synthetic cassettes, however, is generally used in cell culture and does not affect the cell metabolism in the concentrations applied.
Certainly, all described methods have assets and drawbacks. Most of the alternatively described perturbation strategies cannot (properly) be regulated. Consequently either no or maximal perturbation by the respective method is possible. Indeed, regulation of the perturbator can give further information about both, the perturbator and/or the gene/network of interest, as demonstrated in the present work. Thus, the strong and strict perturbation of NS3/4A-H on IFN-β TurboGFP at relative low intracellular levels was demonstrated (fig. 23B).
Taken together, synthetic perturbation as described in this work has the advantage to be regulable and reversible compared to other methods. Since the perturbator is arbitrary, the effect achieved by it can be specific or acting on multiple levels. Also, knock-down or knock-out can be achieved as desired.

4.9 Towards a stable, synthetic oscillator in mammalian cells

The composition of systems for the controlled expression of a transgene is quite simple and already well established in eukaryotes (compare with chapters 1.4 and 1.5 of the introduction). Indeed, combination of these circuits to higher order synthetic circuits is challenging.
While oscillating expression circuits could be established in prokaryotic systems (Elowitz & Leibler, 2000; Stricker et al, 2008), so far only systems for transient oscillation have been implemented in mammalian cells (Tigges et al, 2010; Tigges et al, 2009). Accordingly, the construction of mammalian cells with a stable, oscillating circuit is challenging. In this work, such a higher order synthetic network was aimed. While the single components were demonstrated to work, the final cell with all necessary constructs integrated does not show oscillation. Reasons for this could be that oscillations are not properly visualized by the reporters or that the interplay between or composition of the components does not fit. To get suggestions, under which conditions the circuit as established in this work, could oscillate, a mathematical model was developed by Ana Teixeira (Animal Cell Technology Lab, ITQB/IBET in Oeiras, Portugal). This gave rise to the definition of some conditions that need to be taken into account to successfully implement such a network. Also, the diverse variables would be difficult to handle without a representative model. This is discussed in the following chapter.

4.9.1 Mathematical model development

For the underlying approach, a deterministic modeling was performed which should represent single-cell oscillations. In this model, production and degradation of the three regulatory proteins tTA, CouTA and KRAB as well as the reporters tRFP and tGFP is considered. Also the interactions between them were included. Transcriptional and translational processes were modeled for each parameter as well as mRNA and protein translocations between nucleus and cytoplasm. The time-delays between the different oscillation steps were also taken into account since they are essential to obtain proper oscillation.

Some parameters were assumed as follows:

- Association of RNA polymerase with DNA does not work limiting
- No limitation of nucleotides and amino acids
- A comparable translation rate exists for the proteins
- Components are homogenously distributed within the nucleus/cytoplasm
- The regulatory proteins bind to the respective promoters as dimers

Furthermore, the absence of doxycycline and the constant presence of coumermycin were ascertained (Teixeira, unpublished).

4.9.2 Model simulation and improvement of the potential oscillator

A model simulation was performed with varying parameters to ensure the best conditions to obtain sustained oscillations. Indeed, conditions could be defined that would lead to oscillations in cells proving that the designed synthetic network has the potential to oscillate. Initially, equal transcription rates for the respective genes and equal affinities for the activator as for the repressor were assumed. Like this, it was found out that the copy number of the Tet-Unit should be 3-fold higher than for the Cou-Unit. However, it is not likely that the transcription rate of all genes will be equal since it mainly depends on the integration site (compare with chapter 4.6). Rather, this suggests that the Tet-Unit expression level should be 3-fold higher than the Cou-Unit to obtain sustained oscillations.
In this study, a screening for clones was performed that exhibit this feature. However, such clones could not be identified. This indicates that the probability to meet these requirements randomly might be rather low. Accordingly, strategies that allow the prediction of expression levels seem to be required to balance transcription rates of the various components. For this purpose, a rational design of cells seems to be mandatory. This would include the usage of pre-defined chromosomal loci to integrate the synthetic cassettes together with regulatory elements such as silencers, insulators and/or enhancers.
Elowitz and Leibler (2000) already found that comparable protein and mRNA decays support the generation of oscillations. Also in this work, protein and mRNA of tTA, CouTA and KRAB should have appropriate half-lives. To visualize oscillations in this circuit, also the reporter half-life should match (fig. 42). Proper oscillations only occur for low half-lives (2 - 4 h). Long protein half-life (12 – 24 h) would cause accumulation of the reporters with increasing oscillations and quickly lead to synchronization of oscillations (Teixeira, unpublished).

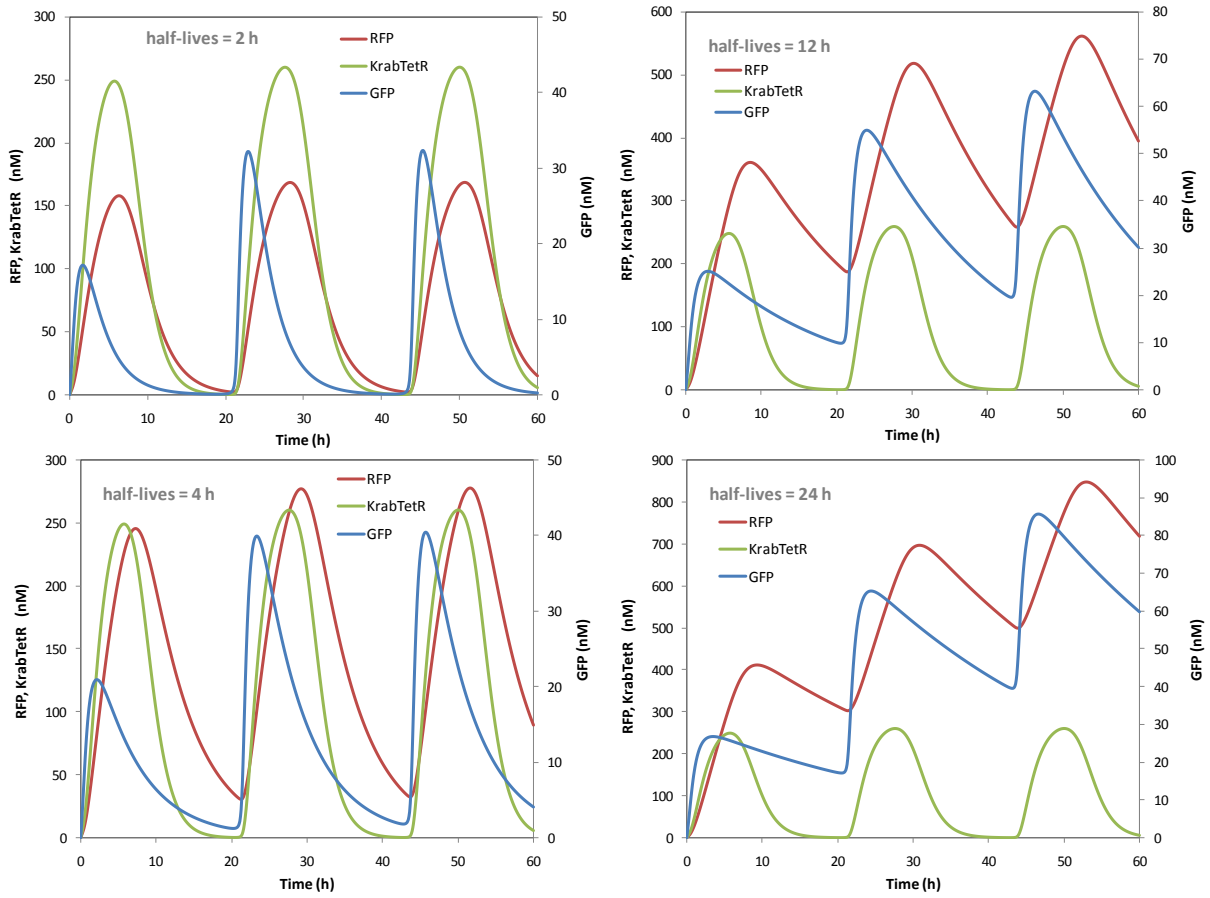

Figure 42: Oscillations of the components according to their half-life.

Oscillation of the system is demonstrated for different half-lives of the components. Proper oscillation can be obtained for low half-lives since for long ones, accumulation of the proteins and subsequent synchronization of the signal occurs. Oscillations according to half-lives of 2 h (upper left), 4 h (lower left), 12 h (upper right) and 24 h (lower right) were simulated with the model. These data were kindly provided by Ana Teixeira (Animal Cell Technology Lab, ITQB/IBET in Oeiras, Portugal).

In the experimental part, the usage of the destabilized proteins, especially tGFP, was limited since the protein could hardly be visualized both in flow cytometry and in time-lapse microscopy. This suggests that the half-life of these proteins might be too short to be visualized. Loss of at least the Tet-Unit in the single cells could be excluded, since tTA was demonstrated to work properly in context with non-destabilized eGFP (fig. 41B). Consequently, future work on this circuit will incorporate an improvement in stable reporter gene expression. It is considered to choose different destabilizing tags which might provide slightly enhanced half-life, thereby allowing visualization of the reporters.
Also, tTA, KRAB and CouTA should be fused to destabilizing tags to obtain comparable, short half-lives of the proteins. Then, proper relation of the

components to each other could be obtained by the use of defined chromosomal loci for the units or by the use of insulators.
It has to be taken into account that tTA and KRAB build heterodimers due to an equal dimerization domain. Heterodimers are probably non-functional and would reduce the concentration of proteins that could form homodimers. Generally, this multimerization could be circumvented by providing different dimerization domains as performed by Forster and co-workers (1999).
The results underline the complexity and challenge of building a higher order synthetic network. Indeed, the mathematical model could provide hints for the improvement of the circuit to aim at the stable implementation of a mammalian oscillator.

5 Outlook

Perturbation experiments are usually performed to get insight into the function of a protein or a cellular network. In this work, a synthetic biology approach was performed to specifically interfere with an intracellular network, namely the IFN system. Perturbation was performed by means of natural, viral perturbators that are stably expressed from a tetracycline-dependent promoter within reporter cells. Selected items that would further the development of such systems as well as future applications are described in the following.

A: Achieving predictable expression of transgenes in mammalian cells

The heterogenous expression behavior of single clones after random integration relies on the position effect meaning the influence of neighboring sequences and effectors on the integrated cassette. As a consequence, varying expression levels of the GOI can be obtained. Inducible promoters are exceptionally affected by promoter crosstalk leading to variation in basal leakiness and maximal inducibility between stable cell clones as could be observed in this work. In order to achieve predictable transgene expression in future approaches, some recently established methods could be performed.

i) A pre-defined chromosomal locus could be exploited for targeted integration of the construct of choice via recombinase-mediated cassette exchange (RMCE). The benefit of this method is the predictable expression from the previously characterized locus which should provide similar expression in single clones. This method can be further improved by the modification of a certain chromosomal site by integration of insulators. The composition of the locus would be arranged in a way that allows targeted integration of a construct of choice in between two insulators. Expression from the construct is not influenced by the environment due to shielding attributes of the insulators.

   Insulators can also be positioned up- and downstream of the region of interest on vector DNA. However, integrating the DNA randomly into a host can cause interruption within the vector constellation making targeted integration more precise.

ii) BAC constructs are used to achieve predictable expression of a GOI after host cell integration. In contrast to RMCE performed in mammalian cells, the construct of interest is integrated into a pre-defined locus in bacteria. The BAC containing the DNA of interest in a defined locus is subsequently transferred to the host cell.

By means of the described methods, predictable expression of a GOI within mammalian cells can be obtained in a reproducible manner.

B: Precise regulation of protein levels

In the present work, NS1-H and NS3/4A-H were demonstrated to efficiently perturb IFN-β TurboGFP induction. However, tight regulation could not be achieved for NS3/4A-H, since low levels already showed drastic effects. In this case, transcriptional regulation by means of the Tet system does not seem to be an appropriate tool, since basal leakiness of the inducible promoter can cause accumulation and consequently a high steady state level of the transgene within the cells. Also, reversion of inducible transgene expression by withdrawal of the inducer takes some time. Here, two possibilities will be described how to overcome this problem by enhanced degradation or post-translational regulation of NS3/4A-H.

i) A combined approach using the Tet system and fusing a destabilizing sequence as PEST (Li et al, 1998; Rogers et al, 1986; also used for destabilizing the reporters in the oscillator approach) to HTV-7 would be feasible. The native half-life of HTV7 is 6 h, but it can be down-regulated to ~ 2 h by this fusion (Yamaguchi et al, 2009). The constant presence of destabilized HTV7 also causes lower steady state levels in the cell. These findings could be implemented to obtain lower basal levels and increased protein turnover of NS3/4A-H.

ii) An approach to regulate intracellular levels of NS3/4A-H solely on the protein level could be advantageous. One system to perform this implies the fusion of NS3/4A-H to a destabilizing sequence of a mutant of the *E. coli* dihydrofolate reductase (ecDHFR). It should allow tight regulation of the protein levels by the small-molecule ligand trimethoprim (TMP) which rapidly and reversibly stabilizes the destabilizing domain (Iwamoto et al, 2010). By administration of the respective amount of TMP, dose-dependent stabilization of the fusion protein can be triggered. With this tool, intracellular NS3/4A-H levels could be regulated and even reduced to a minimum. By this method, a more homogenous presence of NS3/4A-H could be obtained. Though, the system is not as well established as the Tet system.

C: Synthetic perturbation of pathway progression

The perturbation of IFN-β induction was demonstrated to be efficient, regulable and reproducible. By means of this approach, insights into the spatiotemporal dynamics of virus-induced IFN-β induction could be gained. Indeed, the

perturbators used in this work are highly specific for this cascade. It would be of interest to analyze whether the herein described approach could be transferred to different intracellular signaling pathways as e.g. pathways for apoptosis, proliferation or differentiation to get insight into their dynamics. For this purpose, different (viral) perturbators that are known to specifically interfere with the network of interest would need to be exploited.
The perturbation of a unique pathway was successfully implemented in this work. A future perspective is the perturbation and visualization of the respective effect on multiple signaling networks in one cell. By means of such an approach, interactions and spatiotemporal dynamics between pathways can additionally be elucidated. With this work, a similar attempt was initiated combining NS1-H-mediated perturbation of IFN-β induction with HCV core-mediated perturbation of JAK/STAT signaling. As independent progression of the Tet and the Cou system could be demonstrated before (Kästner, 2007), these expression systems can be used for the regulation of the two perturbators. Indeed, reporter cells for the visualization of an early IFN as well as an ISG as Mx2 will needed to be developed.
Synthetic pathway perturbation was demonstrated within mammalian cells in this work. In order to validate the function of the synthetic cassettes *in vivo*, the use of an animal model would be beneficial. Proven functionality in such a model can give rise to the further establishment of synthetic approaches for network analyses in living organisms.

Future perspectives for the synthetic biology technologies

By the synthetic perturbation approach, information cannot only be gained on the cellular level, but also for the perturbators as demonstrated in this work for NS1-H and NS3/4A-H. The reporter cells harboring NS1-H or NS3/4A-H described in this work could be excellent tools to screen for components acting against NS1 or NS3/4A, since both factors are clinically extremely relevant. Especially in the case of NS3/4A, the search for efficient protease inhibitors could be performed.
Further, such synthetic perturbation approaches could be validated for gene therapy, since diseases are often related to the deregulation of intracellular pathways. So far, gene therapeutic approaches mainly depend on the overexpression of genes which might act in a rather unspecific manner and can cause severe side effects. Indeed, it could be beneficial to specifically interfere with the respective pathways to verify a specific counteraction of the disease. Thereby, more pronounced effects of the perturbator could be obtained. Also,

the regulation of the respective perturbator level can be of benefit, since high doses might cause side effects. The use of clinically approved inducers like doxycycline would also be advantageous.
For this purpose, the establishment of the above mentioned *in vivo* mouse model would also be of interest as a proof of principle in a living organism.

6 Materials and Methods

6.1 Equipment

Table top centrifuge	Heraeus Biofuge 13
	Heraeus Biofuge PICO 17
Cooling centrifuges	Beckman GS-15R Heraeus Megafuge 1.0 Sigma 3K20 Heraeus Biofuge fresco Sorvall Superspeed RC5C Inflexible rotors: GSA, GS3, SS34 Swinging rotor: HB4
Photometer	Nanodrop Spectrophotometer ND-1000, Peqlab
ELISA Reader	Multiskan EX reader, Thermo Electron Corporation
Gelelectrophoresis systems	BRL Horizon 58 BRL Horizon 1114 BRL Horizon 2025 Owl Separation System A2 BioRad (Protean II XL)
Western Blot cell	Bio-Rad Trans-Blot Cell
Power supplies	Gibco BRL ST 504 Biorad Power PAC 200 Biotec-Fischer Phero-STAB 550
Autoclave	BelimedDampf Sterilisator 6-6-6 HS1, FD
Microscopes	Nikon TMS Leitz Labovert FS Olympus CK2

	Olympus CK X41
Fluorescence microscopes	Olympus IX81 Zeiss Axiovert TV 135 Zeiss LMS 510 META
Micropipettes	Gilson
UV-chamber	Hanau
Phosphoimager	Molecular Dynamics Storm 860
Videograph	Biotec Fischer Video densitometer Mitsubishi thermo printer and personal computer
FACS machines and Software	FACSAria, Becton Dickinson FACSCalibur, Becton Dickinson FACSVantage SE, Becton Dickinson LSR II, BD Biosciences Macintosh Quadra 650
Luminometer	Berthold Lumat LB 9501
Cell Counter	Casy-DT 1, Schaerfe Systems
Cell culture incubators	Forma Scientific Water jacketed Incubator 3336 Labotect C200
Safety benches	Sterile Gard Class II Type A/B3, Baker SG 400E Herasafe, Heraeus HSP 18 Herasafe, Heraeus KS15 BDK-SK 1500
Sterile work benches	Mecaplex, Sterilgard Hood VBM600 and SG400 Heraeus HLB 2448

	Heraeus HSP 18
ph Meter	Beckmann M340
Thermomixer	Eppendorf Thermomixer 5436 Eppendorf Thermomixer compact
Vortexer	Scientific Industries Vortex Genie 2 Heidolph REAX 2000
Shaker	Heidolph Duomax 1030
Dionized Water Supply	Millipore MilliQ
Electroporator	Biorad Gene Pulser and Pulse Controller
Thermocycler	T3 Thermocycler, Biometra
Precision Weighing Scale	Sartorius
Microwave	Whirlpool
Water Bath	GFL
4°C refrigerator	Liebherr Comfort
-20°C freezer	Liebherr
-70°C freezer	Thermo Forma

6.2 Materials

6.2.1 Chemicals

The used chemicals were purchased from: Amersham Biosciences, Bayer, Biolabs, Bioline, Biorad, BRL Difco, Gibco, Merck, Miles, Pharmacia, Prenner, Qiagen, R&D Systems, Roche, Seromed, Serva and Sigma.

Enzymes were purchased from New England BioLabs (NEB), Bioline, Roche, Invitrogen and Amersham Biosciences.
Antibodies were obtained from Santa Cruz Biotechnology, Calbiochem and Cell Signalling.
Oligonucleotides were purchased from Eurofins MWG and TIB MolBiol.
DNA-sequencing was done by the "Genome Analysis" department of the Helmholtz Centre for Infection Research.

6.2.2 Consumables

Cell culture plates (96-well, 48-well, 24-well, 12-well and 6-well)	Nunc, Corning
Tissue culture dishes (100mm * 20mm, 145mm * 20mm)	Corning, Greiner Bio-one
Tissue culture flasks (25 and 75 mm^2)	Nunc
Falcon tubes (15 ml and 50 ml)	Greiner Bio-one
Flow cytometry / luminescence Measurement tubes (5 ml)	Sarstedt
CombiTips (0.5 ml, 1.25 ml, 2.0 ml, 2.5 ml, 5 ml)	Eppendorf
Safe Lock Tubes (1.5 ml, 2.0 ml)	Eppendorf
PCR Tubes	Biozym

Cryogenic vials	Corning
Pipette tips (20 µl, 200 µl, 1000 µl)	Star Labs
Microscopic chambered cell slides	Nunc / ibidi
Syringes (1 ml, 5 ml, 20 ml)	Omnifix®
Syringe filters (0.2 µM and 0.45 µM)	Sartorius

6.2.3 Applied Software

This manuscript was written employing the *Microsoft Office* 2007 package (*Word, Power Point*, and *Excel*). *Microsoft Office Access* was used for database entries.

Flow cytometry data were performed with the *BD Cellquest pro* and *BD FACSDiva* software, *Cyflogic* or *FlowJo v7.6* and earlier. For the design of primers and cloning strategies Vector NTI AdvanceTM10 from Invitrogen was used.
The analyses of microscopical images was performed with *ImageJ* (National Institute of Health) and corresponding plugins. Zeiss *LSM510* software was also used.
The *Quantity One* software (Bio-Rad) was used for the Western Blot analysis and quantification.
Sequencing results were analyzed with *Chromas* version 2.32 from Technelysium Pty Ltd.

6.3 Basic methods

6.3.1 Sterilisation

Heat sterilization was performed in Belimed autoclaves. Glass ware was sterilized at 180°C for 4 h. Solutions and plastic ware (pipette tips, eppendorf tubes) was sterilized at 121°C, 1 Bar for 25 minutes (min). Sterile filtering was performed in the case of non-autoclaveable solutions (sterile filter, pore diameter 0.22 µm).

6.3.2 Agarose gelelectrophoresis

(According to Maniatis et al, 1982)

1 x TAE-Buffer	40 mM Tris/acetate, pH 7.5 ; 20 mM NaOAc ; 1 mM EDTA
5 x loading buffer	15 % Ficoll, 50 mM EDTA, 1 x TAE; 0.05% Bromophenolblue; 0.05 % Xylenecyanole

Agarose gelelectrophoresis is used to separate double-stranded DNA according to its size. DNA moves from the cathode to the anode within an electrical field since it is negatively charged.
In this work, 1 % agarose gels were used for the separation. To produce a 1 % gel, 1 g of agarose was dissolved in 100 ml TAE by boiling in a microwave oven and 1 µl of ethidiumbromide (10 mg/ml) was added. The gel was poured into a tray and after becoming solid, it was transferred to an electrophoresis chamber filled with 1 x TAE. The DNA samples were mixed with the respective amount of 5 x loading buffer and loaded onto the gel. A marker (Hyperladder I, Bioline) as loaded in parallel to determine the size of DNA fragments. Gel electrophoresis was performed at 100 V and 30 mA. Gels were monitored under UV light (360 nm).

6.3.3 Purification of DNA

Purification of agarose gels:

The DNA bands of the desired size are cut out under UV-light using a scalpel. From those DNA containing agarose pieces, DNA is extracted and purified using the “QIAquick” gel extraction kit (Qiagen) according to the manufacturer’s instructions.

Purification of PCR samples:

DNA from PCR samples was purified using the “QIAquick” PCR purification kit (Qiagen) according to the manufacturer’s instructions.

6.4 Modification of DNA

6.4.1 Restriction of DNA

To determine the size of DNA fragments or for cloning strategies, restriction of DNA plasmids and PCR fragments was performed. For these purposes, restriction enzymes were used that recognize specific nucleotide sequences of a length of 4 - 8 base pairs. The enzymes cut within this region providing overhanging or blunt ends. Each enzyme reacts optimally under conditions (temperature and buffer) recommended by the manufacturer (NEB, Bioline). The reaction was stopped by heat inactivation for 20 min at 65°C/80°C or by purifying with the "QIAquick" purification kit (Qiagen).

6.4.2 Fill in reaction of 5' overhangs

10 x Klenow buffer	50 mM Tris/HCl in ddH_2O, pH 7.2; 10 mM $MgSO_4$; 0.1 mM DTT
dNTP-Mix	1 mM of dATP, dCTP, dGTP, and dTTP each

In a total volume of 50 µl, 1 µg of DNA with overhanging 5' ends was treated with 1 U of Klenow enzyme (NEB) in the presence of 3 µl of dNTP mix. After 30 min of incubation at RT, the reaction was stopped by heat inactivation (20 min at 80°C) or by the use of "QIAquick" purification kit (Qiagen) according to the manufacturers' instructions.

6.4.3 Dephosphorylation of DNA fragments

10 x NEB buffer 3	500 mM Tris/HCl, 1 M NaCl; 100 mM $MgCl_2$, 10 mM DTT; adjusted to pH 7.9

3' and 5' overhanging ends were dephosphorylated by alkaline phosphatase (calf intestinal phosphatase, CIP; NEB) to prevent relegation of a restricted vector. 20 – 100 pmol of the restricted DNA was incubated with the appropriate buffer (NEB) and 1 – 2 U CIP in a total volume of 50 µl. Incubation occurs at 37°C for 30 min. Afterwards, the DNA is purified using the "QIAquick" purification kit (Qiagen) according to the manufacturers' instructions.

6.4.4 Ligation of DNA fragments

10 x Ligase buffer	500 mM Tris/HCl; 100 mM $MgCl_2$; 10 mM ATP; 100 mM DTT; adjusted to pH 7.5

In a total volume of 10 µl, 2 µl of the ligase buffer were incubated with 1 – 2 U of T4-DNA ligase (NEB) as well as the insert and backbone DNA (relation > 10 : 1) at RT for 2 h. The ligation was then directly used for transformation into *E. Coli*.

6.4.5 Polymerase Chain Reaction (PCR)

PCR was performed to amplify the DNA sequences of IAV NS1, HCV core and HCV NS3/4A genes from appropriate vectors. Oligo-nucleotide primers for DNA synthesis were obtained from MWG or TIP. Elongation of the two primers that hybridize to the 5'- and the 3'- end of the sequence to be amplified occurs over repeated reaction steps. In the first step, denaturation of the DNA is performed at 94°C. Afterwards, temperature is reduced to the optimum for primer annealing to the complementary DNA sequence. Then, temperature is shifted to the polymerase optimum. This cycle is repeated 25 – 35 times, thereby amplifying the sequence of interest exponentially.

The Expand Long Template PCR System (Roche) was used for amplification of long DNA sequences (>1000 bp).

Average PCR sample:

Supplied PCR buffer (10 x conc) containing MgCl2	5 µl
10 pmol/µl forward primer	5 µl
10 pmol/µl reverse primer	5 µl
10 mM dNTP Mix (10 mM of each dNTP)	4 µl
DMSO	1 µl
DNA polymerase mix (Roche)	0.5 µl
DNA template as required	
ddH2O	ad 50µl

Average PCR programme (using T3 Thermocycler, Biometra):

Temperature [°C]	Time	Step
1) 94°C	5 min	denaturation
2) 92°C	1 min	denaturation
3) ~55°C	1 min	annealing
4)* 68°C	2 min	elongation
5) 70°C	5 min	final elongation
6) 4°C	pause	

*steps 2-4 were repeated 30 times before proceeding to step 5.

The annealing temperatures rely on the GC content and the length of the primers. The elongation time depends on the length of the DNA fragment to be amplified (30s/kb).

6.5 Work with *E. Coli*

6.5.1 Laboratory strains of *E. Coli*

TOP10 F- mrcA Δ (mrr-hsdRMS-mcrBC) Φ80dlacZM15, ΔlacX74 recA1 araD139 Δ (ara-leu) 7697 galU galK rpsL (StrR) endA1 nupG

XL1-Blue recA1, endA1, gyrA96, thi-1, hsdR17, suppE44, relA1, lac *F' proAB, lacI q Z) M15, Tn10, (Tet r)]

6.5.2 Culture medium and selective drugs for bacteria

LB-Medium 10 g/L Bacto-Trypton, 10 g/L Bacto-Yeast extract, 5 g/L NaCl

Agar plates 15 g of solid agar are added to 1 L of LB-medium

Antibiotic	stock solution	LB-medium	agar plate
Ampicillin	5 mg/ml in ethanol	5 µg/ml	25 mg/ml
Chloramphenicol	5 mg/ml in ethanol	2.5 µg/ml	12.5 µg/ml
Kanamycin	5 mg/ml in H_2O	2.5 µg/ml	12.5 µg/ml
Tetracycline	20 mg/ml in ethanol	5 µg/ml	10 µg/ml

Stock solutions were sterile filtered before use.

6.5.3 Preparation of chemical competent bacteria

Bacteria are pre-incubated overnight in 5-10 ml LB-medium under shaking (180 rpm) at 37°C. The next day, the bacteria culture is diluted in 1L LB-medium and cultivated at 37°C (180 rpm shaking) until an O.D. value of 0.5 - 0.6 at 600 nm is reached. Afterwards, the bacteria suspension is pelletted by centrifugation in a cooled GSA-rotor at 4°C and 5000 rpm for 10 minutes. The supernatant is removed and the bacterial pellet is continuously kept on ice. The pellet is resuspended in 100 ml ice-cold 100mM MgCl2 and incubated on ice for 20 - 30 min. Then, cells are spinned down at 4000 rpm for 10 min at 4°C and the supernatant is removed. The pellet is again kept on ice and resuspended in 10 ml of ice-cold 100 mM $CaCl_2$-15%. Aliquots of 50 µl were frozen and stored at –70°C.

6.5.4 Transformation of chemically competent bacteria

A 50 µl aliquot of the chemically competent cells was thawed on ice for 10 to 15 min and thoroughly mixed with 0.5 - 1 µl DNA or ligation. This mixture was incubated on ice for 5 min and subsequent heat-shock was performed at 37°C. Afterwards, the cells were resuspended in 1 ml of LB medium and incubated for phenotypical expression of antibiotic resistance for 1 h at 37°C. Then, cells were plated on a selective solid medium and incubated overnight at 37°C.

6.5.5 Preservation of *E. Coli* strains

For short time storage, *E. Coli* was expanded overnight at 37°C on agar plates and subsequently kept at 4°C. For long-term storage, 500 µl of a bacteria suspension were mixed with 87 % glycerol and stored in special glass vials at -80°C.

6.5.6 Small scale plasmid DNA isolation

STET buffer	80g/l Sucrose; 0,5% Triton X100; 50 mM EDTA; 10 mM tris/HCl pH8,0
TE buffer	0,1 mM EDTA;10 mM Tris/HCL, pH 8,0
Lysozyme	10 mg/ml lysozyme in TE buffer
Ammonium acetate	8 M NH_4OAc
TE RNase	10 µg/ml RNase A in TE buffer

2 ml of LB medium containing the respective antibiotic(s) are inoculated with the bacteria containing the desired plasmid DNA. Those are cultivated under shaking at 37°C for 12 – 16 h. Afterwards, the bacteria are transferred to eppendorf tubes and centrifuged for 1 min at 13.000 rpm. Then cells are resuspended in 500 l of STET buffer and 50 µl lysozyme are added. The mixture is carefully mixed and after 2 – 3 min of room temperature incubation, the reaction is heat inactivated at 95°C for 90 sec. The viscous pellet is removed using a toothpick. 50 µl of ammonium acetate and 500 µl of isopropanol are mixed with the left solution and carefully mixed. Then, the mixture is centrifuged at 13000 rpm for 5 min. The supernatant is decanted and after air-drying, the pellet is dissolved in 50 µl TE-RNase (according to Maniatis et al, 1982).

6.5.7 Large-scale plasmid DNA isolation

For large-scale isolation of plasmid DNA, the Plasmid Maxi Kit from Qiagen, the PureYield Plasmid Midiprep from Promega or the PhoenIX™ Filter Maxiprep Kit (Qbiogene) was used according to the manufacturer's instructions. 200 ml LB medium containing the appropriate antibiotic were inoculated with the desired bacteria and incubated overnight at 37°C (180 rpm). Centrifugation at 4500 rpm was performed for at 4°C 20 min to pellet the bacteria (GS3 rotor). The pellets were treated as described in the kit's manual and DNA was finally dissolved in an appropriate amount of TE buffer.

6.6 Culture and manipulation of eukaryotic cells

6.6.1 Cell lines used

NIH3T3: embryonic mouse fibroblast (MEF) cell line, ATCC CRL 1658

HEK-293T: human embryonic kidney cell line transformed by adenovirus type 5 (DSMZ ACC 110), into which the temperature sensitive gene for SV40 T-antigen was inserted

6.6.2 Media components

DMEM (Dulbecco's Modified Eagle's Medium)	13.63 g/L DMEM powder (Sigma), 3.67 g/L (44 mM) NaHCO3, 2.6 g/L 10mM HEPES, pH 7.2
PBS	140 mM NaCL, 27 mM KCl, 7.2 mM Na_2HPO_4, 14.7 mM KH_2PO_4, pH 6.8-7.0
TEP (trypsin EDTA)	6 mM EDTA, 0.1 % trypsin (Gibco) in PBS
100 x Pen/Strep	6.06 mg/ml ampicillin (10,000 U/ml), 10 mg/ml streptomycin, set pH to 7.4 by addition of NaOH for dissolving (stored at –20°C)
100 x Glutamine	29.23 mg/ml glutamine, filter sterile, (stored at –20°C)
FCS (Fetal Calf Serum)	Lonza
G418	100 mg/ml G418 in ddH_2O, filter sterile, (stored at -20°C)
Puromycin	5 mg/ml Puromycin in ddH_2O, filter sterile, (stored at -20°C)
Hygromycin	480 U/µL Hygromycin in ddH_2O, filter sterile, (stored at 4°C)
Gentamycin	50 µg/ml (Sigma), (stored at -20°C)
Doxycycline	2 mg/ml doxycycline-hyclate (Sigma) in 70% ethanol, filter sterile, (stored at -20°C)

Coumermycin	5 µM in 100 % DMSO, filter sterile, (stored at -20°C)

6.6.3 Media composition

DMEM 3+	1 x Pen/Strep 1 x Glutamine 10% FCS DMEM

6.6.4 Supplementation of media with antibiotics

Strain	Antibiotic	Concentration
NIH3T3	G418	1 mg/ml
NIH3T3	Puromycin	2.5 µg/ml
NIH3T3	Hygromycin	150 - 300 U/ml
HEK-293T	Puromycin	0.3 µg/ml
HEK-293T	Hygromycin	300 U/ml
NIH3T3/HEK-293T (if not depicted differently)	Doxycycline	2 µg/ml
NIH3T3/HEK-293T	Coumermycin	5 nM

6.6.5 Cultivation of eukaryotic cells

Cells are cultivated in appropriate culture plates or flasks at 37°C and 5 % CO_2 at maximal humidity. The medium was changed every 3 – 4 days. Confluent cells were passaged into new culture plates or flasks containing fresh DMEM 3+. For passaging, cells were once washed with PBS and subsequently trypsinized for some minutes. Then, cells were removed from the surface by thoroughly shaking the cell flask. For the inactivation of trypsine, the cell suspension was diluted into 2 volumes of FCS containing medium. Afterwards, cells were transferred to a new culture flask containing fresh medium.

For determination of the cell number, an aliquot of the cell suspension was counted with the Casy-1 DT cell counter (Schaerfe Systems, Germany).

6.6.6 Long-term storage of eukaryotic cells

For the storage of eukaryotic cells, exponentially growing cells were washed, trypsinized and centrifuged (1000 rpm, 5 min). The cell pellet is resuspended in cold FCS containing 5 % of DMSO and transferred to Cryo vials (Corning).

After 30 min on ice, the vials containing the cell suspension were transferred to isolating boxes and stored at -70°C. 1 - 2 d later, cells were transferred into liquid nitrogen for long-term storage.

Thawing of cells was quickly performed in a 37°C water bath since DMSO could damage the cells. The cell suspension was diluted into 5 ml of pre-warmed DMEM 3+. The suspension was transferred into a 15 ml Falcon tube and centrifuged at 1000 rpm for 5 min. Afterwards, the supernatant was removed, the cell pellet was resuspended in fresh medium and cells were seeded on a new cell culture flask.

6.6.7 IFN-β stimulation of cells

Recombinant murine IFN-β was produced in-house using supernatants of stably transfected BHK-1 cells. The IFN-β titers were determined by an antiviral assay or by a bioassay which is based onNIH3T3 cells stably expressing *Mx2*-driven luciferase (Pulverer, 2008). Standard curves were determined with commercially available IFN-β.

For stimulation of the cells, 500 U/ml were directly added to the supernatant.

6.6.8 Viral infection

Prior to virus infection, cells were seeded on appropriate cell culture plates. To prevent inhibition of viral replication by FCS, cells were washed three times with antibiotic- and FCS-free medium. Infection was also performed in this medium. The virus was left on the cells for 1 h and afterwards, cells were again washed three times with DMEM3+.

Newcastle Disease virus (NDV) [20,000 HAU/ml] (Lohmann Tierzucht GmbH, Cuxhaven, Germany) was used in 1:250 dilution.

Influenza A/PR8_FRE_EMG_0901 (provided by Prof. Dr. Klaus Schughart, department for infection genetics, Helmholtz Centre for Infection Research, Braunschweig) was used at an MOI of 1 or 5.

6.6.9 Gene transfer methods

6.6.9.1 Transfection by calcium phosphate/DNA precipitation

2 x HEBS buffer	280 mM NaCl, 50mM HEPES, 1.5 mM Na_2HPO_4, pH 7.1 (filter sterile)
CaCl2 solution	2.5 M CaCl2 in ddH_2O (filter sterile)

1 x 10^5 NIH3T3 or 3 x 10^5 HEK-293T cells were seeded on a 6-well. The next day, the DNA(s) to be transfected were mixed with CaCl2 solution in a 5 ml tube (15 µL $CaCl_2$, 1-10 µg DNA und H_2O (Σ = 150 µL)). Afterwards, the mixture is dropped into 150 µl of 2 x HEBS buffer under vortexing. This mixture is then incubated at room temperature (RT) for 3 – 10 min and then dropped onto the cells which are subsequently carefully pivoted to dispense the solution and then cultured as described before (chapter 5.5.5). One day after transfection, medium was changed and selection pressure was imposed 2 days after transfection if necessary.

6.6.9.2 Lipofection

Transfection was also performed using Metafectene (Biontex Laboratories GmbH). 0ne day prior to transfection, cells were seeded as described in chapter 5.5.9.1. The respective amount of DNA was mixed with 5 µl of Metafectene (mixed before use) in 45 µl of DMEM and incubated for 10 - 15 min at RT. This mixture was then added to the cells and stored in the incubator. The next day, medium was changed and selection pressure was imposed 2 days after transfection if necessary.

6.6.9.3 Infection with lentivirus

Virus production:

Medium for production:	1x Pen/Strep, 1x glutamin 10 % (v/v) FCS DMEM 20 mM HEPES

Day 1: 1.2 x 10^6 HEK-293T cells are seeded on a 55 cm^2 cell culture dish.

Day 2: HEK-293T cells are transfected with the transfer plasmid as well as the helper plasmids (ViraPowerTM Lentiviral Expression System, Invitrogen) (table 1) by calciumphosphate/DNA precipitation (chapter 5.5.9.1) in 5 ml of DMEM3+.

Day 3: The medium is exchanged for 5 ml of production medium.

Day 4 and 5: The production medium (virus supernatant) is collected and replaced by fresh production medium. After filtration (0.4 µm pore diameter, the virus supernatant is immediately frozen at -70°C and stored until its use.

Plasmid	amount
Transfer plasmid:	7.7 µg
Helper plasmids (Invitrogen):	
pLP1 (gag/pol)	5 µg
pLP2 (rev)	1.9 µg
pVSV-G	3.5 µg

Virus infection:

The cells to be infected were seeded at a density of 2 x 10^5 (NIH3T3) on a 55 cm^2 dishes. The next day, the virus supernatant is supplemented with 8 µg/ml polybrene and administered to those cells. After 24 h, the medium is exchanged and 48 h pi, selection and expansion of the transduced cells is induced.

6.6.10Isolation of selected clones

When single colonies were grown up after the respective drug selection, those clones were marked at the bottom of the dish. Cell clones were washed with PBS and fresh PBS was added to cover the surface of the cell culture plate. A microscope was placed under a clean bench and colonies were gently removed with a 20 µl Gilson pipette. Cells were transferred to a microtiter plate harboring

150 µl of fresh DMEM3+ containing the respective antibiotic and distributed by up-and down-pipetting. From this plate, cells are expanded.

If single clones could not be picked, cells were sorted onto microtiterplates by Fluorescence Activated Cell Sorting (FACS, 5.5.11) using FACSVantage or FACSAria (Becton Dickinson). The medium within the single wells (each 150µl) contains 50 µg/ml of gentamycin to avoid contamination of the plates.

6.6.11Fluorescence Activated Cell Sorting (FACS)

FACS was performed to determine amounts and intensities of cells expressing a respective fluorescent marker.

For HaloTag detection, the respective cells were stained overnight with 100 nM TMR or with 333 nM for 30 min. Oregon Green was used overnight at a concentration of 1 nM. Meanwhile staining, the cells are incubated at 37°C. Since the HaloTag ligands are very light-sensitive, all works with it were performed in the absence of flashy light.
For the measurement, cells were washed with PBS, trypsinized and harvested in measurement tubes (Sarstedt). After centrifugation (1000 rpm, 5 min), the supernatant was removed and the cells were resuspended in FACS buffer (PBS containing 2 % FCS). Analysis of the cells was performed in a FACSCalibur machine (Becton Dickinson). Debris was eliminated from the analysis by setting the forward scatter < 200.
Sorting of cells was performed with a FACSVentage or FACSAria (Becton Dickinson).

6.7 Microscopy

6.7.1 Fluorescence Microscopy

Fluorescence microscopy allows the visualization of fluorescently labeled proteins within a cell. In this work, it was performed with a Zeiss Axiovert 135 TV microscope. By the use of a mercury arc lamp, the extinction of fluorophores could be achieved and visualization occured by the use of Omega Optical Filters.

6.7.2 Time-Lapse Microscopy

The visualization of single cells or even cell components can be performed overtime using a fluorescence microscope in combination with an incubation chamber and position automation.
The respective microscope used in this work uses an Xe-Arc burner excitation light source, an automated objective revolver as well as a wheel harboring harboring the fluorescent filters (BFP, CFP, eGFP, dsRED, mcherry). The objective used in this work was the 20 x (UPLSAPO 20 x immersion oil).
During the experiments, the cells, seeded on a special microscopy slide (ibidi), were applied to the automated PRIOR stage, which was heated to 37°C and was verbunden with a CO_2 source to provide optimal culture conditions. In order to maintain maximal humidity, fresh, destilled water was provided within a reservoir every 24 h.
The cells (10^5 cells/ml) were seeded onto a collagen IV-treated chambered microscopy slide (ibidi, µ-slide 8-well). Using collagen-treated slides, the movement of the cells should be inhibited to increase the number of cells resting within the determined area during long-term experiments.
The time series pictures were taken from multiple positions per slide in 20 or 30 minutes intervals. CellM software (version 3.1) was used for the data acquisition and for positioning as well as autofocus function. The autofocus function was used on bright field pictures, which were additionally taken at any chosen time point and position, to avoid photobleaching effects.
The image series were analyzed using imageJ software (National Institute of Health). Before the analyses, background substraction was equally performed for al taken pictures. To facilitate the tracking of single cells in image series as well as the measurement of basic track statistics, the plugin MTrackJ (Meijering, Biomedical Imaging Group Rotterdam) was used.

6.8 Protein analysis

6.8.1 Preparation of cell extracts

Cell solubilization buffer	50 mM Tris/HCl pH 7,5, 150 mM NaCl, 2 mM EDTA, 1 % Triton, 0,5 % Nonidet p-40 (Sigma), 100 x Protease Inhibitor Cocktail SetI (Calbiochem)

For the determination of firefly luciferase expression levels, it was necessary to extract all water soluble proteins from the cells. To this end, cells were harvested from a 6-well and resuspended in 50 µl Tris-HCl (pH 7.6) by vortexing. Cells were solubilized by 4 x repeated freeze and thaw cycles in liquid nitrogen and a 37°C water bath. Afterwards, centrifugation was performed (13.000 rpm, 10 min, 4°C). The supernatant was used for BCA- and luciferase assay.

6.8.2 Luciferase assay

Luciferase buffer	25 mM glycylglycine, 15 mM $MgSO_4$ in ddH_2O, pH 7.8 (stored at 4°C)
ATP solution	5 mM ATP in ddH_2O, pH7.5 (stored at –20°C)
Luciferin solution	0.1 mM synthetic D-luciferin (Promega), 25 mM glycylglycine in ddH_2O, pH 7,8 (stored at –20°C)
Reaction buffer	1:5 ATP solution: luciferase buffer

The oxidation of D-luciferin to oxyluciferin is catalyzed by firefly luciferase. Emitted photons are detected for the determination of expression levels of the luciferase reporter gene.
For the luminometric assay, 10 µl of the protein supernatant from chapter 5.6.1 was added to 400 µl of of the reaction buffer. 50 µl of luciferin were injected at the luminometer. Light of 610 nm is emitted since luciferase utilizes luciferin as a substrate and detection occurs via the luminometer.

6.8.3 BCA assay

(according to Smith et al, 1985)

BCA A solution	1 g bicinchoninic acid 1.71 g Na_2CO_3 0.95 g $NaHCO_3$ 0.16 g Na_2Tartrat 100 ml ddH_2O pH set to 11.25 with 10 N NaOH (stored at 4°C)
BCA B solution	4 g $CuSO_4$ x 5 H_2O/100 ml dissolved in ddH_2O (stored at 4°C)
Reaction solution	98 % BCA A, 2 % BCA B, freshly prepared
Protein standard	3 mg/ml lysozyme in ddH_2O (stored at –20°C)

The protein content of the luciferase samples (chapter 5.6.2) or samples used for the Western Blot (chapter 5.8.3) was determined by a BCA assay. By relating them to the total protein content of the luciferase samples, the results for them were normalized. Equal amounts of protein levels were calculated and used for the Western Blot.
Into the first row of a 96-well microtiter plate for optical tests, each 190 µl of the reaction solution was pipetted into the wells. Into the other rows each 100 µl of the reaction solution were added. In order to determine the background signal of the reaction, 10 µl of Tris-HCl (pH 7.6) were pipetted into the first well of the first row. To the right, 10 µl of the protein standard were added. Into the other wells of the first row, each 10 µl of a protein sample are given. In each well, the solution is carefully mixed by up- and down-pipetting via a multichannel pipette, avoiding bubble formation, and 100 µl of the first row are then transferred and mixed with the reaction solution in the second row. This procedure was repeated until the last row was reached and final 100 µl were discarded so that each well harbors 100 µl in the end. Then, the plate was incubated at 37°C for 30 – 60 min and absorption was measured at 595 nm by a Multiskan EX reader (Thermo Electron Corporation). Background levels (first column) were automatically subtracted and protein contents were calculated on the basis of a calibration curve.

6.8.4 SDS Polyacrylamide gel electrophoresis

Preparation of the cell lysate:

Table 1: Composition of cell lysis (RIPA) buffer

Substance	Concentration of stock solution	Target concentration	Volume
Tris-HCl, pH 7.5	1 M	10 mM	2 ml
NaCl	4 M	150 mM	7.5 ml
Triton X-100	100 %	1 %	2 ml
SDS	10 %	0.1 %	2 ml
Deoxycholic Acid = Na-Deoxycholat	10 %	1 %	20 ml
DTT	1 M	1 mM	0.2 ml
Na_3VO_4	1 M	1 mM	0.2 ml
NaF	1 M	1 mM	0.2 ml
PICIII	-	1/1000	0.2 ml
ddH_20	-	-	165.7 ml
Total volume			200 ml

*DTT, Na_3VO_4, NaF and PICIII have to be freshly added

The cell pellets were lysed in 40 µl RIPA buffer and incubated for 20 min at 4°C. Afterwards, centrifugation was performed at 13.000 rpm and 4°C for 10 min. The supernatant was further used.

Performance of SDS-PAGE

Separating gel	14.4 ml acrylamid (30 %), 11.1 ml 1.5 M Tris-HCL (pH 8.8), 450 µl 10 % SDS, 225 µl 10 % APS, 18.9 ml ddH_2O, 18 µl TEMED
Stacking gel	2 ml acrylamid (30 %), 4 ml 0.5 M Tris-HCL (pH 6.8), 160 µl 10 % SDS, 160 µl 10 % APS, 9.6 ml ddH_2O, 16 µl TEMED
SDS-PAGE running buffer (10 x)	144 g glycin, 30.3 g Tris, 10 g SDS, made up with ddH_2O to 1l

SDS-polyacrylamide gel electrophoresis (Laemmli 1970) is used to separate proteins in a polyacrylamide gel matrix. This occurs according to their size. Before the samples are applied on a gel, a sample buffer, containing SDS as an anionic detergent that denatures proteins and charges them negatively is administered (NuPAGE® LDS sample buffer, Invitrogen). Consequently, the proteins are separated by electrophoresis without the influence of protein charge

and conformation. The Polyacrylamide gels used in this work consist of a stacking and a separating gel (10%). They were prepared of different polyacrylamide concentrations and with buffers of different pHs. By this method, the proteins are focused on the border between the two gels to guarantee an equal starting point for the proteins. Gel electrophoresis was performed in vertical electrophoresis chambers by BioRad (Protean II XL).
After polymerisation of the gel, combs were removed and the slots were washed with SDS running buffer. The supernatant of each sample was mixed with SDS loading buffer and boiled at 95°C for 5 min to fully denature proteins. Afterwards, equivalent protein values (30 µg) were applied to each chamber of the gel, which is assembled in the electrophoresis chamber. A prestained Molecular Weight marker (Invitrogen, Benchmark™ pre-stained protein ladder) was placed at the beginning and at the end of the gel.
The gel run was performed in 1 x SDS-PAGE running buffer at 100 – 120 mA for 2 – 2.5 h.

6.8.5 Western Blotting

TBS	20 mM TRIS pH 7.5, 150 mM NaCl
TBST	TBS, 0.05% TWEEN-20
TBSTM	TBST, 5% non-fat dry milk

In order to detect the desired proteins, Western blotting was performed using the Bio-Rad Trans-Blot Cell. For this reason, they were transferred to a nitrocellulose membrane (Amersham Biosciences; Towbin et al, 1979). The membrane was activated by 15 s incubation in methanol. The membrane was placed face-to-face with the gel and enclosed by whatman paper as well as fiber pads which were soaked with transblot buffer before. The blot cell was placed in a blotting tank filled with transblot buffer with the membrane facing the anode. Blotting was performed in a 4°C room at 300 mA for 2 – 3 h. Afterwards, the membrane was washed 3 x with TBST and 1 x with TBS for each 5 min. Then, the membrane was blocked with TBSTM for 1 h at RT or overnight at 4°C in order to saturate unspecific protein interactions. Then, TBSTM was removed and replaced by a 1:500 dilution of the primary antibody (anti-NS1, sc-130568, Santa Cruz Biotechnology) in 20 ml of fresh TBSTM. After overnight incubation at 4°C, the membrane was washed as described before and then incubated for 1 h in a 1:20.000 dilution of the secondary antibody, an anti-mouse HRP conjugate, in TBSTM. Another washing step as described before was performed. Detection of the protein was performed in a BioRad ChemiDoc XRS system after administration of the detection reagent (Lumigen TMA-6).

Acquisition and quantification of the data was performed using the Quantity One program.

Membrane stripping:

To reuse the membrane for a second round of protein detection, antibody bindings had to be solved. For this reason, the membrane was 1 x washed with TBST and 1 x with TBS for 5 min at RT and the membrane was incubated with 20 ml of 1 x strip reagent (ReBlot Plus Mild Antibody stripping solution, Millipore) for 15 min at RT. Afterwards washing was performed by 3 x incubation with TBST and 1 x with TBS. Blocking and antibody staining were performed as described above, despite the antibody concentrations. For the primary antibody (anti actin HRP conjugate, Calbiochem) a dilution of 1:15.000 was used and for the secondary antibody (same as above), a 1:5000 dilution was used.

7 Vectors and Oligonucleotides

7.1 Applied vectors

pCCLEF1aPuroKRABrtTA3 (#3561)	Schulze, HZI (2008)
pCMVBL-IRF3-5D (#1908)	(Lin et al, 1999)
pCMVKRAB (#2271)	(Forster et al, 1999)
pCMVRTA2HYG (#2288)	May, HZI (2002)
pCuR.luc.HTV7 (#3248)	Promega
pFK_i389lucEI.JFH1 dGDD (#3484)	Th. Pietschmann, TWINCORE
pFK-JFH1/wt_dg (#3578)	Th. Pietschmann, TWINCORE
pNS1.S8.SS2.NIBSC (#3579)	Timo Frensing, MPI Magdeburg
pTREtight (#3891)	Clontech
pturboGFP-PRL-dest1 (#3863)	Evrogen
pturboRFP.dest1 (#3882)	Evrogen
pCR-Blunt	Invitrogen
pUHD13-3 (#947)	(Gossen & Bujard, 1992)
pUHRT62-1 (#2209)	(Urlinger et al, 2000)

7.2 Cloned vectors

pTet-Unit2 (#4024)	Tet-Unit-encoding construct: The vector ptet.tGFPest (#4025) was cut with *SalI* and filled in by Klenow. pTet-Unit (#3879) was cut with *XhoI* and *ScaI* and filled in with Klenow. The 5234 bp fragment of pTet-Unit containing *hyg*, EMCV IRES, tTA, $P_{bidiTet}$ and CouTA was ligated into the backbone of ptet.tGFPest.
pbidi.Cou-Unit (#4023)	Cou-Unit-encoding construct: The vector pbidi.Cou (#3883) was cut with *HindIII* and *XhoI* (loss of TurboGFP) and was filled in by Klenow. pCou-Unit (#3878) was cut with *SmaI* and *HindIII* and was filled in by Klenow. The 1048 bp fragment containing KRAB was ligated into the pbidi.Cou backbone.
pKrab.PGK.puro (#3860)	KRAB-expressing construct: The vector pKrab.rtTA2.PGK.Puro (#3880) was cut with *SnaBI* and *NotI* (loss of rtTA2). Overhanging ends were blunted by Klenow and religation was performed.
pCMV.CouTA.puro (#3877)	CouTA-expressing vector: The vector prtTA2.Krab.PGK.Puro (#3861) was cut with *HpaI* (loss of rtTA2, EMCV IRES, KRAB and part of SV40 polyA). The vector pTETproCurTA (#3368) was cut with *BamHI* and *HpaI*. Overhanging ends were filled in by Klenow. The 1878 bp fragment containing the CouTA and the complementing part of SV40 polyA was ligated to the backbone of prtTA2.Krab.PGK.Puro.

ptight.NS1-HTV7 (#4019)	NS1-H-expressing construct: The vector pTREtight.Hyg (#4018) was cut with *MluI* and *EcoRV*. The vector ptet.NS1-HTV7delta neo (#3874) was cut with *XbaI* and filled in by Klenow. It was further digested with *MluI*. The 1661 bp fragment containing NS1-H was ligated to the backbone of pTREtight.Hyg.
prtTA2.PGK.puro (#4022)	rtTA2-expressing construct: The vector prtTA2.Krab.PGK.puro (#3861) was cut with *AvrII* and *NotI* (loss of KRAB). Overhanging ends were filled in by Klenow. The vector was religated.
ptet.NS1-HTV7 (#3589)	NS1-H-expressing construct: The vector ptet.Core (#3584) was digested with *MluI* and *NotI* (loss of core). pconst.NS1-HTV7 (#3582) was cut with *MluI* and *NotI*. The 1772 bp fragment containing NS1-H was ligated to the backbone of ptet.Core.
ptet.NS3/4A-HTV7 (#3587)	NS3/4A-H-expressing construct: The vector ptet.NS1-HTV7 (#3589) was digested with *MluI* and *BglII* (loss of NS1). A PCR fragment was amplified with the Primers NS3/4A_3' (# 3754) and NS3/4A_5' (# 3755) using pFK_i389lucEI JFH1 dGDD (# 3484) as a template. This fragment was filled in by Klenow and ligated with pCR-Blunt (Invitrogen).The target sequence was excised by cutting with *MluI* and *BamHI* and ligated with the backbone of ptet.NS1-HTV7, thereby fusing NS3/4A to HaloTag V7.

ptet.NS3/4A-HTV7Δneo (#3869)	NS3/4A-H-expressing construct: The vector ptet.NS3/4A-HTV7 (#3587) was digested with *BstBI* and *PstI* and overhanging ends were filled in by Klenow reaction. The 3708 bp fragment was ligated to the 2345 bp fragment of ptet.NS1 (#3588) which was digested with *AatII* and *NheI* and filled in by Klenow reaction.
ptet.NS3/4A-HTV7Δneo (#3869)	NS3/4A-H-expressing construct: The vector ptet.NS1 (#3588) was digested with *AatII* and *NheI* (loss of neomycin phosphotransferase, $P_{bidiTet}$ and NS1) and filled in by Klenow. The vector ptet.NS3/4A-HTV7 (#3587) was digested with *BstBI* and *PstI* and overhanging ends were filled in by Klenow reaction. The 3708 bp fragment containing $P_{bidiTet}$ and NS3/4A-H was ligated to the backbone of ptet.NS1.

7.3 Oligonucleotides

pNS1 3‘ (#3760):

5’ GGAACAATTAGGTCAGAAGTTTGGCAGATCTTCGCGACTAGCGGC CGCAAATTAA 3’

pNS1 5‘ (#3761):

5’ TTAATTTCGATCGACGCGTCCATGGATCCAAACACTGTGTCAAG C 3’

pNS3/4A 3‘ (#3754):

5’ GCTTTTGATGAGATGGAGGAATGCGGGATCCTCGCGACTAGCGGC CGCAAATTAA 3’

pNS3/4A 5‘ (#3755):

5’ TTAATTTCGATCGACGCGTCCATGGCTCCCATCACTGCTTATGC 3’

8 Appendix

8.1 Abbreviations

α	alpha
β	beta
γ	gamma
δ	delta
ε	epsilon
κ	kappa
λ	lambda
μ	my and micro
ω	omega
aa	amino acids
ATP	adenosintriphoshate
a.u.	arbitrary units
BAC	bacterial artificial chromosome
bp	base pair
β-gal	β-galactosidase
C-terminus	carboxy-terminus
CARD	caspase recruitment domain
CAT	chloramphenicol acetyltransferase
CBP	CREB-binding protein
CFP	cyan fluorescent protein
CMV	cytomegalovirus
Cou	Coumermycin
CouTA	coumermycin transactivator
CpG	cytosine phosphatidyl guanine
Da	dalton
DC	dendritic cell
DMEM	Dulbecco's modified Eagle's medium
DNA	desoxyribonucleic acid
dNTP	desoxynucleotide triphosphate
Dox	doxycycline

dsRNA	double-stranded RNA
E. coli	Escherichia coli
eGFP	enhanced GFP
EMCV	encephalomyocarditis virus
FACS	fluorescence activated cell sorting
FCS	fetal calf serum
Fig.	figure
G418	aminoglycosid-2´-deoxystreptin
GFP	green fluorescent protein
GOI	gene of interest
GTPase	guanosine triphosphatase
GyrB	gyrase B subunit
h	hours
HAU	haemagglutinating unit
HCV	hepatitis C virus
HMG	high-mobility group
HTV7	HaloTag V7
Hyg	hygromycin phosphotransferase
IAV	influenza A virus
IFN	interferon
IFNAR	IFN-α receptor
IKK	IκB kinase
IPS-1	IFN-β promoter stimulator
IRAK	IL-1-receptor-associated kinase
IRF	IFN regulatory factor
ISG	IFN stimulated gene
ISGF	IFN stimulated gene factor
ISRE	IFN stimulated response elements
JAK	Janus activated kinase
KRAB	Krüppel-associated box

L	liter
LGP-2	laboratory of genetics and physiology-2
LIF	leukemia inhibitory factor
LPS	lipopolysaccharide
Luc	luciferase
m	milli or meter
M	molarity
mCherry	monomeric Cherry (red fluorescent protein)
MDA-5	melanoma-differentiation-associated gene 5
MDCK	Madin-Darby canine kidney
MEF	murine embryonic fibroblast
min	minute
MOI	multiplicity of infection
mRNA	messenger RNA
Mx	myxovirus resistance gene
MyD88	myeloid differentiation primary-response gene 88
n	nano
N-terminus	amino terminus
NDV	Newcastle disease virus
NF-κB	nuclear factor κB
NS	non-structural protein
NS1-H	fusion of NS1 to HaloTag V7
NS3/4A-H	fusion of NS3/4A to HaloTag V7
NLS	nuclear localization signal
NoLS	nucleolar localization signal
NTR	Non-translated region
OAS	oligoadenylate synthetase
OD	optical density
OG	Oregon Green
ORF	open reading frame
p	piko
PABPII	poly(A)-binding protein II
PAMP	pathogen-associated molecular pattern
$P_{bidiTet}$	bidirectional tetracycline-responsive promoter

PBS	phosphate buffer saline
PCR	polymerase chain reaction
P_{Cou}	coumermycin-responsive promoter
PGK	phosphoglycerate kinase
P_{hCMV*}	human minimal Cytomegalus promoter
PKR	protein kinase R
polyA	polyadenylation signal
poly I:C	polyinosinic-polycytidylic acid
PR8	influenza A/PR/8/34
PRR	pathogen recognition receptor
P_{Tet}	tetracycline-responsive promoter
P_{Tight}	tight tetracycline-responsive promoter
RFP	Red fluorescent protein
RIG-I	retinoic-acid-inducible gene I
RLR	RIG-I-like receptors
RMCE	recombinase-mediated cassette exchange
RNA	ribonucleic acid
RNAi	RNA interference
RNase	ribonuclease
Rpm	rounds per minute
RT	room temperature
rtTA	reverse tetracycline transactivator
s	second
ssRNA	single-stranded RNA
SD	standard deviation
SDS	sodium dodecyl sulfate
SOCS	suppressor of cytokine signaling
STAT	signal transducer and activator of transcription
STING	stimulator of IFN genes
SV40	simian virus 40
TBK-1	TANK-binding kinase 1
tdTomato	tandem dimer Tomato
Tet	tetracycline
tetO	tetracycline operator
Tet-On	tetracycline-dependent expression system

Tet-Off	tetracycline-dependent expression system
tetR	tetracycline repressor
tGFP	destabilized turbo green fluorescent protein
TurboGFP	Turbo green fluorescent protein
tRFP	destabilized turbo red fluorescent protein
TIR	TLR-interleukin-1 receptor
TLR	toll-like receptor
TMR	Tetramethylrhodamin
TNFα	tumor necrosis factor alpha
TRAF	TNF-receptor associated factor
TRIF	TIR-domain-containing adapter-inducing interferon-β
TRIM25	tripartite-motif 25
Tris	tris-hydroxymethyl-aminomethan
tTA	tetracycline transactivator
Tyk2	tyrosin kinase 2
U	unit
YFP	yellow fluorescent protein

8.2 References

Agha-Mohammadi S, O'Malley M, Etemad A, Wang Z, Xiao X, Lotze MT (2004) Second-generation tetracycline-regulatable promoter: Repositioned tet operator elements optimize transactivator synergy while shorter minimal promoter offers tight basal leakiness. *Journal of Gene Medicine* **6**(7)**:** 817-828

Ahlquist P, Schwartz M, Chen J, Kushner D, Hao L, Dye BT (2005) Viral and host determinants of RNA virus vector replication and expression. *Vaccine* **23**(15 SPEC. ISS.)**:** 1784-1787

Alexopoulou L, Holt AC, Medzhitov R, Flavell RA (2001) Recognition of double-stranded RNA and activation of NF-κB by Toll-like receptor 3. *Nature* **413**(6857)**:** 732-738

Arias CF, Escalera-Zamudio M, de los Dolores Soto-Del Río M, Georgina Cobían-Güemes A, Isa P, López S (2009) Molecular Anatomy of 2009 Influenza virus A (H1N1). *Archives of Medical Research* **40**(8)**:** 643-654

Aubel D, Fussenegger M (2010) Mammalian synthetic biology - From tools to therapies. *BioEssays* **32**(4)**:** 332-345

Barchet W, Blasius A, Cella M, Colonna M (2005a) Plasmacytoid dendritic cells: In search of their niche in immune responses. *Immunologic Research* **32**(1-3)**:** 75-83

Barchet W, Cella M, Colonna M (2005b) Plasmacytoid dendritic cells - Virus experts of innate immunity. *Seminars in Immunology* **17**(4)**:** 253-261

Baron U, Freundlieb S, Gossen M, Bujard H (1995) Co-regulation of two gene activities by tetracycline via a bidirectional promoter. *Nucleic Acids Research* **23**(17)**:** 3605-3606

Berens C, Hillen W (2003) Gene regulation by tetracyclines: Constraints of resistance regulation in bacteria shape TetR for application in eukaryotes. *European Journal of Biochemistry* **270**(15)**:** 3109-3121

Berg CP, Schlosser SF, Neukirchen DK, Papadakis C, Gregor M, Wesselborg S, Stein GM (2009) Hepatitis C virus core protein induces apoptosis-like caspase independent cell death. *Virology Journal* **6**

Berger SM, Pesold B, Reber S, Schönig K, Berger AJ, Weidenfeld I, Miao J, Berger MR, Gruss OJ, Bartsch D (2010) Quantitative analysis of conditional gene inactivation using rationally designed, tetracycline-controlled miRNAs. *Nucleic Acids Research* **38**(17)**:** e168-e168

Bode JG, Ludwig S, Ehrhardt C, Albrecht U, Erhardt A, Schaper F, Heinrich PC, Häussinger D (2003) IFN-alpha antagonistic activity of HCV core protein involves induction of suppressor of cytokine signaling-3. *The FASEB journal : official publication of the Federation of American Societies for Experimental Biology* **17**(3)**:** 488-490

Boo KH, Yang JS (2010) Intrinsic cellular defenses against virus infection by antiviral type I interferon. *Yonsei Medical Journal* **51**(1)**:** 9-17

Bornkamm GW, Berens C, Kuklik-Roos C, Bechet JM, Laux G, Bachl J, Korndoerfer M, Schlee M, Hölzel M, Malamoussi A, Chapman RD, Nimmerjahn F, Mautner J, Hillen W, Bujard H, Feuillard J (2005) Stringent doxycycline-dependent control of gene activities using an episomal one-vector system. *Nucleic acids research* **33**(16)

Boshart M, Weber F, Jahn G (1985) A very strong enhancer is located upstream of an immediate early gene of human cytomegalovirus. *Cell* **41**(2)**:** 521-530

Botezatu L, Sievers S, Gama-Norton L, Schucht R, Hauser H, Wirth D (submitted) Cell line development from a synthetic biology perspective.

Chaturvedi A, Pierce SK (2009) How location governs toll-like receptor signaling. *Traffic* **10**(6)**:** 621-628

Chen S, Short JAL, Young DF, Killip MJ, Schneider M, Goodbourn S, Randall RE (2010) Heterocellular induction of interferon by negative-sense RNA viruses. *Virology* **407**(2)**:** 247-255

Chen Z, Li Y, Krug RM (1999) Influenza A virus NS1 protein targets poly(A)-binding protein II of the cellular 3'-end processing machinery. *EMBO Journal* **18**(8)**:** 2273-2283

Cheng G, Zhong J, Chisari FV (2006) Inhibition of dsRNA-induced signaling in hepatitis C virus-infected cells by NS3 protease-dependent and -independent mechanisms. *Proceedings of the National Academy of Sciences of the United States of America* **103**(22)**:** 8499-8504

Childs K, Stock N, Ross C, Andrejeva J, Hilton L, Skinner M, Randall R, Goodbourn S (2007) mda-5, but not RIG-I, is a common target for paramyxovirus V proteins. *Virology* **359**(1)**:** 190-200

Civas A, Génin P, Morin P, Lin R, Hiscott J (2006) Promoter organization of the interferon-A genes differentially affects virus-induced expression and responsiveness to TBK1 and IKKε. *Journal of Biological Chemistry* **281**(8)**:** 4856-4866

Clontech (2003) pTRE-Tight Vectors. *Clontechniques* **18**
(3)**:** 13-14

Cutrone EC, Langer JA (2001) Identification of Critical Residues in Bovine IFNAR-1 Responsible for Interferon Binding. *Journal of Biological Chemistry* **276**(20)**:** 17140-17148

Dansako H, Ikeda M, Ariumi Y, Wakita T, Kato N (2009) Double-stranded RNA-induced interferon-beta and inflammatory cytokine production modulated by hepatitis C virus serine proteases derived from patients with hepatic diseases. *Archives of Virology* **154**(5)**:** 801-810

Dansako H, Ikeda M, Kato N (2007) Limited suppression of the interferon-β production by hepatitis C virus serine protease in cultured human hepatocytes. *FEBS Journal* **274**(16)**:** 4161-4176

Dauber B, Schneider J, Wolff T (2006) Double-stranded RNA binding of influenza B virus nonstructural NS1 protein inhibits protein kinase R but is not essential to antagonize production of alpha/beta interferon. *Journal of Virology* **80**(23)**:** 11667-11677

Davey RE, Onishi K, Mahdavi A, Zandstra PW (2007) LIF-mediated control of embryonic stem cell self-renewal emerges due to an autoregulatory loop. *FASEB Journal* **21**(9)**:** 2020-2032

De Wet JR, Wood KV, DeLuca M (1987) Firefly luciferase gene: Structure and expression in mammalian cells. *Molecular and Cellular Biology* **7**(2)**:** 725-737

Deuschle U, Meyer WKH, Thiesen HJ (1995) Tetracycline-reversible silencing of eukaryotic promoters. *Molecular and Cellular Biology* **15**(4)**:** 1907-1914

Ehrhardt C, Seyer R, Hrincius ER, Eierhoff T, Wolff T, Ludwig S (2010) Interplay between influenza A virus and the innate immune signaling. *Microbes and Infection* **12**(1)**:** 81-87

Elowitz MB, Leibler S (2000) A synthetic oscillatory network of transcriptional regulators. *Nature* **403**(6767)**:** 335-338

Failla C, Tomei L, De Francesco R (1994) Both NS3 and NS4A are required for proteolytic processing of hepatitis C virus nonstructural proteins. *Journal of Virology* **68**(6)**:** 3753-3760

Fenner JE, Starr R, Cornish AL, Zhang JG, Metcalf D, Schreiber RD, Sheehan K, Hilton DJ, Alexander WS, Hertzog PJ (2006) Suppressor of cytokine signaling 1 regulates the immune response to infection by a unique inhibition of type I interferon activity. *Nature Immunology* **7**(1)**:** 33-39

Fitzgerald KA, McWhirter SM, Faia KL, Rowe DC, Latz E, Golenbock DT, Coyle AJ, Liao SM, Maniatis T (2003) IKKE and TBKI are essential components of the IRF3 signalling pathway. *Nature Immunology* **4**(5)**:** 491-496

Ford E, Thanos D (2010) The transcriptional code of human IFN-β gene expression. *Biochimica et Biophysica Acta - Gene Regulatory Mechanisms* **1799**(3-4)**:** 328-336

Forster K, Helbl V, Lederer T, Urlinger S, Wittenburg N, Hillen W (1999) Tetracycline-inducible expression systems with reduced basal activity in mammalian cells. *Nucleic Acids Research* **27**(2)**:** 708-710

Foy E, Li K, Sumpter Jr R, Loo YM, Johnson CL, Wang C, Fish PM, Yoneyama M, Fujita T, Lemon SM, Gale Jr M (2005) Control of antiviral defenses through hepatitis C virus disruption of retinoic acid-inducible gene-I signaling. *Proceedings of the National Academy of Sciences of the United States of America* **102**(8)**:** 2986-2991

Freundlieb S, Schirra-Müller C, Bujard H (1999) A Tetracycline Controlled Activation/Repression System with Increased Potential for Gene Transfer into Mammalian Cells. *Journal of Gene Medicine* **1**(1)**:** 4-12

Fussenegger M, Morris RP, Fux C, Rimann M, Von Stockar B, Thompson CJ, Bailey JE (2000) Streptogramin-based gene regulation systems for mammalian cells. *Nature Biotechnology* **18**(11)**:** 1203-1208

Gack MU, Albrecht RA, Urano T, Inn KS, Huang IC, Carnero E, Farzan M, Inoue S, Jung JU, García-Sastre A (2009) Influenza A Virus NS1 Targets the Ubiquitin Ligase TRIM25 to Evade Recognition by the Host Viral RNA Sensor RIG-I. *Cell Host and Microbe* **5**(5)**:** 439-449

Gack MU, Shin YC, Joo CH, Urano T, Liang C, Sun L, Takeuchi O, Akira S, Chen Z, Inoue S, Jung JU (2007) TRIM25 RING-finger E3 ubiquitin ligase is essential for RIG-I-mediated antiviral activity. *Nature* **446**(7138)**:** 916-920

García-Sastre A, Egorov A, Matassov D, Brandt S, Levy DE, Durbin JE, Palese P, Muster T (1998) Influenza A virus lacking the NS1 gene replicates in interferon- deficient systems. *Virology* **252**(2)**:** 324-330

Gaszner M, Felsenfeld G (2006) Insulators: Exploiting transcriptional and epigenetic mechanisms. *Nature Reviews Genetics* **7**(9)**:** 703-713

Geiss GK, Salvatore M, Tumpey TM, Carter VS, Wang X, Basler CF, Taubenberger JK, Bumgarner RE, Palese P, Katze MG, García-Sastre A (2002) Cellular transcriptional profiling in influenza A virus-infected lung epithelial cells: The role of the nonstructural NS1 protein in the evasion of the host innate defense and its potential contribution to pandemic influenza. *Proceedings of the National Academy of Sciences of the United States of America* **99**(16)**:** 10736-10741

Gossen M, Bujard H (1992) Tight control of gene expression in mammalian cells by tetracycline- responsive promoters. *Proceedings of the National Academy of Sciences of the United States of America* **89**(12)**:** 5547-5551

Gossen M, Freundlieb S, Bender G, Muller G, Hillen W, Bujard H (1995) Transcriptional activation by tetracyclines in mammalian cells. *Science* **268**(5218)**:** 1766-1769

Grakoui A, McCourt DW, Wychowski C, Feinstone SM, Rice CM (1993) Characterization of the hepatitis C virus-encoded serine proteinase: Determination of proteinase-dependent polyprotein cleavage sites. *Journal of Virology* **67**(5)**:** 2832-2843

Greenspan D, Palese P, Krystal M (1988) Two nuclear location signals in the influenza virus NS1 nonstructural protein. *Journal of Virology* **62**(8)**:** 3020-3026

Hale BG, Randall RE, Ortin J, Jackson D (2008) The multifunctional NS1 protein of influenza A viruses. *Journal of General Virology* **89**(10)**:** 2359-2376

Haller O, Kochs G, Weber F (2006) The interferon response circuit: Induction and suppression by pathogenic viruses. *Virology* **344**(1)**:** 119-130

Haller O, Weber F (2009) The interferon response circuit in antiviral host defense. *Verhandelingen - Koninklijke Academie voor Geneeskunde van BelgiÃ«* **71**(1-2)**:** 73-86

Hampf M, Gossen M (2007) Promoter Crosstalk Effects on Gene Expression. *Journal of Molecular Biology* **365**(4)**:** 911-920

Han H, Cui ZQ, Wang W, Zhang ZP, Wei HP, Zhou YF, Zhang XE (2010) New regulatory mechanisms for the intracellular localization and trafficking of influenza A virus NS1 protein revealed by comparative analysis of A/PR/8/34 and A/Sydney/5/97. *Journal of General Virology* **91**(12)**:** 2907-2917

Han HJ, Jung EY, Lee WJ, Jang KL (2002) Cooperative repression of cyclin-dependent kinase inhibitor p21 gene expression by hepatitis B virus X protein and hepatitis C virus core protein. *FEBS Letters* **518**(1-3)**:** 169-172

Hayakawa T, Yusa K, Kouno M, Takeda J, Horie K (2006) Bloom's syndrome gene-deficient phenotype in mouse primary cells induced by a modified tetracycline-controlled trans-silencer. *Gene* **369**(1-2)**:** 80-89

Hayman A, Comely S, Lackenby A, Murphy S, McCauley J, Goodbourn S, Barclay W (2006) Variation in the ability of human influenza A viruses to induce and inhibit the IFN-β pathway. *Virology* **347**(1)**:** 52-64

Heil F, Hemmi H, Hochrein H, Ampenberger F, Kirschning C, Akira S, Lipford G, Wagner H, Bauer S (2004) Species-Specific Recognition of Single-Stranded RNA via Toll-like Receptor 7 and 8. *Science* **303**(5663)**:** 1526-1529

Helbig KJ, Yip E, McCartney EM, Eyre NS, Beard MR (2008) A screening method for identifying disruptions in interferon signaling reveals HCV NS3/4a disrupts Stat-1 phosphorylation. *Antiviral Research* **77**(3)**:** 169-176

Hemmi H, Takeuchi O, Kawai T, Kaisho T, Sato S, Sanjo H, Matsumoto M, Hoshino K, Wagner H, Takeda K, Akira S (2000) A Toll-like receptor recognizes bacterial DNA. *Nature* **408**(6813)**:** 740-745

Hiscott J (2007) Triggering the innate antiviral response through IRF-3 activation. *Journal of Biological Chemistry* **282**(21)**:** 15325-15329

Honda K, Taniguchi T (2006) Toll-like receptor signaling and IRF transcription factors. *IUBMB Life* **58**(5-6)**:** 290-295

Hop C, De Waard V, Van Mourik JA, Pannekoek H (1997) Lack of gradual regulation of tetracycline-controlled gene expression by the tetracyclin-repressor/VP16 transactivator (tTA) in cultured cells. *FEBS Letters* **405**(2)**:** 167-171

Horvath CM, Stark GR, Kerr IM, Darnell Jr JE (1996) Interactions between STAT and non-STAT proteins in the interferon- stimulated gene factor 3 transcription complex. *Molecular and Cellular Biology* **16**(12)**:** 6957-6964

Hu J, Sealfon SC, Hayot F, Jayaprakash C, Kumar M, Pendleton AC, Ganee A, Fernandez-Sesma A, Moran TM, Wetmur JG (2007) Chromosome-specific and noisy IFNB1 transcription in individual virus-infected human primary dendritic cells. *Nucleic Acids Research* **35**(15)**:** 5232-5241

Irshad M, Dhar I (2006) Hepatitis C virus core protein: An update on its molecular biology, cellular functions and clinical implications. *Medical Principles and Practice* **15**(6)**:** 405-416

Iwamoto M, Björklund T, Lundberg C, Kirik D, Wandless TJ (2010) A general chemical method to regulate protein stability in the mammalian central nervous system. *Chemistry and Biology* **17**(9)**:** 981-988

Jia D, Rahbar R, Chan RWY, Lee SMY, Chan MCW, Wang BX, Baker DP, Sun B, Malik Peiris JS, Nicholls JM, Fish EN (2010) Influenza virus non-structural protein 1 (NS1) disrupts interferon signaling. *PLoS ONE* **5**(11)

Jolma IW, Laerum OD, Lillo C, Ruoff P (2010) Circadian oscillators in eukaryotes. *Wiley interdisciplinary reviews Systems biology and medicine* **2**(5)**:** 533-549

Kain SR, Ganguly S (2001) Overview of genetic reporter systems. *Current protocols in molecular biology / edited by Frederick M Ausubel [et al]* Chapter **9**

Kästner P (2007) Etablierung von Genregulationssystemen in Säugerzellen für die Konstruktion künstlicher Regulationskreisläufe. Diplomarbeit an der Technischen Universität Braunschweig.

Kim J, Choi BH, Jang KL, Min DS (2004) Phospholipase D activity is elevated in hepatitis C virus core protein-transformed NIH3T3 mouse fibroblast cells. *Experimental and Molecular Medicine* **36**(5)**:** 454-460

Kim TK, Kim TH, Maniatis T (1998) Efficient recruitment of TFIIB and CBP-RNA polymerase II holoenzyme by an interferon-β enhanceosome in vitro. *Proceedings of the National Academy of Sciences of the United States of America* **95**(21)**:** 12191-12196

Kochs G, García-Sastre A, Martínez-Sobrido L (2007) Multiple anti-interferon actions of the influenza A virus NS1 protein. *Journal of Virology* **81**(13)**:** 7011-7021

Koerner I, Kochs G, Kalinke U, Weiss S, Staeheli P (2007) Protective role of beta interferon in host defense against influenza a virus. *Journal of Virology* **81**(4)**:** 2025-2030

Kramer BP, Fussenegger M (2005) Hysteresis in a synthetic mammalian gene network. *Proceedings of the National Academy of Sciences of the United States of America* **102**(27)**:** 9517-9522

Kramer BP, Viretta AU, Baba MDE, Aubel D, Weber W, Fussenegger M (2004) An engineered epigenetic transgene switch in mammalian cells. *Nature Biotechnology* **22**(7)**:** 867-870

Kumar H, Kawai T, Akira S (2011) Pathogen recognition by the innate immune system. *International Reviews of Immunology* **30**(1)**:** 16-34

Lam AMI, Frick DN (2006) Hepatitis C virus subgenomic replicon requires an active NS3 RNA helicase. *Journal of Virology* **80**(1)**:** 404-411

Levy DE, Kessler DS, Pine R, Darnell Jr JE (1989) Cytoplasmic activation of ISGF3, the positive regulator of interferon-alpha-stimulated transcription, reconstituted in vitro. *Genes & development* **3**(9)**:** 1362-1371

Li K, Foy E, Ferreon JC, Nakamura M, Ferreon ACM, Ikeda M, Ray SC, Gale Jr M, Lemon SM (2005) Immune evasion by hepatitis C virus NS3/4A protease-mediated cleavage of the Toll-like receptor 3 adaptor protein TRIF. *Proceedings of the National Academy of Sciences of the United States of America* **102**(8)**:** 2992-2997

Li X, Zhao X, Fang Y, Jiang X, Duong T, Fan C, Huang CC, Kain SR (1998) Generation of destabilized green fluorescent protein as a transcription reporter. *Journal of Biological Chemistry* **273**(52)**:** 34970-34975

Lin R, Heylbroeck C, Pitha PM, Hiscott J (1998) Virus-dependent phosphorylation of the IRF-3 transcription factor regulates nuclear translocation, transactivation potential, and proteasome- mediated degradation. *Molecular and Cellular Biology* **18**(5)**:** 2986-2996

Lin R, Mamane Y, Hiscott J (1999) Structural and functional analysis of interferon regulatory factor 3: Localization of the transactivation and autoinhibitory domains. *Molecular and Cellular Biology* **19**(4)**:** 2465-2474

Lin W, Choe WH, Hiasa Y, Kamegaya Y, Blackard JT, Schmidt EV, Chung RT (2005) Hepatitis C virus expression suppresses interferon signaling by degrading STAT1. *Gastroenterology* **128**(4)**:** 1034-1041

Lin W, Kim SS, Yeung E, Kamegaya Y, Blackard JT, Kim KA, Holtzman MJ, Chung RT (2006) Hepatitis C virus core protein blocks interferon signaling by interaction with the STAT1 SH2 domain. *Journal of Virology* **80**(18)**:** 9226-9235

Lindström S, Andersson-Svahn H (2010) Overview of single-cell analyses: Microdevices and applications. *Lab on a Chip - Miniaturisation for Chemistry and Biology* **10**(24)**:** 3363-3372

Liu XY, Wei B, Shi HX, Shan YF, Wang C (2010) Tom70 mediates activation of interferon regulatory factor 3 on mitochondria. *Cell Research* **20**(9)**:** 994-1011

Loew R, Heinz N, Hampf M, Bujard H, Gossen M (2010) Improved Tet-responsive promoters with minimized background expression. *BMC Biotechnology* **10**

Loo YM, Owen DM, Li K, Erickson AK, Johnson CL, Fish PM, Carney DS, Wang T, Ishida H, Yoneyama M, Fujita T, Saito T, Lee WM, Hagedorn CH, Lau DTY, Weinman SA, Lemon SM, Gale Jr M (2006) Viral and therapeutic control of IFN-β promoter stimulator 1 during hepatitis C virus infection. *Proceedings of the National Academy of Sciences of the United States of America* **103**(15)**:** 6001-6006

Lu Y, Wambach M, Katze MG, Krug RM (1995) Binding of the influenza virus NS1 protein to double-stranded RNA inhibits the activation of the protein kinase that phosphorylates the eIF-2 translation initiation factor. *Virology* **214**(1)**:** 222-228

Lukyanov KA, Serebrovskaya EO, Lukyanov S, Chudakov DM (2010) Fluorescent proteins as light-inducible photochemical partners. *Photochemical and Photobiological Sciences* **9**(10)**:** 1301-1306

Ma Y, Yates J, Liang Y, Lemon SM, Yi M (2008) NS3 helicase domains involved in infectious intracellular hepatitis C virus particle assembly. *Journal of Virology* **82**(15)**:** 7624-7639

Maiwald T, Schneider A, Busch H, Sahle S, Gretz N, Weiss TS, Kummer U, Klingmüller U (2010) Combining theoretical analysis and experimental data generation reveals IRF9 as a crucial factor for accelerating interferon-α induced early antiviral signalling. *FEBS Journal* **277**(22)**:** 4741-4754

Maniatis T, Fritsch EJ, Sambrook J (1982) Molecular cloning: a laboratory manual. *Cold Spring Harbor, NY: Cold Spring Harbor Laboratory*

Margolin JF, Friedman JR, Meyer WKH, Vissing H, Thiesen HJ, Rauscher Iii FJ (1994) Krüppel-associated boxes are potent transcriptional repression domains. *Proceedings of the National Academy of Sciences of the United States of America* **91**(10)**:** 4509-4513

Marié I, Durbin JE, Levy DE (1998) Differential viral induction of distinct interferon-α genes by positive feedback through interferon regulatory factor-7. *EMBO Journal* **17**(22)**:** 6660-6669

Marié I, Smith E, Prakash A, Levy DE (2000) Phosphorylation-induced dimerization of interferon regulatory factor 7 unmasks DNA binding and a bipartite transactivation domain. *Molecular and Cellular Biology* **20**(23)**:** 8803-8814

Martinez-Moczygemba M, Gutch MJ, French DL, Reich NC (1997) Distinct STAT structure promotes interaction of STAT2 with the p48 subunit of the interferon-α-stimulated transcription factor ISGF3. *Journal of Biological Chemistry* **272**(32)**:** 20070-20076

May T, Eccleston L, Herrmann S, Hauser H, Goncalves J, Wirth D (2008) Bimodal and hysteretic expression in mamalian cells from a synthetic gene circuit. *PLoS ONE* **3**(6)

May T, Hauser H, Wirth D (2004) Transcriptional control of SV40 T-antigen expression allows a complete reversion of immortalization. *Nucleic Acids Research* **32**(18)**:** 5529-5538

McInerney GM, Karlsson Hedestam GB (2009) Direct cleavage, proteasomal degradation and sequestration: Three mechanisms of viral subversion of type i interferon responses. *Journal of Innate Immunity* **1**(6)**:** 599-606

McLauchlan J (2009) Lipid droplets and hepatitis C virus infection. *Biochimica et Biophysica Acta - Molecular and Cell Biology of Lipids* **1791**(6)**:** 552-559

Melén K, Kinnunen L, Fagerlund R, Ikonen N, Twu KY, Krug RM, Julkunen I (2007) Nuclear and nucleolar targeting of influenza A virus NS1 protein: Striking differences between different virus subtypes. *Journal of Virology* **81**(11)**:** 5995-6006

Min JY, Krug RM (2006) The primary function of RNA binding by the influenza A virus NS1 protein in infected cells: Inhibiting the 2'-5' oligo (A) synthetase/RNase L pathway. *Proceedings of the National Academy of Sciences of the United States of America* **103**(18)**:** 7100-7105

Miyoshi H, Fujie H, Shintani Y, Tsutsumi T, Shinzawa S, Makuuchi M, Kokudo N, Matsuura Y, Suzuki T, Miyamura T, Moriya K, Koike K (2005) Hepatitis C virus core protein exerts an inhibitory effect on suppressor of cytokine signaling (SOCS)-1 gene expression. *Journal of Hepatology* **43**(5)**:** 757-763

Moradpour D, Englert C, Wakita T, Wands JR (1996) Characterization of cell lines allowing tightly regulated expression of hepatitis C virus core protein. *Virology* **222**(1)**:** 51-63

Nemeroff ME, Barabino SML, Li Y, Keller W, Krug RM (1998) Influenza virus NS1 protein interacts with the cellular 30 kDa subunit of CPSF and inhibits 3' end formation of cellular pre-mRNAs. *Molecular Cell* **1**(7)**:** 991-1000

Nemeroff ME, Qian XY, Krug RM (1995) The influenza virus NS1 protein forms multimers in vitro and in vivo. *Virology* **212**(2)**:** 422-428

Neumann H, Neumann-Staubitz P (2010) Synthetic biology approaches in drug discovery and pharmaceutical biotechnology. *Applied Microbiology and Biotechnology* **87**(1)**:** 75-86

Noah DL, Twu KY, Krug RM (2003) Cellular antiviral responses against influenza A virus are countered at the posttranscriptional level by the viral NS1A protein via its binding to a cellular protein required for the 3' end processing of cellular pre-mRNAS. *Virology* **307**(2)**:** 386-395

Onoguchi K, Yoneyama M, Fujita T (2011) Retinoic acid-inducible Gene-I-Like receptors. *Journal of Interferon and Cytokine Research* **31**(1)**:** 27-31

Pichlmair A, Schulz O, Tan CP, Näslund TI, Liljeström P, Weber F, Reis E Sousa C (2006) RIG-I-mediated antiviral responses to single-stranded RNA bearing 5'-phosphates. *Science* **314**(5801)**:** 997-1001

Pluta K, Luce MJ, Bao L, Agha-Mohammadi S, Reiser J (2005) Tight control of transgene expression by lentivirus vectors containing second-generation tetracycline-responsive promoters. *Journal of Gene Medicine* **7**(6)**:** 803-817

Postle K, Nguyen TT, Bertrand KP (1984) Nucleotide sequence of the repressor gene of the TN10 tetracycline resistance determinant. *Nucleic Acids Research* **12**(12)**:** 4849-4863

Pulverer JE (2008) Monitoring Interferon Responses by Novel Reporter Systems in vitro and in vivo. Doctoral thesis at the Hannover Medical School.

Pulverer JE, Rand U, Lienenklaus S, Kugel D, Zietara N, Kochs G, Naumann R, Weiss S, Staeheli P, Hauser H, Köster M (2010) Temporal and spatial resolution of type I and III interferon responses in vivo. *Journal of Virology* **84**(17)**:** 8626-8638

Purcell O, Savery NJ, Grierson CS, Di Bernardo M (2010) A comparative analysis of synthetic genetic oscillators. *Journal of the Royal Society Interface* **7**(52)**:** 1503-1524

Rand U (2010) Dynamics of type I interferon induction and action. Doctoral thesis at the Hannover Medical School.

Randall RE, Goodbourn S (2008) Interferons and viruses: An interplay between induction, signalling, antiviral responses and virus countermeasures. *Journal of General Virology* **89**(1)**:** 1-47

Rang A, Will H (2000) The tetracycline-responsive promoter contains functional interferon-inducible response elements. *Nucleic Acids Research* **28**(5)**:** 1120-1125

Rogers S, Wells R, Rechsteiner M (1986) Amino acid sequences common to rapidly degraded proteins: The PEST hypothesis. *Science* **234**(4774)**:** 364-368

Ruggieri A, Franco M, Gatto I, Kumar A, Rapicetta M (2007) Modulation of RANTES expression by HCV core protein in liver derived cell lines. *BMC Gastroenterology* **7**
Sadler AJ, Williams BRG (2008) Interferon-inducible antiviral effectors. *Nature Reviews Immunology* **8**(7)**:** 559-568

Saito T, Hirai R, Loo YM, Owen D, Johnson CL, Sinha SC, Akira S, Fujita T, Gale Jr M (2007) Regulation of innate antiviral defenses through a shared repressor domain in RIG-1 and LGP2. *Proceedings of the National Academy of Sciences of the United States of America* **104**(2)**:** 582-587

Sasaki A, Yasukawa H, Suzuki A, Kamizono S, Syoda T, Kinjyo I, Sasaki M, Johnston JA, Yoshimura A (1999) Cytokine-inducible SH2 protein-3 (CIS3/SOCS3) inhibits Janus tyrosine kinase by binding through the N-terminal kinase inhibitory region as well as SH2 domain. *Genes to Cells* **4**(6)**:** 339-351

Sato M, Hata N, Asagiri M, Nakaya T, Taniguchi T, Tanaka N (1998) Positive feedback regulation of type I IFN genes by the IFN-inducible transcription factor IRF-7. *FEBS Letters* **441**(1)**:** 106-110

Sato M, Suemori H, Hata N, Asagiri M, Ogasawara K, Nakao K, Nakaya T, Katsuki M, Noguchi S, Tanaka N, Taniguchi T (2000) Distinct and essential roles of transcription factors IRF-3 and IRF-7 in response to viruses for IFN-α/β gene induction. *Immunity* **13**(4)**:** 539-548

Satterly N, Tsai PL, Van Deursen J, Nussenzveig DR, Wang Y, Faria PA, Levay A, Levy DE, Fontoura BMA (2007) Influenza virus targets the mRNA export machinery and the nuclear pore complex. *Proceedings of the National Academy of Sciences of the United States of America* **104**(6)**:** 1853-1858

Scheu S, Dresing P, Locksley RM (2008) Visualization of IFN-β production by plasmacytoid versus conventional dendritic cells under specific stimulation conditions in vivo. *Proceedings of the National Academy of Sciences of the United States of America* **105**(51)**:** 20416-20421

Schindler C, Plumlee C (2008) Interferons pen the JAK-STAT pathway. *Seminars in Cell and Developmental Biology* **19**(4)**:** 311-318

Schucht R, Wirth D, May T (2010) Precise regulation of transgene expression level and control of cell physiology. *Cell Biology and Toxicology* **26**(1)**:** 29-42

Scott JD, Pawson T (2009) Cell signaling in space and time: Where proteins come together and when they're apart. *Science* **326**(5957)**:** 1220-1224

Seo YJ, Hahm B. Type I interferon modulates the battle of host immune system against viruses. *Advances in Applied Microbiology*, Vol. 73, pp. 83-101.

Servant MJ, Tenoever B, Lin R (2002) Overlapping and distinct mechanisms regulating IRF-3 and IRF-7 function. *Journal of Interferon and Cytokine Research* **22**(1)**:** 49-58

Sharma S, TenOever BR, Grandvaux N, Zhou GP, Lin R, Hiscott J (2003) Triggering the interferon antiviral response through an IKK-related pathway. *Science* **300**(5622)**:** 1148-1151

Shimomura O, Johnson FH, Saiga Y (1962) Extraction, purification and properties of aequorin, a bioluminescent protein from the luminous hydromedusan Aequorea. *Journal of cellular and comparative physiology* **59:** 223-239

Smith PK, Krohn RI, Hermanson GT (1985) Measurement of protein using bicinchoninic acid. *Analytical Biochemistry* **150**(1)**:** 76-85

Stricker J, Cookson S, Bennett MR, Mather WH, Tsimring LS, Hasty J (2008) A fast, robust and tunable synthetic gene oscillator. *Nature* **456**(7221)**:** 516-519

Suarez DL, Perdue ML (1998) Multiple alignment comparison of the non-structural genes of influenza A viruses. *Virus Research* **54**(1)**:** 59-69

Sun Y (1997) RIG-I, a human homolog gene of RNA helicase, is induced by retinoic acid during the differentiation of acute propromyelocytic leukemia cell. Thesis. Shanghai Institute of Hematology, Rui-Jin Hospital, Shanghai Second Medical University,

Takaoka A, Wang Z, Choi MK, Yanai H, Negishi H, Ban T, Lu Y, Miyagishi M, Kodama T, Honda K, Ohba Y, Taniguchi T (2007) DAI (DLM-1/ZBP1) is a cytosolic DNA sensor and an activator of innate immune response. *Nature* **448**(7152)**:** 501-505

Takeuchi O, Akira S (2009) Innate immunity to virus infection. *Immunological Reviews* **227**(1)**:** 75-86

Tang H, Grisé H (2009) Cellular and molecular biology of HCV infection and hepatitis. *Clinical Science* **117**(2)**:** 49-65

Thompson AJV, Locarnini SA (2007) Toll-like receptors, RIG-I-like RNA helicases and the antiviral innate immune response. *Immunology and Cell Biology* **85**(6)**:** 435-445

Thompson JF, Hayes LS, Lloyd DB (1991) Modulation of firefly luciferase stability and impact on studies of gene regulation. *Gene* **103**(2)**:** 171-177

Tigges M, Dénervaud N, Greber D, Stelling J, Fussenegger M (2010) A synthetic low-frequency mammalian oscillator. *Nucleic Acids Research* **38**(8)**:** 2702-2711

Tigges M, Fussenegger M (2009) Recent advances in mammalian synthetic biology-design of synthetic transgene control networks. *Current Opinion in Biotechnology* **20**(4)**:** 449-460

Tigges M, Marquez-Lago TT, Stelling J, Fussenegger M (2009) A tunable synthetic mammalian oscillator. *Nature* **457**(7227)**:** 309-312

Towbin H, Staehelin T, Gordon J (1979) Electrophoretic transfer of proteins from polyacrylamide gels to nitrocellulose sheets: Procedure and some applications. *Proceedings of the National Academy of Sciences of the United States of America* **76**(9)**:** 4350-4354

Triezenberg SJ, Kingsbury RC, McKnight SL (1988) Functional dissection of VP16, the trans-activator of herpes simplex virus immediate early gene expression. *Genes & development* **2**(6)**:** 718-729

Unterholzner L, Keating SE, Baran M, Horan KA, Jensen SB, Sharma S, Sirois CM, Jin T, Latz E, Xiao TS, Fitzgerald KA, Paludan SR, Bowie AG (2010) IFI16 is an innate immune sensor for intracellular DNA. *Nature Immunology* **11**(11)**:** 997-1004

Urlinger S, Baron U, Thellmann M, Hasan MT, Bujard H, Hillen W (2000) Exploring the sequence space for tetracycline-dependent transcriptional activators: Novel mutations yield expanded range and sensitivity. *Proceedings of the National Academy of Sciences of the United States of America* **97**(14)**:** 7963-7968

Van Gelder RN, Herzog ED, Schwartz WJ, Taghert PH (2003) Circadian rhythms: In the loop at last. *Science* **300**(5625)**:** 1534-1535
Versteeg GA, García-Sastre A (2010) Viral tricks to grid-lock the type I interferon system. *Current Opinion in Microbiology* **13**(4)**:** 508-516

Vester D, Lagoda A, Hoffmann D, Seitz C, Heldt S, Bettenbrock K, Genzel Y, Reichl U (2010) Real-time RT-qPCR assay for the analysis of human influenza A virus transcription and replication dynamics. *Journal of Virological Methods* **168**(1-2)**:** 63-71

Vo N, Goodman RH (2001) CREB-binding Protein and p300 in Transcriptional Regulation. *Journal of Biological Chemistry* **276**(17)**:** 13505-13508

Walsh MJ, Jonsson JR, Richardson MM, Lipka GM, Purdie DM, Clouston AD, Powell EE (2006) Non-response to antiviral therapy is associated with obesity and increased hepatic expression of suppressor of cytokine signaling 3 (SOCS-3) in patients with chronic hepatitis C, viral genotype 1. *Gut* **55**(4)**:** 529-535

Wang W, Riedel K, Lynch P, Chien CY, Montelione GT, Krug RM (1999) RNA binding by the novel helical domain of the influenza virus NS1 protein requires its dimer structure and a small number of specific basic amino acids. *RNA* **5**(2)**:** 195-205

Wathelet MG, Lin CH, Parekh BS, Ronco LV, Howley PM, Maniatis T (1998) Virus infection induces the assembly of coordinately activated transcription factors on the IFN-β enhancer in vivo. *Molecular Cell* **1**(4)**:** 507-518

Weber F, Wagner V, Rasmussen SB, Hartmann R, Paludan SR (2006) Double-stranded RNA is produced by positive-strand RNA viruses and DNA viruses but not in detectable amounts by negative-strand RNA viruses. *Journal of Virology* **80**(10)**:** 5059-5064

Weber W, Fussenegger M (2010) Synthetic gene networks in mammalian cells. *Current Opinion in Biotechnology* **21**(5)**:** 690-696

Weber W, Fux C, Daoud-El Baba M, Keller B, Weber CC, Kramer BP, Heinzen C, Aubel D, Bailey JE, Fussenegger M (2002) Macrolide-based transgene control in mammalian cells and mice. *Nature Biotechnology* **20**(9)**:** 901-907

West AG, Fraser P (2005) Remote control of gene transcription. *Human Molecular Genetics* **14**(SPEC. ISS. 1)**:** R101-R111

Yamaguchi K, Inoue S, Ohara O, Nagase T (2009) Pulse-chase experiment for the analysis of protein stability in cultured mammalian cells by covalent fluorescent labeling of fusion proteins. *Methods in molecular biology (Clifton, NJ)* **577:** 121-131

Yeow WS, Au WC, Juang YT, Fields CD, Dent CL, Gewert DR, Pitha PM (2000) Reconstitution of virus-mediated expression of interferon α genes in human fibroblast cells by ectopic interferon regulatory factor-7. *Journal of Biological Chemistry* **275**(9)**:** 6313-6320

Yie J, Senger K, Thanos D (1999) Mechanism by which the IFN-β enhanceosome activates transcription. *Proceedings of the National Academy of Sciences of the United States of America* **96**(23)**:** 13108-13113

Zawatzky R, De Maeyer E, De Maeyer-Guignard J (1985) Identification of individual interferon-producing cells by in situ hybridization. *Proceedings of the National Academy of Sciences of the United States of America* **82**(4)**:** 1136-1140

Zhang X, Brann TW ZM, Yang J, Oguariri RM, Lidie KB, Imamichi H, Huang DW, Lempicki RA, Baseler MW, Veenstra TD, Young HA, Lane HC, Imamichi T (2011) Cutting Edge: Ku70 is a novel cytosolic DNA sensor that induces Type III rather than Type I IFN.

Zhao HF, Boyd J, Jolicoeur N, Shen SH (2003) A Coumermycin/Novobiocin-Regulated Gene Expression System. *Human Gene Therapy* **14**(17)**:** 1619-1629

8.3 List of tables and figures

Danksagung

Mit den folgenden Worten möchte ich mich bei allen bedanken, die dazu beigetragen haben, dass diese Arbeit erfolgreich durchgeführt werden konnte.

Zu allererst möchte ich mich bei meiner Betreuerin Dr. Dagmar Wirth für die Ermöglichung dieser Arbeit und die Unterstützung in den vergangenen Jahren bedanken. Vielen Dank für zahlreiche Diskussionen und Anregungen und natürlich, insbesondere in der letzten Zeit, für das Korrekturlesen.

Desweiteren möchte ich mich bei Dr. Hansjörg Hauser für die Teilnahme an meinem Thesis Komitee, sowie seine Ideen bezüglich dieser Arbeit bedanken.

Meinem Co-Supervisor Dr. Mario Köster möchte ich neben seiner Teilnahme an meinem Thesis Komitee für seine stets positive Denkweise und den einen oder anderen netten Gedankenaustausch danken.

Ich möchte meinem Co-Supervisor Prof. Dr.-Ing. Udo Reichl für die Teilnahme an meinem Thesis Komitee herzlich danken.

Ich möchte mich bei Prof. Dr. Petra Dersch für die Übernahme der Mentorenschaft, des Referats und für die Teilnahme an meiner Prüfungskommission bedanken. Bei Prof. Dr. Peter Paul Müller möchte ich mich für die Übernahme des Ko-Referats herzlich bedanken. Prof. Dr. Michael Steinert und Prof. Dr. André Fleißner danke ich für die Teilnahme an der Prüfungskommission.

Bei Prof. Dr. Klaus Schughart möchte ich mich für die Bereitstellung des Influenza Virus bedanken.

Ein ganz besonderer Dank geht an Dr. Ulfert Rand, der mich insbesondere im letzten Jahr dieser Arbeit unterstützt und ertragen hat. Vielen Dank für unzählige Diskussionen und die Einführung und Begeisterung für die Mikroskopie.

Many thanks go to Dr. Ana Margarida Palma Teixeira: Muito obrigada para a colaboracao e muito successo como todos os teus alvos.

Lukas Kemper möchte ich für die Unterstützung beim Western Blot danken.

Maria Höxter danke ich für ihren unermüdlichen Einsatz rund um das FACS.

A special thank goes to the MSYS group, that I was part of during the last years. Thanks to all of you for a nice working atmosphere.

I would like to thank Lacra for her support in compensation and for the motivation in the past months.

Marcin and Sara: My lab-buddies… thanks for the nice atmosphere during work. I am still fascinated by all the wonderful things that happened during our time together.

Sabrina: Danke für deine Unterstützung und viele, nette Gespräche auch am Rande der Arbeit.

Dr. Tobias May: Danke für das Vermitteln einer ganz „speziellen“ Atmosphäre.

Insbesondere bedanke ich mich bei meiner Familie, die mich außerhalb des Labors stets unterstützt hat! Danke an meine Eltern, die immer für mich da waren und mich immer wieder ermutigt haben! Meiner Schwester, meinem Schwager und den drei Rabauken (Almeida-Bande) danke ich für ihr Vertrauen und dafür, dass sie immer für mich da sind!

Mein größter Dank gilt meinem geliebten Alexis, der mich mit seiner Liebe und Geduld stets unterstützt und gestärkt hat. Du warst während der gesamten Dauer dieser Arbeit für mich da! Ich bin froh und glücklich, dass es dich gibt! Vielen Dank für’s immer da sein!

Lebenslauf

Angaben zur Person

Geburtsdatum und –ort:	03.11.1982, Goslar
Familienstand:	ledig
Staatsangehörigkeit:	deutsch

Schulausbildung

08/1989 – 06/1993	Grundschule Jürgenohl – Goslar
08/1993 – 06/1995	Orientierungsstufe Goldene Aue – Goslar
08/1995 – 06/2002	Christian – von – Dohm – Gymnasium – Goslar

Studium

10/2002 – 10/2007	Studium der Biologie an der TU Braunschweig
01/2007 – 10/2007	Diplomarbeit am Institut für Mikrobiologie, Arbeitsgruppe von Prof. Dr. Petra Dersch; Thema: „Influence of global regulators on the expression of the virulence regulator RovA in *Yersinia pseudotuberculosis*"

Berufstätigkeit

01/2008 – 04/2011	Wissenschaftliche Mitarbeiterin (Doktorandin) am Helmholtz Zentrum für Infektionsforschung, Braunschweig in der Arbeitsgruppe „Modellsysteme für Infektion und Immunität" von Dr. Dagmar Wirth

Publikationen

Botezatu L, Sievers S, Gama-Norton L, Schucht R, Hauser H, Wirth D: "Cell line development from a synthetic biology perspective", submitted.